

Altered Intranuclear Dynamics of Mutant Thyroid Hormone Receptors in Resistance to
Thyroid Hormone

Hannah Page Tofil

Great Falls, Virginia

Bachelor of Arts, University of Vermont, 2019

A Thesis presented to the Graduate Faculty of The College of William & Mary in
Candidacy for the Degree of
Master of Science

Department of Biology

College of William & Mary
August, 2022

APPROVAL PAGE

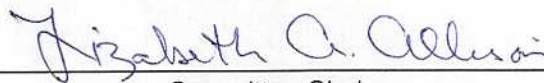
This Thesis is submitted in partial fulfillment of
the requirements for the degree of

Master of Science



Hannah Page Tofil

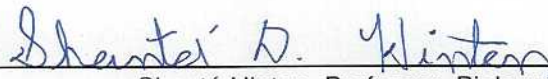
Approved by the Committee July 2022



Committee Chair
Elizabeth Allison, Professor, Biology
College of William & Mary



Co-Chair
Diane Shakes, Professor, Biology
College of William & Mary



Shantá Hinton, Professor, Biology
College of William & Mary

ABSTRACT

A protein's intracellular location is an integral part of its function. Mislocalization caused by mutations within a protein can lead to protein dysfunction and leave an individual susceptible to diseases such as type II diabetes, certain cancers, and Resistance to Thyroid Hormone Syndrome (RTH). Such is the case for the thyroid hormone receptor $\alpha 1$ (TR $\alpha 1$), as certain mutations in TR $\alpha 1$'s ligand binding domain can cause RTH. TR $\alpha 1$ binds to thyroid hormone (T3) and acts as a transcription factor in the nucleus. As such, maintenance of TR $\alpha 1$'s nucleocytoplasmic shuttling and intranuclear dynamics is essential to ensure proper protein function. Prior studies have demonstrated that certain RTH TR $\alpha 1$ mutants have an increased affinity to one of TR $\alpha 1$'s coregulators, nuclear corepressor 1 (NCoR1), and form a more stable complex compared to wild type TR $\alpha 1$. This finding suggests that the intranuclear mobility of RTH TR $\alpha 1$ mutants would decrease relative to their wild-type counterpart, and that nucleocytoplasmic shuttling would be impacted due to having one of several nuclear export motifs (NES-H12) compromised. The major aim of this thesis was to evaluate the intranuclear dynamics of RTH TR $\alpha 1$ mutants E403X, Ala382ProfsX7, and F397fs406X in response to increased levels of NCoR1. The intranuclear dynamics of each mutant RTH TR $\alpha 1$ was evaluated in human cells using fluorescence recovery after photobleaching (FRAP), and statistically analyzed for a significant difference compared to wild type TR $\alpha 1$. A mutant NCoR1 that lacks TR interaction domains, NCoR Δ ID, was used to control for wild type NCoR1's increased binding affinity to RTH TR $\alpha 1$ mutants. While overexpressing NCoR1 did not significantly impact RTH TR $\alpha 1$ mutant intranuclear mobility, NCoR Δ ID overexpression significantly decreased RTH-F397fs406X intranuclear mobility, with RTH-E403X showing a similar trend. Interestingly, RTH-A383PfsX7 did not appear to be affected by NCoR Δ ID. As a second measure of intracellular dynamics, the nucleocytoplasmic shuttling ability of RTH-A383PfsX7 and wild type TR $\alpha 1$ was evaluated using heterokaryon assays. Despite having a compromised or missing NES-H12, RTH-A383PfsX7 maintained shuttling capabilities qualitatively similar to those of wild type TR $\alpha 1$. These findings offer new insight into RTH TR $\alpha 1$'s molecular phenotype and warrant further investigation into the interaction between NCoR1/ NCoR Δ ID with TR $\alpha 1$ and RTH-E403X, Ala382ProfsX7, and F397fs406X, as well as evaluation of RTH-E403X and F397fs406X's nucleocytoplasmic shuttling.

TABLE OF CONTENTS

Acknowledgements	ii
List of Tables	iii
List of Figures	iv
Chapter 1. General Information	1
What is Resistance to Thyroid Hormone?	1
Hypothalamus-Pituitary-Thyroid Axis	3
Thyroid Hormone Receptor α	5
TR α 1 DNA Binding and Dimerization	8
TR α 1 Ligand Binding	11
Nucleocytoplasmic Shuttling	13
Nuclear Receptor Corepressor 1	15
Resistance to Thyroid Hormone α	17
Specific Aims	21
Chapter 2. Methods	23
Chapter 3. Experimental Results	28
Chapter 4. Discussion	55
Chapter 5. Conclusion	62
Appendix	65
References	99

ACKNOWLEDGEMENTS

I would like to take this opportunity to thank everyone who has helped me get here. It has been a process, especially during COVID and quarantine. I first want to thank Dr. Allison – thank you for all of your unwavering support as I worked on this thesis while handling my health issues. I am so incredibly grateful to you and all you have done for me. To the oh so fashionable Dr. Hinton – thank you for pushing me to become the best version of me scientifically, professionally, and personally. To Dr. Shakes – thank you for providing so many different perspectives on my work and for sharing my love and geekiness for microscopy. To Vinny Roggero – thank you for putting up with my unceasing questions, for helping with our best friend, the confocal, and just all around being so supportive. To all Allison Lab members, past and present, for making this journey fun even in the middle of a pandemic. To my friends and family for their unwavering support and for being a listening ear, and to my partner, Ayanna, for her love, companionship, and support.

LIST OF TABLES

Chapter 3 Tables

1. FRAP parameters comparing wild-type TR α 1 to RTH-F397fs406X, A382PfsX7, and E403X 35
2. FRAP parameters comparing NCoR1 coexpressed with wild-type TR α 1 to NCoR1 coexpressed with either RTH-F397fs406X, A382PfsX7, or E403X 49
3. FRAP parameters comparing NCoR Δ ID coexpressed with wild-type TR α 1 to NCoR Δ ID coexpressed with either RTH-F397fs406X, A382PfsX7, or E403X 52

LIST OF FIGURES

1. Thyroid hormone synthesis via the Hypothalamus-Pituitary-Thyroid (HPT) axis	5
2. TR α 1 localization signals and domains	7
3. Orientation of TRE consensus half sites, direct repeats, palindrome, and inverted palindrome	10
4. Protein structure of TR α 1's ligand binding domain bound to T3	12
5. Nucleocytoplasmic transport of TR α 1	14
6. TR α 1 action in the presence and absence of NCoR1 when bound to a thyroid response element (TRE)	17
7. The locations of RTH α mutants with increased NCoR1 binding affinity	19
8. No apparent differences in intranuclear mobility between wild-type TR α 1 and the RTH α mutants	32
9. NCoR1 does not impact RTH-F397fs406X intranuclear dynamics, yet NCoR Δ ID reduces its mobility	36
10. Neither NCoR1 nor NCoR Δ ID impact RTH-A382PfsX7 intranuclear dynamics	40
11. NCoR1 does not impact RTH-E403X intranuclear dynamics, yet NCoR Δ ID reduces its mobility	49
12. Intracellular localization of NCoR1 and NCoR Δ ID	50
13. Intracellular localization of NCoR1 and NCoR Δ ID in cotransfected cells	51
14. Deletion of Helix 12 does not impact TR α 1-A382PfsX7 nucleocytoplasmic shuttling	53
15. Suggested Model: NCoR Δ ID may bind to RTH-F397fs406X and E403X	64

Chapter 1: General Introduction

Regulation of protein activity is crucial to maintaining proper cell function, as one mistake could damage the integrity of the cell and, by extension, the body. This is especially true when the protein in question regulates gene expression, such as those in the nuclear receptor (NR) superfamily—a family of transcription factors (Laudet & Gronemeyer, 2002). One of the ways cells modulate proper NR function and associated target gene expression is through monitoring their mobility and localization. For example, dysregulation of NR intranuclear kinetics and their corepressors have been implicated in prostate cancer and spinal and bulbar muscle atrophy (Black & Paschal, 2004; Normanno et al., 2012); increased nuclear localization and reduced nucleocytoplasmic shuttling of glucocorticoid receptors can lead to disease, such as types of cancer (Conway-Campbell et al., 2007); and for thyroid hormone receptor $\alpha 1$ (TR $\alpha 1$), the focus of this thesis, improper shuttling and mislocalization is associated with thyroid cancer, renal and breast cancers, and, most notably, Resistance to Thyroid Hormone Syndrome α (RTH α) (Anyetei-Anum et al., 2018; Astapova et al., 2011; Bonamy and Allison 2006; Bonamy et al. 2005; Bondzi et al. 2011; Bunn et al. 2001; DeLong, et al. 2004; Zhang et al. 2018). This thesis evaluates the impact of nuclear corepressor 1 (NCoR1), TR α 's primary corepressor, on the intranuclear mobility of select RTH α mutants.

A. What is Resistance to Thyroid Hormone?

Resistance to Thyroid Hormone Syndrome (RTH) is a rare genetic disease, clinically characterized by decreased sensitivity of somatic tissues to thyroid hormone activity in

addition to mild hypothyroid-like symptoms (Singh & Yen, 2017). It was first documented in 1937 by Albright et al. as “pseudohypoparathyroidism;” its current name was not coined until 1967 by Refetoff et al. (Weiss & Refetoff, 2000). Between 1967 and 1993, the number of reported cases had risen from one to 347 cases (Refetoff et al., 1993), and a current estimate suggests that 1 in 40,000 live births present with associated symptoms (Rivas & Lado-Abeal, 2016).

As a reflection of its rarity, the genetic cause of RTH was not isolated until 20 years after its classification. In 1986, researchers were able to link RTH to multiple mutations in the gene *THRB*, a gene which encodes for the beta subtype of the thyroid hormone receptor (TR β) (Weinberger et al., 1986). However, Bochukova et al. (2012) classified the first RTH mutation in the *THRA* gene, which encodes the TR α receptor subtype.

This discovery led to the reclassification of RTH into two subtypes—RTH β and RTH α —based on which gene carried mutation(s). Since this discovery, over 100 RTH β and 25 RTH α mutations have been identified in patients (Rurale et al., 2020; *RTH α — Institut de Génomique Fonctionnelle de Lyon*, 2022). Of note, the ExAC database lists 68 mutations from anonymous patients that are predicted to alter TR α 1 function (Rurale et al., 2020; *THRA | GnomAD v2.1.1 | GnomAD*, 2021).

Diagnosing RTH has proven to be difficult as a result of its variable symptoms across cases (Weiss & Refetoff, 2000). However, three symptoms seem to unite all cases: elevated free thyroid hormone levels, specifically triiodothyronine (T3) or thyroxine (T4), normal or slightly elevated thyroid stimulating hormone (TSH) levels, and thyroid swelling, also known as goiter (Refetoff et al, 1993; Weiss & Refetoff, 2000). Other potential symptoms include, but are not limited to, irregular heart rate, developmental

delays, seizures, learning disorders, short stature, hearing loss, and recurrent ear, nose, and throat infections. Another difficulty in diagnosing RTH originates in the variability in severity and the affected tissues. Patients who clinically present as either euthyroid or hypothyroid are diagnosed with “general” RTH; those who are clinically hypermetabolic are diagnosed with pituitary RTH; finally, those with hormone resistance in the periphery are diagnosed with peripheral tissue RTH (Weiss & Refetoff, 2000). The focus of this thesis is on RTH α and associated mutations in TR α 1.

B. Hypothalamus-Pituitary-Thyroid Axis

In order to appreciate the clinical presentation of Resistance to Thyroid Hormone Syndrome, we must first appreciate the baseline presentation of TRs, and of the thyroid gland itself. The thyroid and the hormones it produces are responsible for maintaining homeostasis in the body through processes ranging from gene regulation to metabolism regulation (reviewed in Anyetei-Anum et al., 2018; Davis, Goglia, & Leonard, 2015). Therefore, thyroid activity is heavily regulated by the endocrine and nervous system via the hypothalamus-pituitary-thyroid (HPT) axis, as depicted in Figure 1 (Anyetei-Anum et al., 2018; Ortiga-Carvalho et al., 2016).

To activate the axis, external stimuli notify the brain to induce thyroid hormone (TH) production. To achieve TH production, the brain notifies the hypothalamus to release thyrotropin-releasing hormone (TRH) to stimulate the pituitary gland. Once stimulated, the pituitary gland releases thyroid stimulating hormone (TSH) into the circulatory system. When bound to thyroid stimulating hormone receptors (TSHRs) on thyrocytes, TSH induces the production of the two primary TH isoforms: T3 and T4 (Ortiga-

Carvalho et al., 2016; Singh & Yen, 2017). Once released, thyroid hormones are transported to target cells by thyroxine-binding globulin, transthyretin, and human serum albumin (reviewed in Anyetei-Anum et al., 2018). Upon arrival at the target cell, TH enters the cell through monocarboxylate transporters 8 and 10 (MCT8 and MCT 10) (Gereben et al., 2008; Singh et al., 2017; reviewed in Anyetei-Anum et al., 2018).

The HPT axis is regulated through a negative feedback loop created by T3, as the hormone is able to bind to TRH and inhibit its effects (Ortiga-Carvalho et al., 2016). To help regulate thyroid hormone levels and activity, T3 and T4 are able to be interconverted as needed. T4 is the primary, secreted isoform of TH; however, T3 is the preferred ligand for many TRs and TRH. Accordingly, the concentration of available T3 helps regulate TR activity. To help regulate T3 levels, T4 is converted to T3 by undergoing extra-thyroidal conversion by the enzymes 5'-deiodinases, D1 and D2 (Ortiga-Carvalho et al., 2016).

The body can be further protected from excess hormone by deactivating T4 using the enzyme 5-deiodinase to convert T4 to reverse-T3, which has a lower affinity to TRs and THR (reviewed in Anyetei-Anum et al., 2018; Ortiga-Carvalho et al., 2016). Apart from T3 and T4 concentrations, the HPT axis is also modulated with many other local, neural, and humoral factors as needed to ensure proper hormone signaling (Ortiga-Carvalho et al., 2016).

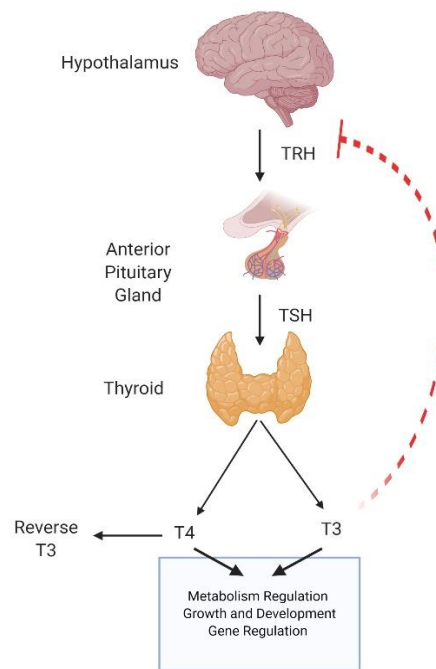


Figure 1. Thyroid hormone synthesis via the Hypothalamus-Pituitary-Thyroid (HPT) axis. The red dotted line represents T3 negative feedback inhibition of TRH and subsequent HPT axis inhibition. (Adapted from Ortiga-Carvalho et al., 2016.) Created with BioRender.

C. Thyroid Hormone Receptor α

All TRs are thought to have originated from one, highly conserved gene found in non-vertebrates that has been duplicated and adapted in vertebrates. Overall, vertebrate TRs are encoded by the two, generalized genes—*NR1A1* and *NR1A2*—with TR α subtypes encoded by *NR1A1* and TR β subtypes encoded by *NR1A2*. Alternative splicing of *NR1A1* and *NR1A2* allows for several different TR isoforms, with predominant isoforms including TR α 1, TR β 1, TR β 2, TR β 3, and TR β 4 (reviewed in Anyetui-Anum et al., 2018).

Human TR α 1 is encoded by the *Homo sapiens*-specific gene *THRA*, located on chromosome 17 (NCBI). p46, TR α 1's full length isoform, is the primary isoform involved

in transcription activation; however, alternative splicing and promotor usage, in combination with multiple initiation codons in *THRA*, can generate four additional isoforms of the protein with diverse, non-transcriptional functions (NCBI, reviewed in Anyetei-Anum et al., 2018). They are named based on molecular mass, and all save one are truncated versions of the protein. The full-length version of TR α 1, p46 is localized primarily to the nucleus, but undergoes nucleocytoplasmic shuttling. Its role is to act as a nuclear transcription factor, repressing or activating gene transcription in response to T3.

All cases of RTH α have been documented in the full-length isoform, p46 TR α 1; therefore, it will be the focus of the remainder of this thesis. As mentioned previously, TR α 1 is a transcription factor, acting as a repressor in apo-form and as an activator in holo-form, with some exceptions where genes are repressed by holo-TR α 1. TR α 1 was shown in vitro to inhibit transcription by blocking the formation of the functional preinitiation complex (Laudet and Gronemeyer, 2002); however, its repressive function is aided by corepressors, specifically nuclear corepressors 1 (NCoR1) and 2 (NCoR2, also known as SMRT [Silencing-Mediator for Retinoid/Thyroid hormone receptors]). It is most highly expressed in bone, gastrointestinal and cardiac tissues, skeletal muscle, and the central nervous system (CNS) (reviewed in Anyetei-Anum et al., 2018).

TR α 1 consists of four domains, as depicted in Figure 2: the A/B domain by the N-terminus, followed by the DNA-binding domain (DBD), the hinge domain, and finally, the ligand-binding domain (LBD) at the C-terminus (reviewed in Anyetei-Anum et al., 2018).

The A/B domain serves as the transactivation domain, containing AF1—a ligand-independent transactivation motif—and may aid the receptor in promotor-binding

specificity (Fernandez et al., 2017). The A/B domain is the least conserved of all four regions. It harbors one of two autonomous transcriptional activation function motifs, AF-1. When linked to the DBD, AF-1 activates transcription, and is not ligand dependent (Laudet & Gronemeyer, 2002).

The DBD helps localize the receptor to specific half-sites of the target DNA sequence which are responsive to TH, known as thyroid hormone response elements (TREs) (Yen, 2001; Zhang and Lazar, 2000). As the name suggests, the hinge domain provides the receptor with flexibility for changing its conformation and stabilizes the protein when bound to DNA. This domain also houses a nuclear localization signal (NLS-1) (Mavinakere et al., 2012; Aranda et al., 2013). Finally, the LBD is responsible for binding of T3 and other TR α 1 regulators, such as corepressors and coactivators (Makowski et al., 2003). TR α 1's LBD is comprised of twelve, stacked α -helices, with different helices likely serving different functions. The exact function of each helix is not fully understood; however, hypotheses have been put forward for the function of some of the helices. For example, helices 1 and 11 aid in nuclear corepressor binding, and are supported by helices 3 and 5, which contact both corepressor and coactivator binding sites (Makowski et al., 2003; Marimuthu et al., 2002).

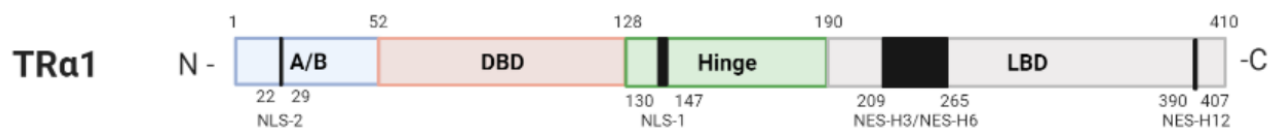


Figure 2. TR α 1 localization signals and domains. The domains, nuclear localization signal (NLS), and nuclear export signal (NES) motifs of full length TR α 1 are shown (not to scale) (adapted from Anyetey-Anum et al., 2018). The location of domains and motifs

are noted by amino acid number, reading from N-terminus to the C-terminus, with black boxes highlighting motif location. Created with BioRender.

TR α 1 is regulated in its role not just by hormone presence, but also by protein-protein interactions between its coactivators and corepressors. TR α 1 responds to several coactivators, mainly Mediator Complex 1 (MED-1), the steroid receptor coactivator (SRC) family, and the vitamin D receptor interacting protein/ TR associated protein (DRIP/TRAP) complex. Upon the TR/T3 complex binding to a positive TRE, coactivators are recruited, prompting assemblage of the transcription machinery (Arnold et al., 2007; Fondell et al., 1999; Mendoza et al., 2017; Rachez et al., 1998). Coactivators such as MED-1 and SRC recruit histone acetyl transferases (HATs) to TR's transcriptional site to induce chromatin restructuring, but DRIP/TRAP complexes do not seem to exhibit this activity. Adding acetyl groups to lysines in the N-terminal tails of histones induces chromatin decondensation, allowing easier access of the transcriptional machinery to the DNA (Arnold et al., 2007; Mendoza et al., 2017, Sinha & Yen, 2018; Rachez & Freedman, 2001).

The second protein-protein interaction of note is TR regulation by corepressors such as NCoR1 and NCoR2. However, due to their hypothesized role in RTH and known roles outside of RTH, they will be covered more in depth in a later section.

D. TR α 1 DNA Binding and Dimerization

One aspect of RTH α mutants that is currently under investigation by the Allison lab is their intranuclear mobility, or how fast the proteins are moving inside the nucleus (Evans, 2019; Femia et al., 2019). Should an RTH α mutant's intranuclear mobility be

altered from that of wild type TR α 1, it could provide some insight as to the mutant's molecular role in the RTH α phenotype. A reduced intranuclear mobility suggests that the TR α 1 mutant is unable to properly regulate transcription of target genes in associated tissues, thus contributing to the RTH α phenotype.

The intranuclear mobility of a transcription factor like TR is dependent on protein size, assuming Brownian diffusion through the nucleoplasm, protein-protein interactions, and finally, DNA binding ability (Boulon et al., 2002; Grünwald et al., 2006; Kues et al., 2001). Protein-protein interactions have already been introduced and will be covered in more depth later in this chapter. Here, TR's DNA binding mechanics, located in its aforementioned DBD, will be examined.

A highly conserved region, the DBD selects the appropriate response element on the DNA. It houses two zinc finger motifs used to recognize and bind to the DNA with high specificity. The N-terminal finger motif is as follows: Cys–X2–Cys–X13–Cys–X2–Cys; the C-terminal finger motif is Cys–X5–Cys–X9–Cys–X2–Cys. The four Cys residues on each finger chelate one Zn²⁺ ion. The C-terminal of the first finger binds to the major groove of DNA (also known as the P-Box) (Laudet & Gronemeyer, 2002). TR α 1's DBD specifically recognizes TREs on the DNA. TREs contain a consensus hexanucleotide sequence with AGGTCA, known as the half-site. This half-site is either used by itself or as a palindrome (AGGTCA-TGACCT). The palindrome contains half-sites with 3-6 nucleotide spacers between the two inverted sequences (IR3 and IR6, respectively). TREs can also have direct repeats, with varying number of nucleotides in between each repeat adding another layer of specificity. TR specifically prefers DR4 (four nucleotides

between each half-site), but evidence of a DR5 (five nucleotides between each half-site) has been documented (Laudet & Gronemeyer, 2002; Yen, 2001).

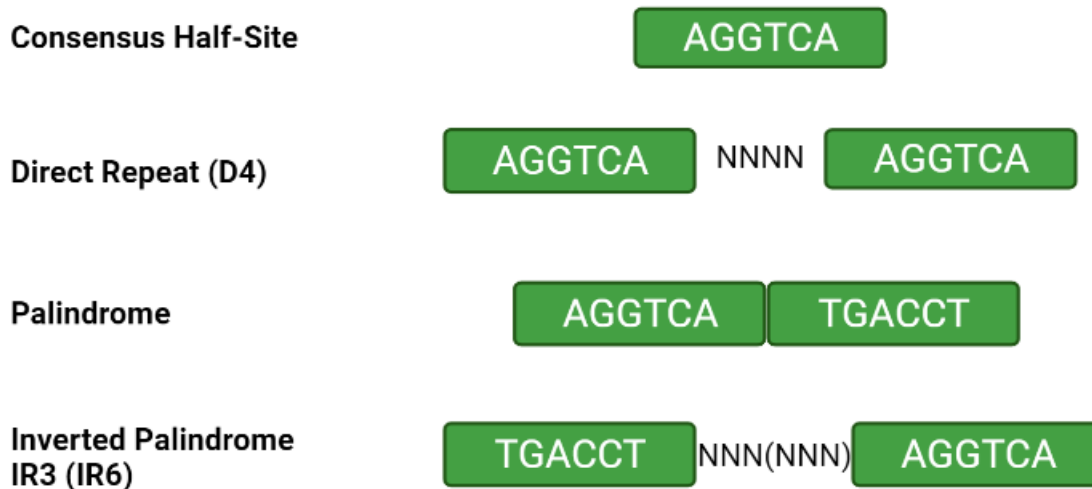


Figure 3: Orientation of TRE consensus half sites, direct repeats, palindrome, and inverted palindrome. Base consensus half-site containing the standard hexanucleotide sequence AGGTCA, and associated reorientations seen in TREs. N represents nucleotides. (Adapted from Yen, 2001.) Created with BioRender.

TR α 1 can interact with TREs independent of TH (reviewed in Passero, 2018). Of note, TREs can either be positive or negative. A positive TRE response to TH would result in repression with the apo-receptor and activation with the holo-receptor, and a negative response would cause general repression when TH is present (Laudet & Gronemeyer, 2002). TR α 1 classically interacts with positive TREs, and, although negative TREs have been identified, they have not been well characterized yet.

TR α 1 is able to bind DNA as a monomer, homodimer, or heterodimer. Monomers and homodimers tend to have weaker bonding than heterodimers, and therefore will have

rapid TRE dissociation. Monomers preferentially bind to TRE hexanucleotide sequences, preceded by the nucleotides T and A as a TA AGGTCA motif. However, they are susceptible to destabilization when half sites and flanking sequences are changed (reviewed in Passero, 2018). Heterodimers are preferred due to their stronger binding. More specifically, heterodimerization of TR with retinoid X receptor (RXR; another nuclear receptor) is especially preferred, whereupon TR α 1's first zinc finger interacts with RXR's second zinc finger. This interaction is strengthened by helix 10 in TR α 1's ligand binding domain. When in this heterodimer, DR4 binding elements are markedly preferred, using the spacing sequence ATCA. TR contacts the 3' elements of the DR4, while RXR contacts the 5' elements. Heterodimers are more tolerant of changes to consensus sequences and flanking nucleotides. Of note, TR α 1 is also able to heterodimerize with retinoic acid receptors (RARs) and vitamin D receptors (VDRs), two other nuclear receptors. When TR is heterodimerized with RAR, the N-terminal of the second zinc finger as well as helix 10 in the LBD both aid in stabilizing the heterodimerization (Laudet & Gronemeyer, 2002).

DNA-binding of TR induces bending of DNA, situating for either easy or lessened DNA access depending on transcription activation or repression, respectively. A TR-TR homodimer and TR-RXR heterodimer will induce a *ca.* 10-degree bend in DR4 but will bend the DNA in opposite directions (Laudet & Gronemeyer, 2002).

E. TR α 1 Ligand Binding

The final and most C-terminal domain of TR α 1 is the LBD. The LBD allows for binding of TH to TR α 1, and as such is the key player in RTH α . As previously mentioned, all

known RTH α mutations are in the LBD, and therefore explain the phenotypical “resistance” to thyroid hormone. All mutations appear to compromise the LBD’s ability to bind to TH, to where TH either binds poorly or cannot bind at all (Moran et al., 2013; *RTH α* — *Institut de Génomique Fonctionnelle de Lyon*, n.d.; Schoenmakers et al., 2013). This thesis focused on three RTH α mutations that result in truncation of the LBD. The LBD contains 12 stacked alpha helices with three beta sheets, one beta turn, and some unstructured sequences, as shown below in Figure 4 (Protein Data Bank).



Figure 4. Protein structure of TR α 1’s ligand binding domain bound to T3. Structure of human TR α 1’s LBD obtained by Nascimento et al. (2006) and shown on the Protein Data Bank. The structure shows twelve stacked alpha helices forming a pocket, in which sits T3. Structure obtained via small X-ray scattering (Nascimento et al., 2006).

The alpha helices are named helices 1 to 12 (H1 to H12), going from the N to C-terminus of the LBD. As mentioned previously, Helix 10 is a major component in TR heterodimer stabilization. To allow for TH binding, the alpha helices stack to form three layers like a sandwich, which allows for the formation of a hydrophobic pocket/cavity for the ligand. More specifically, TR α 1 is proposed to follow a “mousetrap model:” H11 is

repositioned in continuity with H10; H12, which had been exposed prior to TH binding, swings around, flipping over H6 and the N-terminal of H3. H12 then seals the ligand-binding cavity as a lid, protecting hydrophobic TH from the surrounding aqueous environment. When H12 closes as the lid, it exposes a hydrophobic cleft that accommodates coactivator binding, with the motif LXXLL (Laudet & Gronemeyer, 2002, Makowski et al., 2003; Zhang and Lazar, 2000). Both THs, T3 and T4, serve as ligands for TR α 1, but T3 has a seven-fold higher binding affinity than T4 (Wejaphikul et al., 2019). The LBD houses AF-2, the ligand dependent activation function. This motif stabilizes ligand binding and associated TR α 1 activation. There are two known TH binding sites in the LBD. The first is the aforementioned pocket/cavity, where TH will interact with the hydroxyl group on histidine (H) 381, the carboxyl group on R228, and hydrophobic interactions involving a total of 15 residues (Protein Data Bank, Souza et al., 2014). Additional polar interactions have been documented between Q342 and R375, as well as nonpolar interactions with S326, V371, T372, L346, and L368. The secondary binding site is noted to be between helices H9, H10, and H11 (Souza et al., 2014).

F. Nucleocytoplasmic shuttling

TR α 1 regulation of gene expression is aided not just by T3 but also by the receptor's localization and mobility within a cell. TR is unlike some NRs in that it does not require ligand binding to enter the nucleus. The receptor was long-thought to be located solely in the nucleus; however, prior studies in the Allison Lab have demonstrated that TR α 1 undergoes nucleocytoplasmic shuttling, the mechanics of which are detailed in Figure 5

(reviewed in Anyetei-Anum et al., 2018). TR α 1 primarily resides in the nucleus but can be transported out of the nucleus by a class of proteins called exportins. The specific exportins include exportin 1, also known as the calreticulin (CRT)/CMT1 complex, and exportins 4, 5, and 7 (Maruvada et al., 2003; Grespin et al., 2008; Subramanian et al., 2015). Exportins are able to bind to TR α 1 due to at least three different nuclear export signals (NESs), all located in the LBD on helices 3, 6, and 12, as shown in Figure 2 (Mavinakere et al., 2012).

After an exportin shuttles TR α 1 into the cytoplasm, the receptor is free to reenter the nucleus. In this case, a second class of proteins called importins—specifically importins α 1, β 1, and 7—recognize and bind to TR α 1's two nuclear localization signals (NLSs) located in the A/B and hinge domains (Figure 2) (Mavinakere et al., 2012; Zhang et al., 2018). Upon NLS binding, importins escort TR α 1 back into the nucleus, where it can bind to DNA and repress or enhance transcription of the designated target gene (Zhang et al., 2018). Dysregulation of this process, as well as significant changes to the ratio of nuclear to cytoplasmic TR α 1, both contribute to changes in TR α 1-associated gene expression.

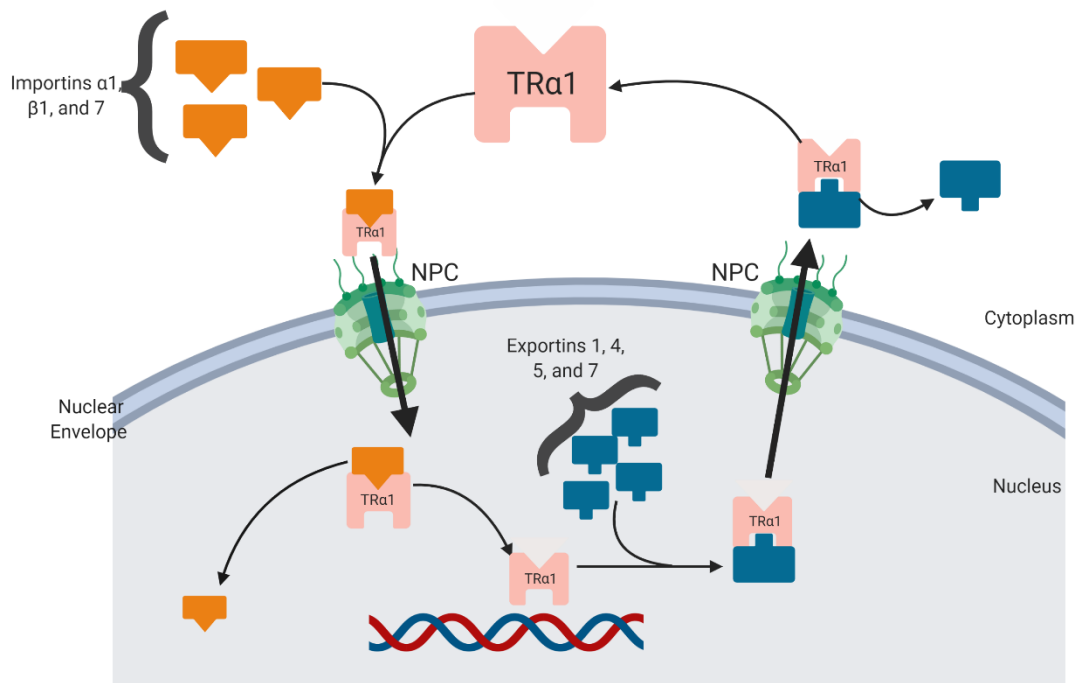


Figure 5. Nucleocytoplasmic transport of TRα1. For TRα1 to modulate gene transcription, it must first be in the nucleus. Once bound to an importin (orange) in the cytoplasm, the importin-TRα1 complex passes into the nucleus through the nuclear pore complex (NPC). Once in the nucleus, the importin dissociates and the TRα1 binds to the DNA at a thyroid hormone response element (TRE). TRα1 can also exit the nucleus with the aid of exportins (blue). The exportin-TRα1 complex exits the nucleus through an NPC. Upon exiting the nucleus, the exportin dissociates from TRα1 and the cycle can begin again (adapted from Evans, 2019). Created with BioRender.

G. Nuclear Receptor Corepressor 1

Nuclear corepressor 1, also known as NCoR1, is the primary corepressor interacting with TRα1. It was discovered along with the nuclear corepressor, SMRT, in 1995, while researchers were attempting to understand NR repression (Mottas et al., 2013). NCoR1

was first found bound to a TR-RAR heterodimer; however, it has since been found to bind to other NRs and certain non-NR transcription factors (Mottas et al., 2013). As a nuclear corepressor, NCoR1 serves as a bridge to chromatin modifying enzymes and transcription factors. Of note, it is now known that SMRT plays little role in thyroid hormone signaling (Mendoza et al., 2017). As such, the focus of this thesis will be on NCoR1 and its potential role in RTH.

NCoR1 has been implicated in tumor suppression, neural cell differentiation, metabolic homeostasis, oxidative phosphorylation, and in adults, adipocyte and myocyte differentiation. It is also important in circadian rhythm management and decreasing inflammatory responses of macrophages (Martinez-Iglesias, Alonso-Merino, & Aranda, 2016). NCoR1 has also been shown to play a minor role in mediating gene expression in congenital hypothyroidism in mice (Mendoza et al., 2017). However, upon publication of the first three RTH α mutants, it has been hypothesized to potentially play a role in RTH α pathogenesis.

To understand the hypothesized role of NCoR1 in RTH α , one must understand its function. The NCoR1 cDNA is a 7,320-base pair-long sequence that encodes the corepressor involved in TR-mediated gene silencing. The corepressor binds to the apo-form of TR α 1 in the absence of TH (Laudet & Gronemeyer, 2002), and in doing so mediates ligand sensitivity (Mendoza et al., 2017). It interacts with TR through its three receptor interacting domains (RIDs) (Webb et al., 2000). Specifically, it uses an isoleucine motif (I/LxxII) in the RIDs to recognize and bind to lysine residues in helix 3 and glutamine residues in helix 12 of TR α 1's LBD (Webb et al., 2000).

Prior research performed by Hager et al. (2000) demonstrated that NCoR1 binding regulates TR activity both directly (inducing a conformational change) and indirectly.

Past studies performed by the Allison lab have shown that NCoR1 knockdown increases TR α 1 nuclear export, while NCoR1 overexpression increases TR α 1 nuclear localization (Sun, 2019).

NCoR1 induces TR repression not just in its interaction with TR, but also by recruiting histone deacetylase 3 (HDAC3). Without HDAC3, acetylation of lysine residues in histone tails activates transcription, promoting opening of chromatin and allowing TRs to bind. HDACs reverse this by deacetylating the lysine, causing the chromatin to close and limiting transcription factor access to chromatin (You et al., 2013). HDAC3 interacts with NCoR1 via a conserved repression domain called SANT (so-named due to its presence in Swi3, Ada2, NCoR1, and TFIIB). SANT, NCoR1's Y478 residue, and a unique N-terminal helical extension are required to activate HDAC3, since it is inactive until bound to NCoR1. The N-terminus extension contains three strong repressor domains with HDAC3 binding sites (Martinez-Iglesias, Alonso-Merino, & Aranda, 2016; Mottis et al., 2013). If interacting with TR α 1, NCoR1 must recruit HDAC3 to be able to repress TR; however, it can recruit other HDACs with HDAC3 attached in a context-dependent manner. Upon HDAC3 binding, other repressor proteins are recruited, including G-protein pathway suppressor and TBL1/TBL1R1, to create the final core-repression complex (Mottis et al., 2013).

It is hypothesized that NCoR1 remains bound to TR α 1, allowing the complex to associate with the target TRE and block transcription. However, when T3 binds to

TR α 1, a conformational change in helix 12 of TR α 1's LBD likely causes NCoR1 to dissociate, providing room for coactivators to bind to the TR and initiate transcription as illustrated in Figure 6.

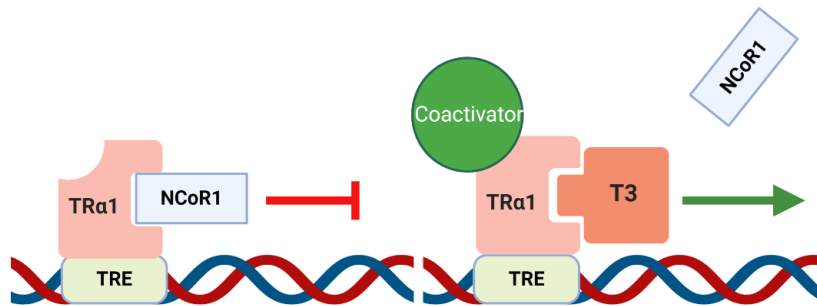


Figure 6. TR α 1 action in the presence and absence of NCoR1 when bound to a thyroid response element (TRE). Binding to NCoR1 induces a conformational change in TR α 1, inhibiting gene transcription. T3 binding induces another conformational change, releasing NCoR1 from TR α 1, and allowing coactivator binding and heightened gene transcription (adapted from Evans, 2019). Created with BioRender.

H. Resistance to Thyroid Hormone α

For the past 30 years, it was commonly accepted that RTH was solely due to mutations in the gene *THRB*, yet within the past decade, researchers have been able to demonstrate dominant negative mutations in *THRA* as well, leading to RTH α . This version of RTH is considerably harder to diagnose compared to its RTH β counterpart, as patients will generally physically present as hypothyroid despite having clinically euthyroid hormone levels, and symptoms are less severe (Espiard et al., 2015). Symptoms include short stature, bradycardia, neurodevelopmental delays, dysmorphic syndrome, constipation, anemia, and skeletal dysplasia (Moran & Chatterjee, 2015; van Gucht et al., 2017; Vlaeminck-Guillem et al., 2015). RTH α patients tend to have

clinically elevated to normal levels of free T3, low to normal free T4, and normal thyroid stimulating hormone (TSH) levels (Rurale et al., 2020).

Thus far, twenty-five RTH α mutations have been characterized, all occurring in TR α 1's LBD (Fozzatti et al, 2013; "RTH α —Institut de Génomique Fonctionnelle de Lyon," 2021). All mutations characterized so far exert a dominant negative effect, meaning that when the cell has one wild type allele, the mutated allele's phenotype will dominate over the wild type and negatively impact TR α 1's function. Of note, these mutations have been heterozygous in patients, noting that mice homozygous for the murine equivalent of the mutation F397fs406X died shortly after birth (Fozzatti et al., 2013; Tyłki-Szymańska et al., 2015; van Mullem et al., 2012; Yen, 2003). The role of each mutation in TR α 1's functionality depends on the location of the mutation, and what impact it has on protein structure. For example, some of the mutations cause a shortened LBD, which alters the receptor's binding affinity to coregulators and T3. As hinted at when mutations to the LBD were introduced, reduced T3 binding renders the cell less responsive to thyroid hormone signaling, leading to hypothyroid symptoms. Should the mutation occur in helix 12, T3, coactivator and corepressor binding affinities can be altered (Fozzatti et al, 2013). Furthermore, it is hypothesized that certain helix 12 mutations allow for increased NCoR1 recruitment to RTH TR α 1, the locations of which are detailed in Figure 7 and are the focus of this thesis (Bochukova et al., 2012; Moran et al., 2013; van Mullem et al., 2012; van Mullem et al., 2013; Zavacki & Larsen, 2013). Going from N to C terminus, the three mutants of interest are as follows. The first mutant, Ala382ProfsX7, is a single-nucleotide deletion that changes the alanine at amino acid 382 to a proline, and also shifts the reading frame, causing a premature stop at position

389. In the second mutant, F397fs406X, a single nucleotide insertion causes a frameshift at phenylalanine 397, causing a premature stop codon at position 406. The final mutant, E403X, is a single nucleotide substitution (c.1207G>T) that changes glutamate 403 to a stop codon. All of these RTH α mutants affect H12 in TR α 1, with the latter two resulting in a truncated H12 and the former with a completely missing H12.



Figure 7. The locations of RTH α mutants with increased NCoR1 binding affinity. These mutations were investigated in this thesis (adapted from Moran & Chatterjee, 2016). Created with BioRender.

NCoR1's increased affinity for certain mutant TR α 1, such as the three of interest to this thesis, could potentially cause two different scenarios: either NCoR1 dissociates from the mutant isoforms slowly, or not at all, thereby decreasing nuclear TR export. In either scenario, TR α 1's intranuclear mobility is predicted to decrease when bound to NCoR1, thereby increasing nuclear retention (Astapova, 2016; Fozzatti et al., 2011; Fozzatti et al., 2013). Preliminary fluorescence recovery after photobleaching (FRAP) assays were performed by a former Master's student in the Allison Lab, Rochelle Evans, to evaluate for any potential effect of NCoR1. Specifically, she bleached a line through the middle of the nucleus to establish the fluorescent mutated isoform's recovery time when coexpressed with NCoR1. Her preliminary findings suggested that Ala382ProfsX7 has a

similar recovery half-time in the presence of either empty GFP or GFP-NCoR1. In contrast, its mobile fractions were quite different at 98% and 77% respectively (Evans, 2019). However, this assay contained a limited number of data points, therefore more were required to fully confirm and determine the significance of these results. As such, we investigated further into NCoR1's impact on the intranuclear mobility of RTH α TR α 1 mutants.

Specific Aims

Changes to TR localization and intranuclear mobility have been implicated in multiple diseases, including but not limited to some forms of cancer and Resistance to Thyroid Hormone Syndrome (RTH), in which the body is resistant to thyroid hormone signaling. Recent studies have shown that NCoR1, a TR α 1 corepressor, has a higher affinity to frameshift mutations and H12 deletions in RTH TR α 1 compared to the wild type (Fozzatti et al., 2013; Fozzatti, Lu, Kim, and Cheng, 2011). Prior studies in the Allison lab have shown no significant difference in intranuclear mobility between three RTH TR α 1 mutants (E403X, Ala382ProfsX7, and F397fs406X—all located in helix 12) and wild type TR α 1 (Evans, 2019) in the presence of endogenous NCoR1. However, preliminary studies performed by Evans (2019) suggested that overexpressed GFP-tagged NCoR1 has a much slower intranuclear mobility compared to overexpressed TR α 1. This raises the question: does NCoR1's increased affinity for RTH mutant isoforms lead to their decreased intranuclear mobility, at least in part, when NCoR1 is overexpressed? Also of note, the truncation or complete loss of H12 in these mutants results in the loss of TR α 1's nuclear export motif located in H12 (NES-H12). As noted earlier, wild type TR α 1 is primarily localized to the nucleus at baseline, despite the presence of multiple NES's, one in the aforementioned H12, two spanning helices 3 and 6 (NES-H3 and NES-H6, Salomon et al., 2020), and an unidentified CRM1-dependent NES. Taken together, these observations also raise the question of whether the loss of H12 impacts the mutants' nucleocytoplasmic shuttling?

This thesis aimed to determine the following:

1. If there is an effect of GFP-NCoR1 overexpression on the intranuclear mobility of three RTH mutants of mCherry-TR α 1, A382PfsX7, F397fs406X, and E403X.
2. If the loss of NES-H12 affects the nucleocytoplasmic shuttling of mCherry-RTH α mutant isoforms compared to wild type TR α 1.

Chapter 2: Experimental Methods

A. Plasmid Preparation

Coding regions for human wild-type TR α 1, A382PfsX7 TR α 1, F397fs406X TR α 1, and E403X TR α 1 were acquired from Invitrogen GeneArt Gene Synthesis (Thermo Fisher Scientific, MA) and subcloned into pmCherry-C1 (Clontech) by Vinny Roggero. mGFP-NCOR1 was acquired from GenScript. The coding region for NCoR Δ ID was synthesized and subcloned into pEGFP-C1 (Clontech) by GenScript. All plasmids were amplified in competent *Escherichia coli*. Once obtained, all plasmids were purified using ZymoPURE™ Plasmid Midiprep (Zymo Research Corporation, Irvine, CA). Quantity and purity of plasmid DNA were assessed with a NanoDrop ND-1000 spectrophotometer, with an A₂₆₀/A₂₈₀ ratio between 1.8 and 1.9, and an A₂₆₀/A₂₃₀ ratio between 2.0 and 2.2, both indicating successful plasmid purification.

B. Cell Culture

HeLa cells were cultured in Minimal Essential Media (MEM) with 10% fetal bovine serum (FBS). Mouse (NIH/3T3) cells were cultured in Dulbecco's Modified Eagle Medium (DMEM) in 10% calf serum (CS). They were incubated at 5% CO₂, 37°C, and 98% humidity in a Thermo Scientific 3578 Napco Series 8000 WJ CO₂ Water-Jacketed Incubator (Thermo Fisher Scientific, Waltham, MA) to simulate a physiological environment. HeLa cells were cultured to 70-90% confluency for transfection.

C. Transfection

For both NCoR1 and heterokaryon analysis, cultured HeLa cells were displaced with 0.25% trypsin and seeded in 6-well plates with sterile glass coverslips at a concentration of 2.0 x 10⁵ to 2.5 x 10⁵ cells per milliliter and left to grow for 24 hours.

They then were transfected with either 4 μ g of GFP-NCoR1, 2 μ g of mCherry -tagged wild type or mutant TR α 1 plasmids or, when cotransfected with mCherry-TR α 1 isoforms, 4 μ g of GFP-NCoR1 and 2 μ g mCherry-mutant or wild type TR α 1.

Transfections were performed using Lipofectamine 3000 (Life Technologies), following instructions provided by the manufacturer. Cells were incubated at 5% CO₂, 37°C, and 98% humidity following transfection. Medium for GFP-NCoR1 single-transfected cells was changed 19-20 hours post transfection according to the protocol outlined by Rochelle Evans (Evans, 2019). Medium for cells transfected with NCoR Δ ID alone, mutant or wild-type TR alone or with NCoR1 or NCoR Δ ID was changed 5-8 hours post transfection to promote cell vitality and protein expression. Cells solely transfected with GFP-NCoR1 and heterokaryons were washed with Dulbecco's phosphate buffer saline (DPBS) and fixed in 3.7% formaldehyde in DPBS prior to analysis using a Keyence BZ-X800 Fluorescence Microscope (Keyence Corporation, Itasca, IL). Cells set for live imaging (FRAP and live heterokaryon imaging) were given MEM media without phenol red prior to imaging, 23-27 hours post transfection.

D. NCoR1 and NCoR Δ ID Intracellular Localization

Baseline NCoR1 and NCoR Δ ID intracellular localizations were determined using HeLa cells transfected with GFP-NCoR1 or GFP-NCoR Δ ID alone. Prior to analysis, cells were washed with DPBS and fixed in 3.7% formaldehyde in DPBS. The nucleus was stained with DAPI to provide a frame of reference for intracellular localization. Fluorescent protein localization was then analyzed using the Keyence.

E. Fluorescence Recovery After Photobleaching (FRAP)

Cells were analyzed 23-27 hours post transfection. Prior work performed by Femia (2018) demonstrated proper cell viability during this time frame. Prior to confocal analysis, living, single- or cotransfected HeLa cells were washed with DPBS and given fresh 10% FBS-MEM. Cells were analyzed using a Nikon A1Rsi confocal microscope Ti-E-PFS (Nikon Inc., Melville, NY), and a 60x oil objective lens. Cells were kept in a stage incubator at 5% CO₂, 98% humidity and 37°C during imaging time. The following laser lines were employed: 488nm laser line of krypton-argon for GFP, 561nm for mCherry, and 405nm at solid state for photobleaching (Femia et al., 2019). Intranuclear mobility was measured using the technique selective fluorescence recovery after photobleaching (FRAP), also known as Strip-FRAP, as described by Koster et al. (2005). Koster et al. had shown success in applying the technique to nucleocytoplasmic shuttling analysis, which was extended by Evans (2019), Anyetei-Anum et al. (2019), and Femia et al. (2019) in the Allison lab to evaluate mutant RTH α and NCoR1 intranuclear dynamics. This protocol allows for selective photobleaching of a fluorescent region—in this case, the nucleus. A single line in the fluorescent region of interest (ROI) in the nucleus was photobleached for one second at 100% laser power, leaving the rest of the nucleus with active GFP or mCherry. FRAP was quantified following the protocol outlined by Houstmuller et al. (2005) and employed by Femia et al. (2019) and Evans (2019). Specifically, fluorescence intensity in the ROI was tracked and plotted from pre- to post-bleach as the ROI recovers to as close to 100% intensity as possible. The resulting plot was normalized following the protocol outlined in Femia et al. (2019). Specifically, fluorescence intensity was normalized to a scale of 0-1, with 0 representing

the lowest intensity, and 1 representing highest intensity, using the following formula from Femia et al. (2019), written as a function of time (t):

$$I(t)_{full} = \frac{I(t)_{double\ norm} - I(t_{postbleach})_{double\ norm}}{1 - I(t_{postbleach})_{double\ norm}}$$

Where I_{full} represents full fluorescence normalization, $I_{double\ norm}$ represents background-corrected, double fluorescence normalization, and $I(t_{postbleach})_{double\ norm}$ represents background-corrected intensity at the time point immediately after photobleaching.

Once normalized, we were able to use the data to calculate the recovery rate, mobile and immobile fractions of the protein again using formulas from Femia et al. (2019). The mobile fraction were calculated with the following formula:

$$F_m = \frac{I(t_{eq}) - I(t_{postbleach})}{I(t_{pre}) - I(t_{postbleach})}$$

Where F_m is the mobile fraction, $I(t_{eq})$ is the normalized intensity when recovery equilibrium is reached, $I(t_{postbleach})$ is the normalized intensity immediately after photobleaching, and $I(t_{pre})$ is the normalized intensity prior to photobleaching. The immobile fraction is the remainder of fluorescent-tagged proteins, represented by the following formula (Femia et al., 2019):

$$F_i = 1 - F_m$$

Where F_i is the immobile fraction and F_m is the mobile fraction.

F. Heterokaryon Assays

Mouse cells were trypsinized and resuspended in Heterokaryon Growth Medium (10% FBS, 20% sterile ddH₂O, 70% DMEM). HeLa cells transfected with either mutant or wild

type TR α 1 and with NCoR1 were resuspended in Heterokaryon Growth Medium 16 hours post-transfection. Mouse cells were then added to each cover slip at a concentration of 1.0×10^6 to 1.4×10^6 cells per milliliter. Cells were then exposed to 50 μ g/mL cycloheximide and incubated at 37°C for 2.5 hours, given fresh medium and 100 μ g/mL cycloheximide, and left to incubate for another 30 minutes. Cells were then rinsed with DPBS, and fused using 50% polyethylene glycol 1500 (PEG, Sigma PT181 HybriMax). Fused cells were incubated for 2 minutes then washed with DPBS and either incubated for 2 hours after fusion at 37°C or analyzed with a Keyence BZ-X800 Fluorescence Microscope. Cells subjected to live cell imaging were stained with Hoechst 33342 stain (Invitrogen) for 20 minutes at a concentration of 100ng/ml, then kept in a stage incubator at 5% CO₂, 98% humidity and 37°C for 2 hours. All cells were fixed for analysis using 3.7% formaldehyde at the end of the incubation period. Cells left to incubate for 2 hours were stained with Hoechst stain for 20 minutes at a concentration of 100ng/ml. All cells were analyzed with the Keyence. Each fixed assay was qualitatively characterized based on whether or not the mCherry-tagged mutant or wild type TR α 1 had entered the mouse nucleus, indicating export from the human nucleus into the shared cytoplasm, followed by import into the mouse nucleus.

G. Statistical Analyses

Data were statistically analyzed for significance with a two-tailed t-test using Microsoft Excel (Microsoft Corporation, Redmond, WA).

Chapter 3: Experimental Results

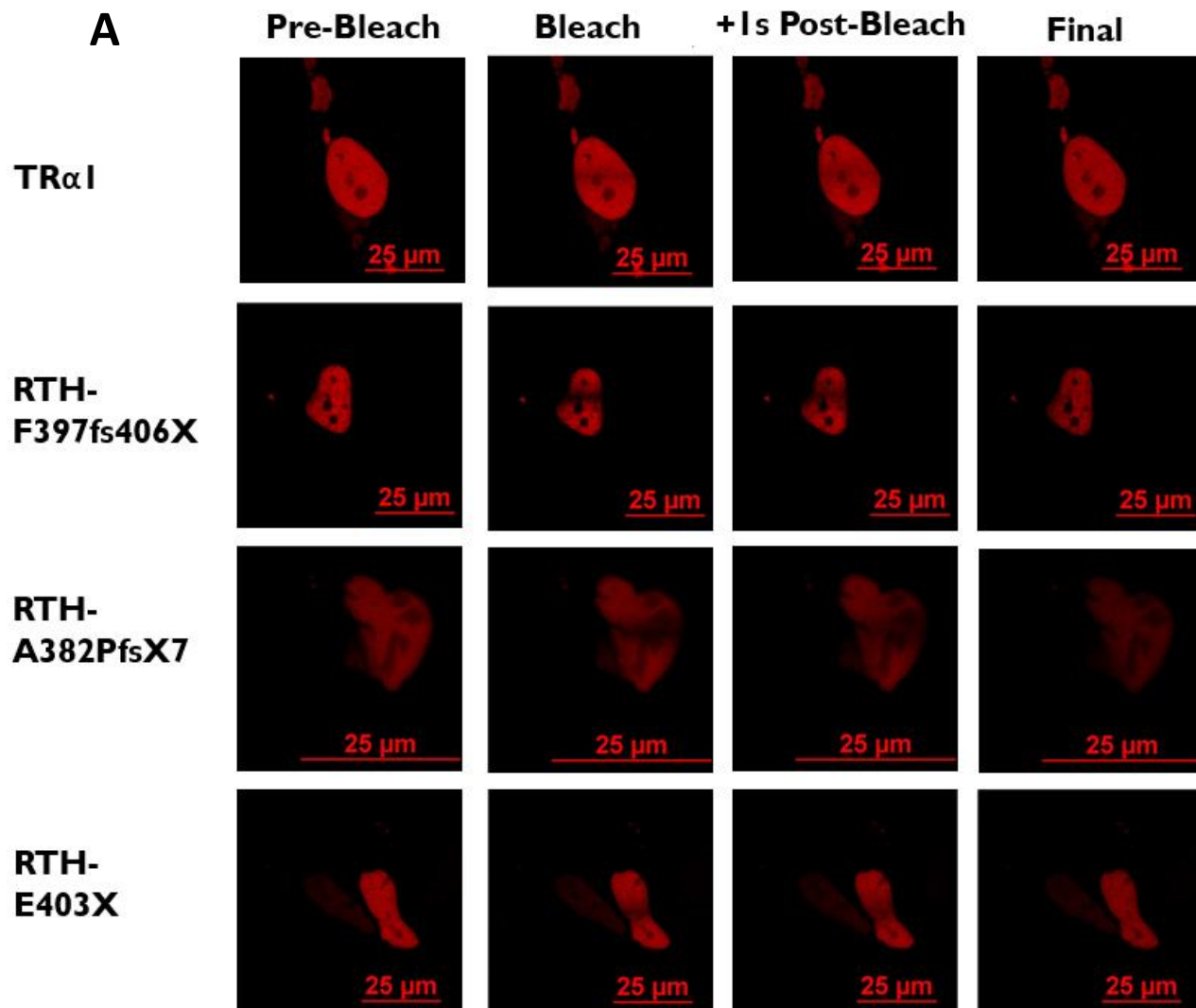
Coexpressing NCoR1 with RTH α mutants does not reduce their intranuclear mobilities, yet NCoR Δ ID decreases RTH-F397fs406X and E403X intranuclear mobility

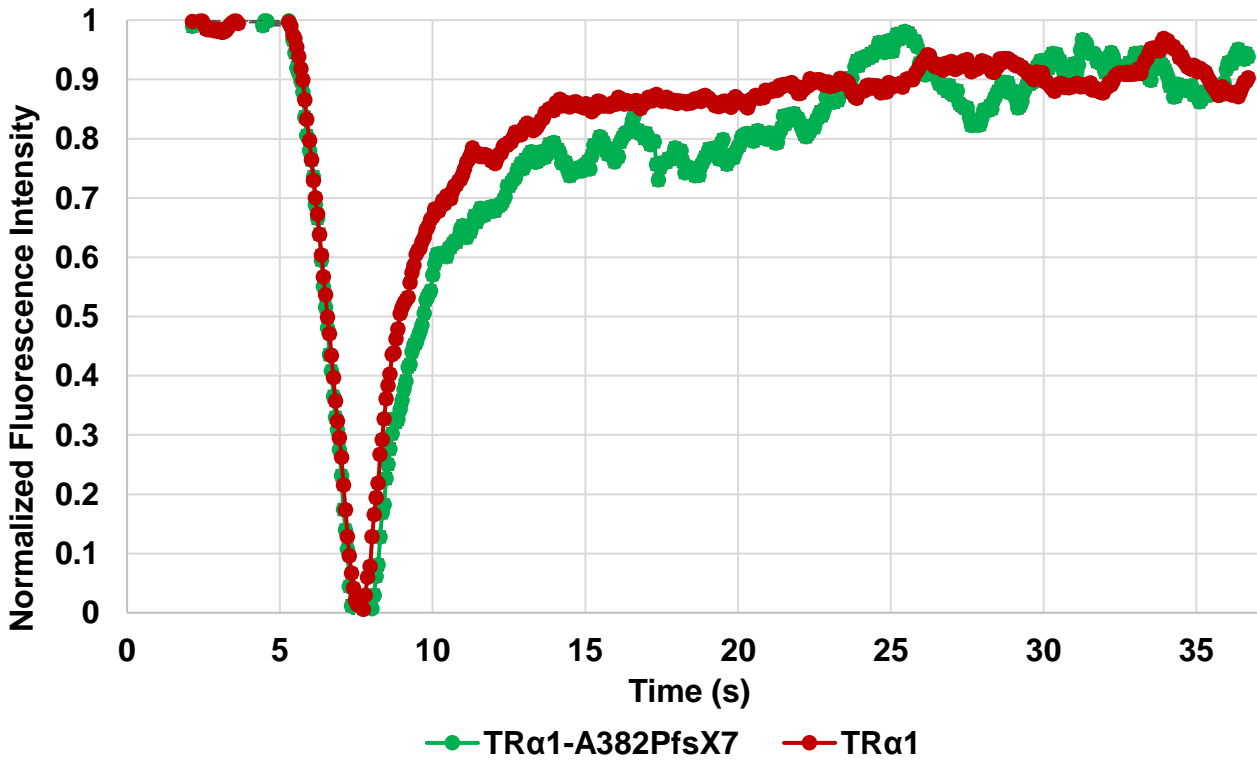
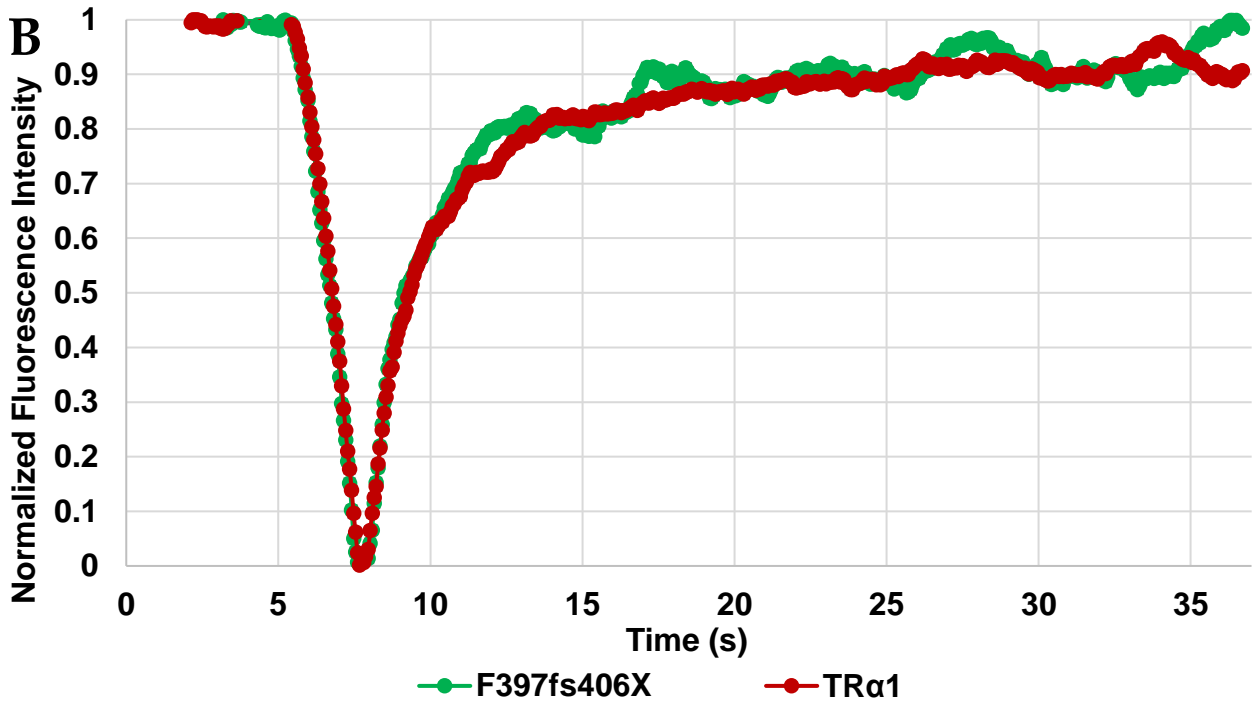
NCoR1 is a very large, 2440 amino acid-long protein, which, assuming Brownian diffusion, would be predicted to have a relatively slow intranuclear mobility. This prediction raised questions as to how this slow rate of diffusion might impact the intranuclear dynamics of RTH α mutants. NCoR1 is recruited to wild-type TR α 1 once the receptor binds to the TRE of a target gene, serving as a bridge between TR α 1 and HDAC3, to allow for limited access to the target gene and repression of gene expression (You et al., 2013; Martinez-Iglesias, Alonso-Merino, & Aranda, 2016; Mottis et al., 2013). NCoR1 does not stay permanently bound to TR α 1, as once T3 binds to TR α 1, NCoR1 will release TR α 1. However, NCoR1 has a higher binding affinity for these RTH α mutants, and it is thought to be due to the missing or truncated helix H12 in these mutants (Bochukova et al., 2012; Moran et al., 2013, van Mullem et al., 2012). It is hypothesized that H12 in TR's LBD is necessary for allowing NCoR1 to dissociate from the receptor upon ligand binding; however, this helix is compromised or missing in the RTH α mutants of interest. If NCoR1 is bound to TR α 1 and cannot dissociate, then it was hypothesized that NCoR1 would remain associated with TR α 1 even if the receptor dissociates from the DNA and therefore would slow down TR α 1 as the two proteins diffused together through the nucleoplasm. Pilot studies showed that the RTH α mutants of interest had similar recovery times compared to wild type TR α 1 in the presence of endogenous levels of NCoR1 (Evans, 2019). However, when A382PfsX7 was cotransfected with GFP-NCoR1, preliminary results demonstrated slow FRAP kinetics of NCoR1, which failed to recover during the standard 35 second time period. In this

preliminary study, the FRAP kinetics of A382PfsX7 were not quantified; however, it was noted that full recovery was achieved by the end of the 35 second time period (Evans, 2019).

To test our hypothesis that NCoR1 would impact the intranuclear mobility of RTH α mutants, we cotransfected either wild-type TR α 1 or an RTH α mutant with either NCoR1 or NCoR Δ ID, a synthetic NCoR1 mutant that does not bind to TR, as NCoR1's RIDs II and III have been deleted. Researchers from other labs have used NCoR Δ ID mouse models to study the physiological effects of the interaction between RTH α and RTH β mutants, TR α 1-PV and TR β 1-PV, respectively. NCoR Δ ID was found to ameliorate the physiological effects of the PV mutants (Astapova et al., 2008; Han, Park & Cheng, 2017). Therefore, because we hypothesized that NCoR1's increased binding affinity would impact mutant TR α 1 intranuclear dynamics, NCoR Δ ID was used as a control for the potentially increased binding affinity of wild type NCoR1.

As shown in Figure 8 and Table 1, first we confirmed Evan's work (Evans, 2019), showing that the RTH α -A382PfsX7, F397fs406X, and E403X did not have significantly different intranuclear mobilities compared to wild type TR α 1 in the presence of endogenous levels of NCoR1.





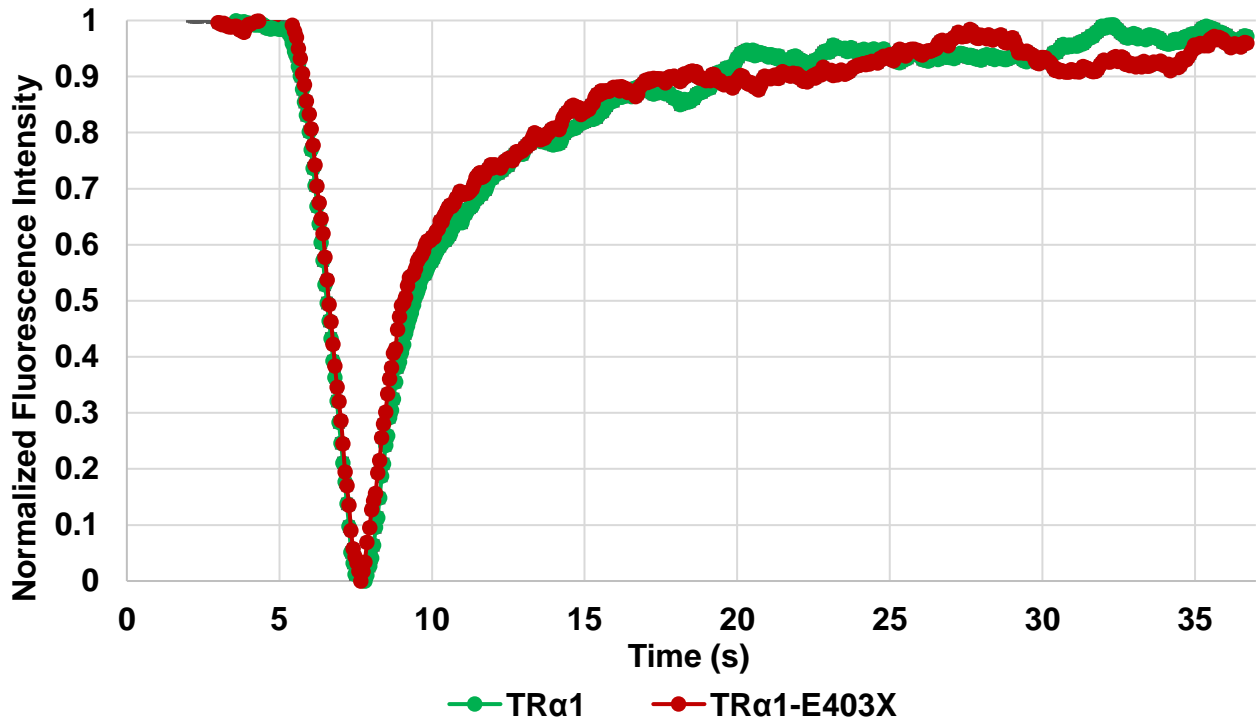


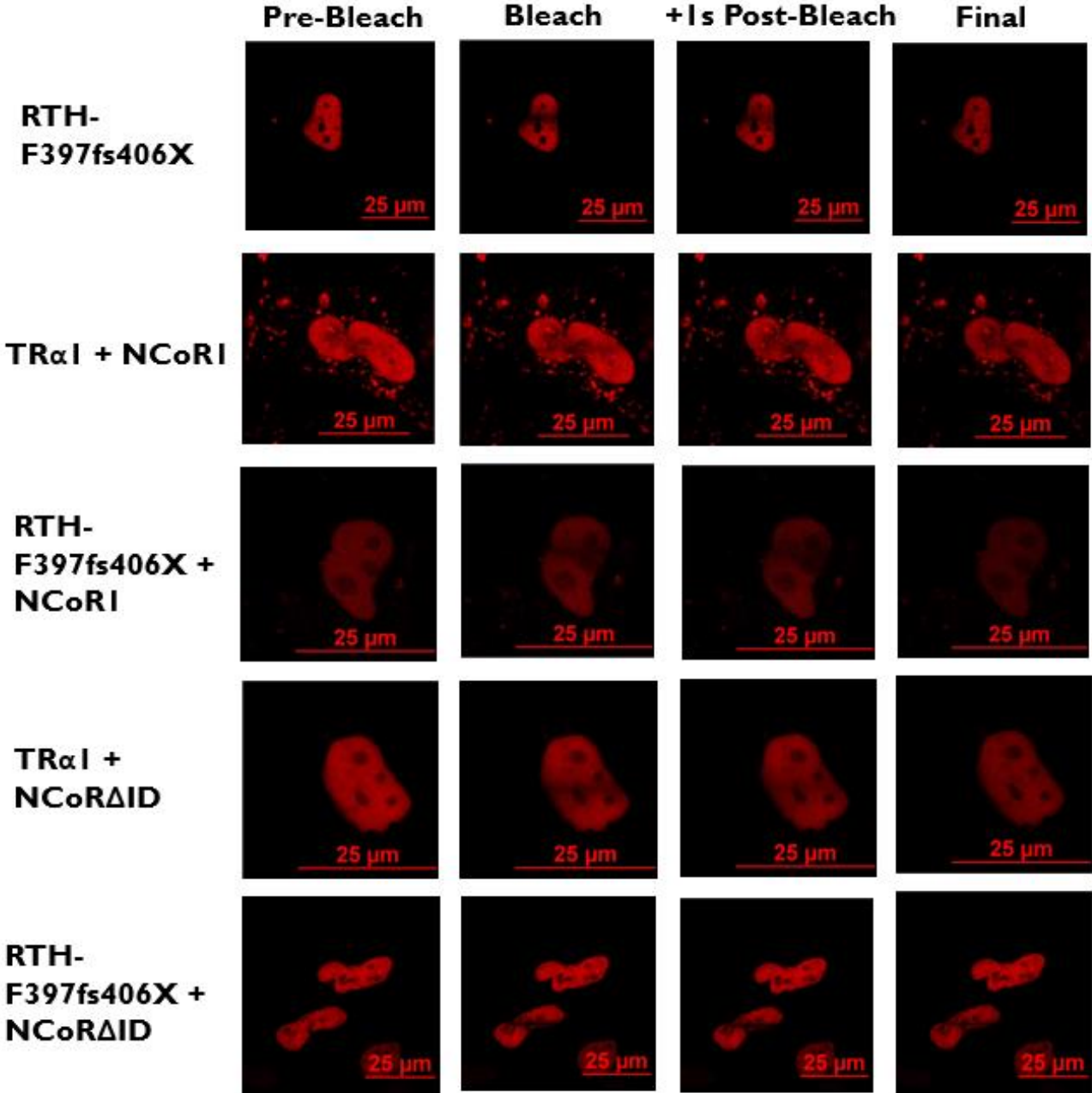
Figure 8. No apparent differences in intranuclear mobility between wild type TR α 1 and the RTH α mutants. FRAP curve and representative images of HeLa nuclei, comparing respective mCherry RTH α mutants to mCherry TR α 1. **(A)** HeLa cells were transfected with expression plasmids for either mCherry F397fs406X, mCherry A382PfsX7, mCherry E403X, or mCherry TR α 1. **(B)** Strip-FRAP was conducted on 5 nuclei for each replicate, with the fluorescence intensities quantified in the graph. A total of three biological replicates were performed for RTH-F397fs406X (N=3, 5 nuclei per replicate). Data were normalized to a scale of 0 to 1, and bars represent \pm SEM, $p > 0.05$. Two biological replicates were performed for RTH-A382PfsX7 and RTH-E403X (N=2, 5 nuclei per replicate). Data were normalized to a scale of 0 to 1 and averaged, and bars represent \pm SEM.

	Mobile Fraction	Immobile Fraction	t-half (s)	t-half Slope
TR α 1-F397fs406X	0.976258587	0.023741413	1.328158766	0.222161401
TR α 1	0.922262162	0.077737838	1.325700606	0.213999054
P-Value	0.244914127	0.244914127	0.989637131	0.800970409
TR α 1-A382PfsX7	1.003798407	- 0.003798407	1.661932266	0.170954241
TR α 1	0.915052399	0.084947601	1.148266833	0.25836812
TR α 1-E403X	0.971369223	0.027024289	1.485045426	0.22775898
TR α 1	0.970790516	0.029209484	1.676764528	0.165121574

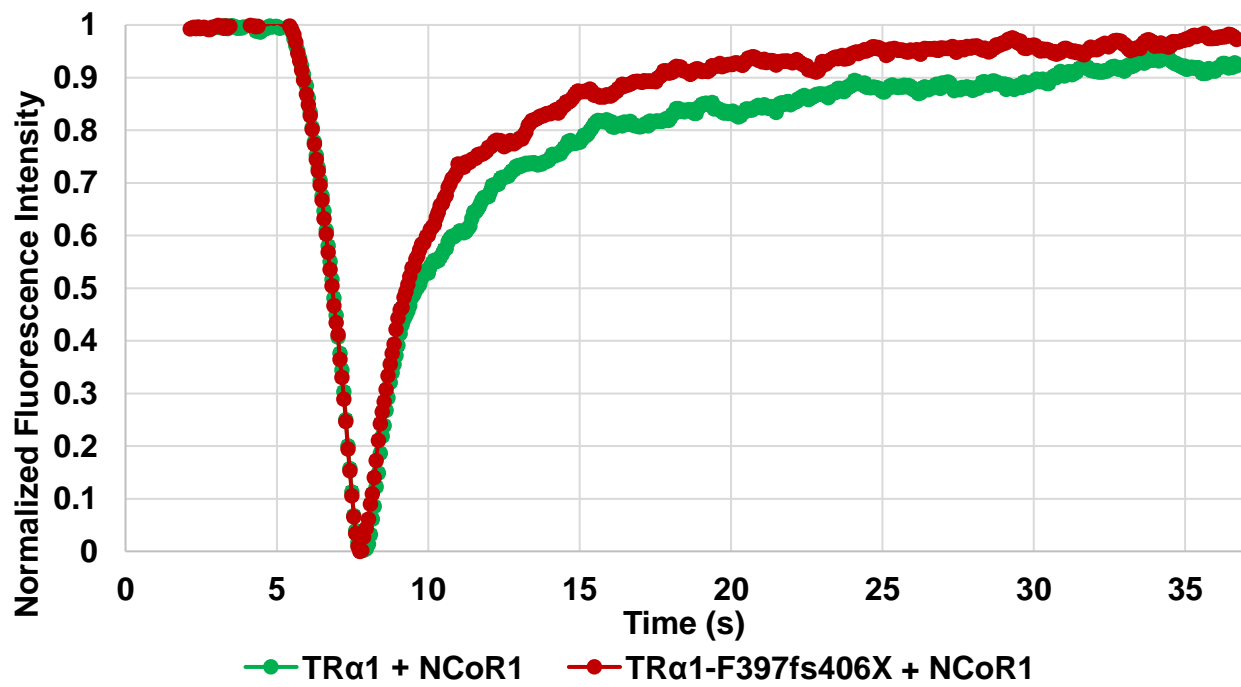
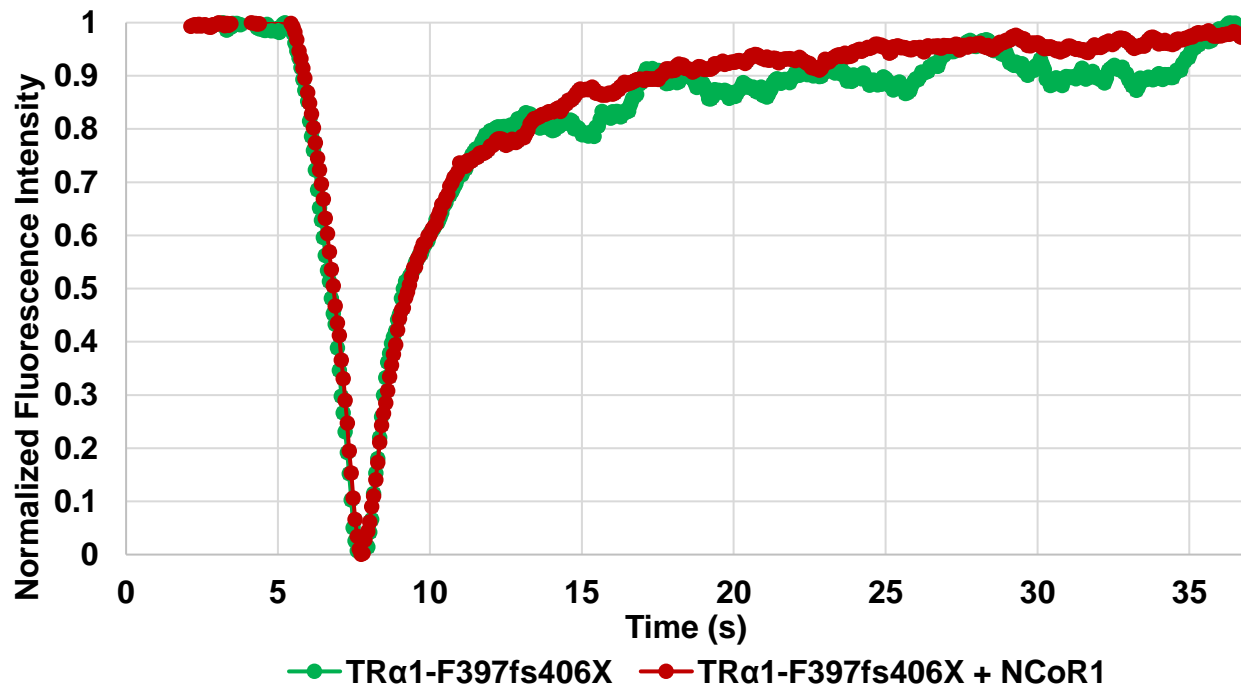
Table 1: FRAP parameters comparing wild-type TR α 1 to RTH-F397fs406X, A382PfsX7, and E403X. FRAP analysis parameters (averages) and statistics for RTH α mutants and TR α 1. HeLa cells were transfected with expression plasmids for either mCherry TR α 1 or mCherry RTH-F397fs406X, A382PfsX7, or E403X. Strip-FRAP was conducted on cells 23-27 hours post transfection. For RTH-F397fs406X, N=3, p>0.05. For RTH-A382PfsX7 and E403X, N=2.

We next investigated the effect of NCoR1 on the intranuclear mobility of wild-type and RTH mutant TR. NCoR Δ ID was used as a control for NCoR1's reported increased binding affinity to RTH-F397fs406X, A382PfsX7, and E403X.

A



B



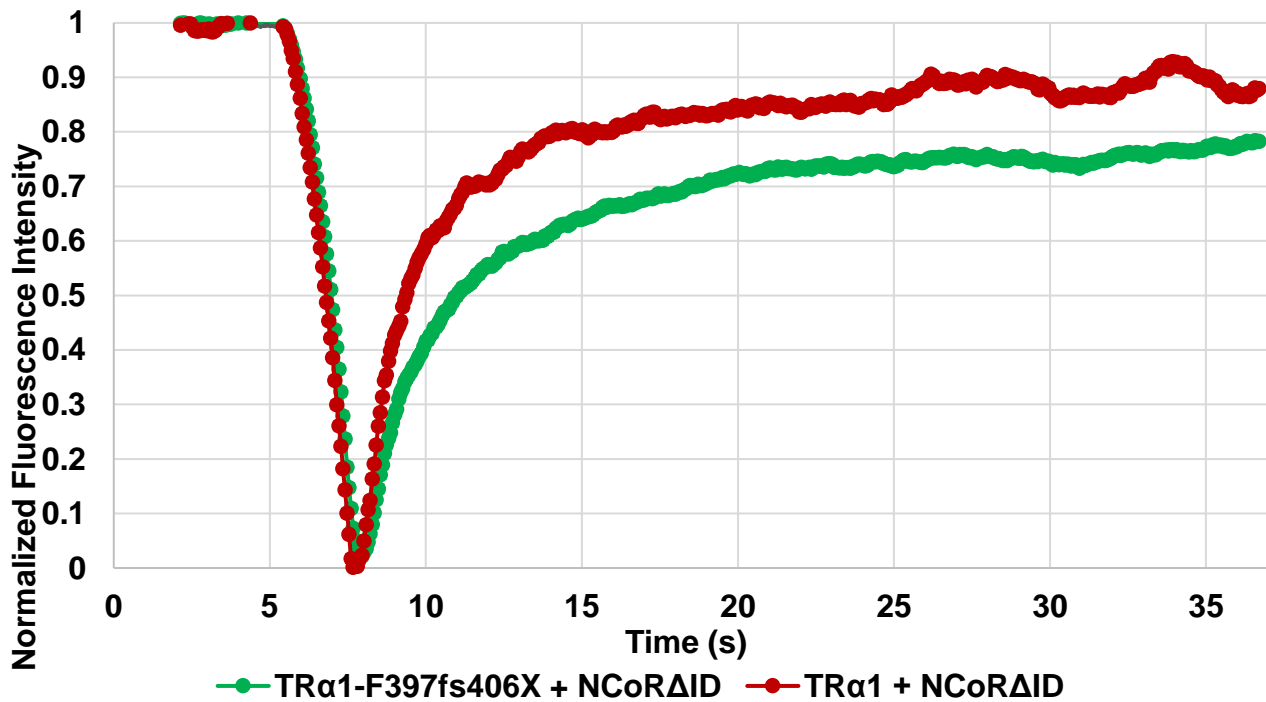
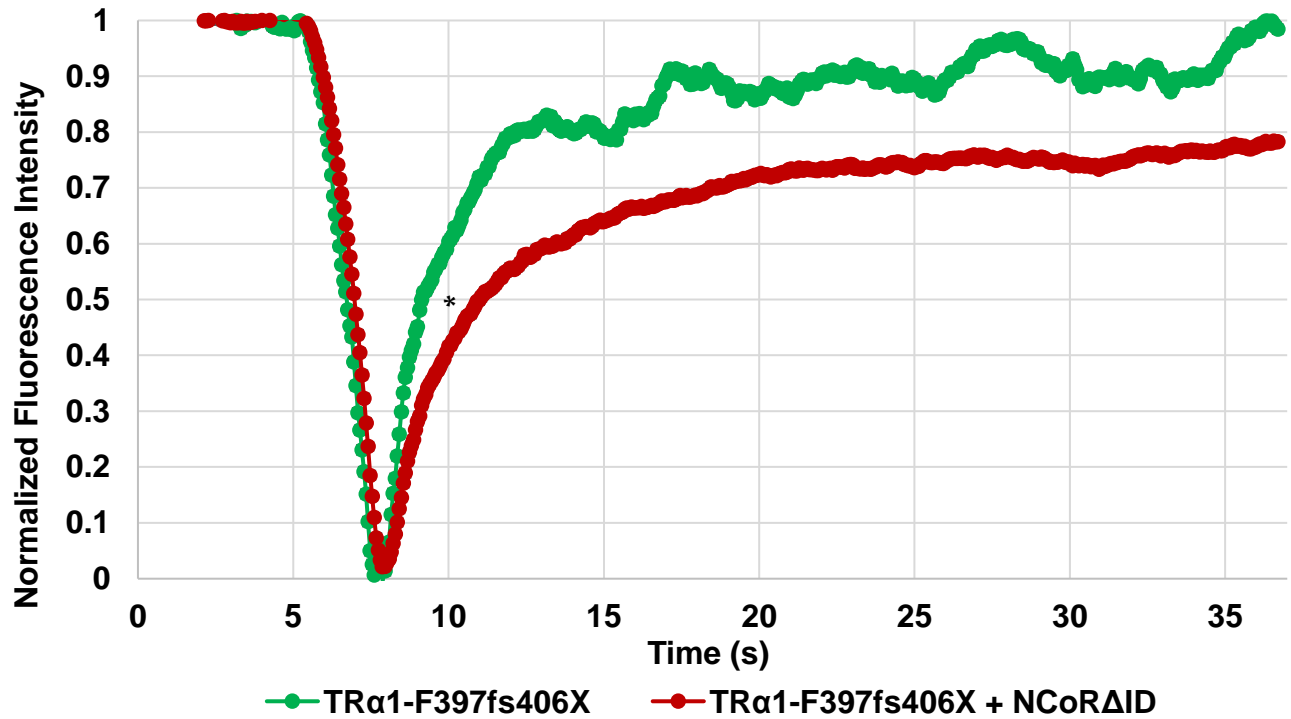
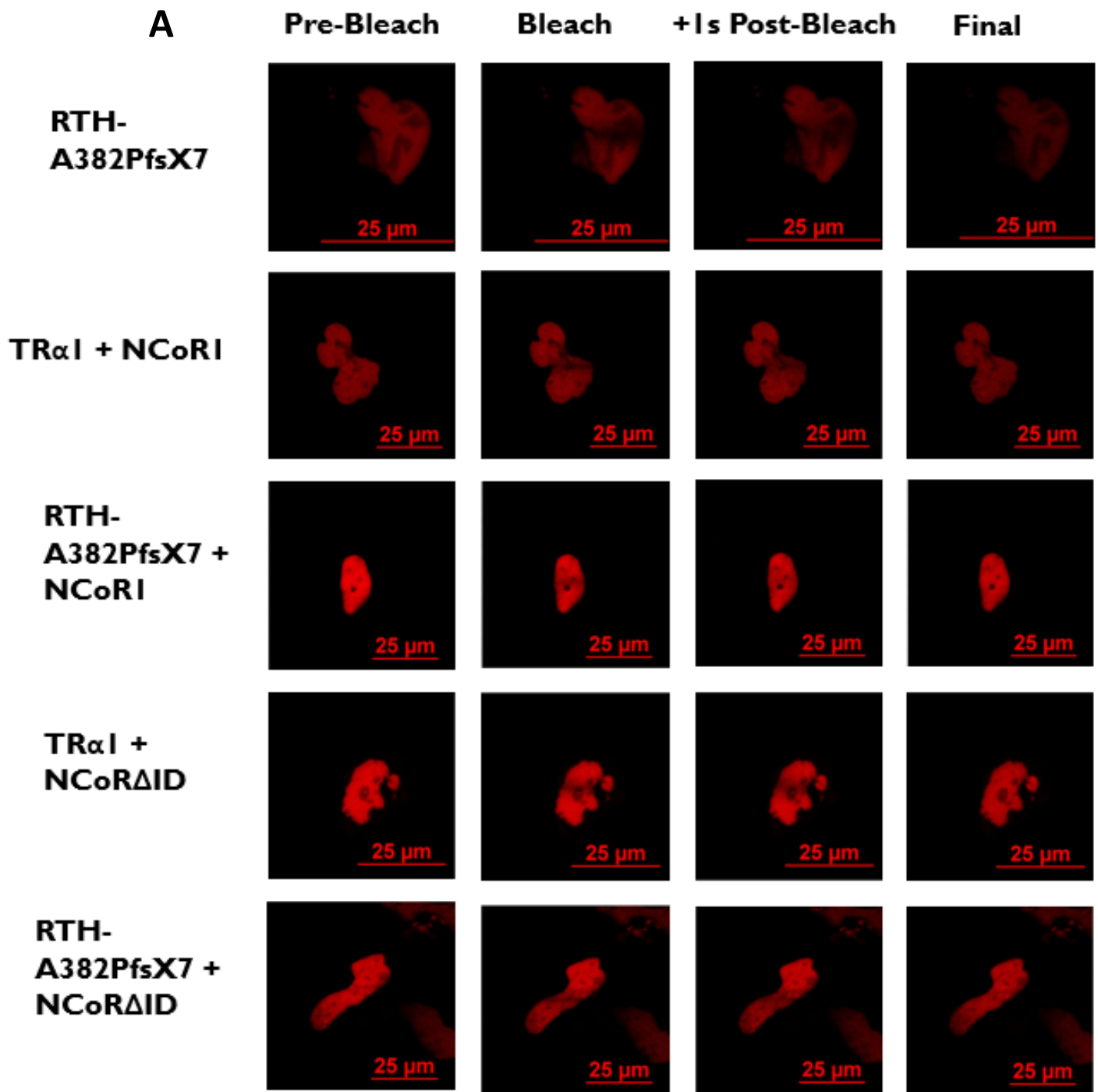
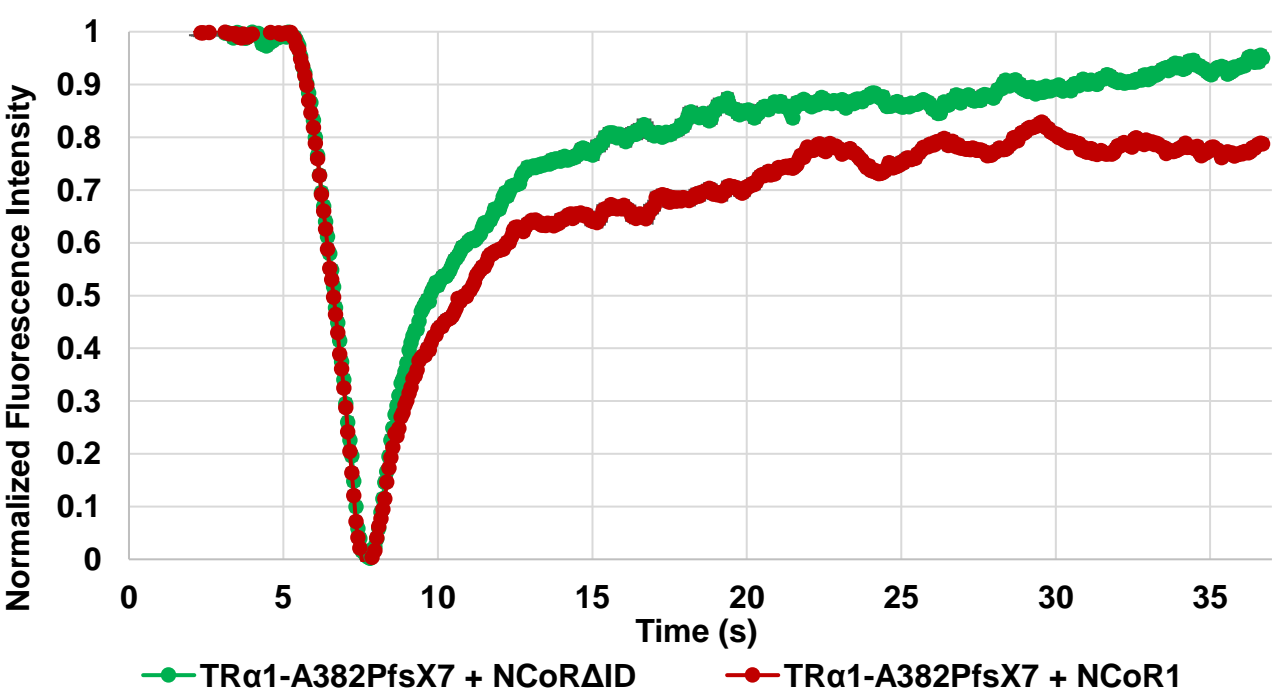
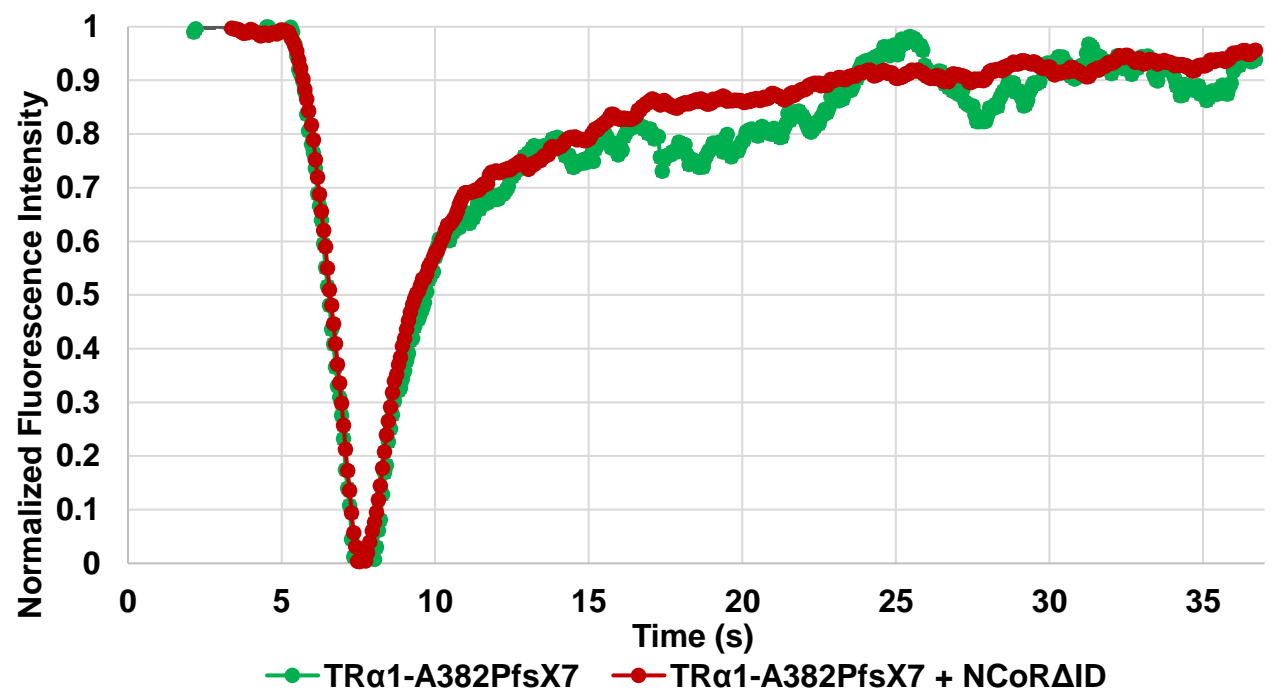


Figure 9: NCoR1 does not impact RTH-F397fs406X intranuclear dynamics, yet NCoRΔID reduces its mobility. FRAP curve and representative images of HeLa nuclei, comparing either mCherry TRα1 or mCherry RTH TRα1-F397fs406X alone to mCherry RTH TRα1-F397fs406X cotransfected with GFP-NCoR1 or GFP-NCoRΔID (GFP-NCoR1/ΔID). **(A)** HeLa cells were transfected with expression plasmids for either mCherry TRα1 or mCherry RTH TRα1-F397fs406X alone, or cotransfected with

mCherry RTH TR α 1- F397fs406X and GFP-NCoR1/ Δ ID as well at a ratio of 2:1, TR to NCoR1/ Δ ID. **(B)** Strip-FRAP was conducted on 5 nuclei for each of three biological replicates. Data were normalized to a scale of 0 to 1 and averaged. Bars represent \pm SEM. *P<0.05 for t-half and for t-half slope.



B



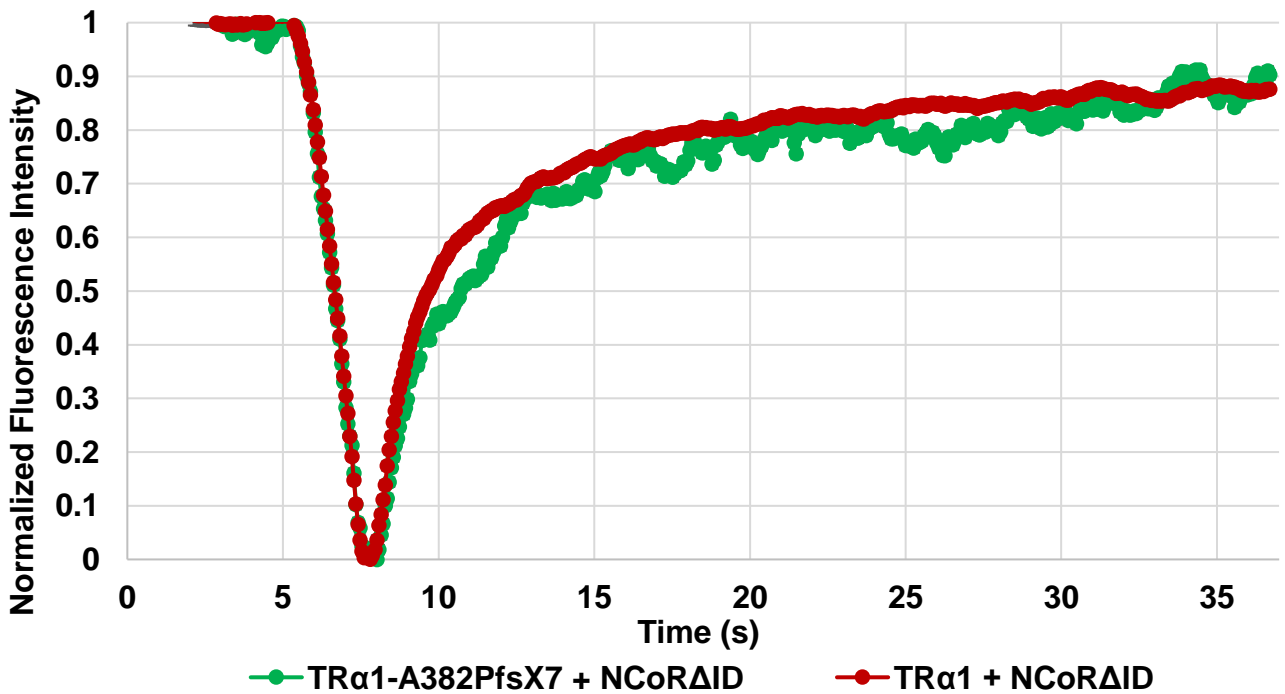
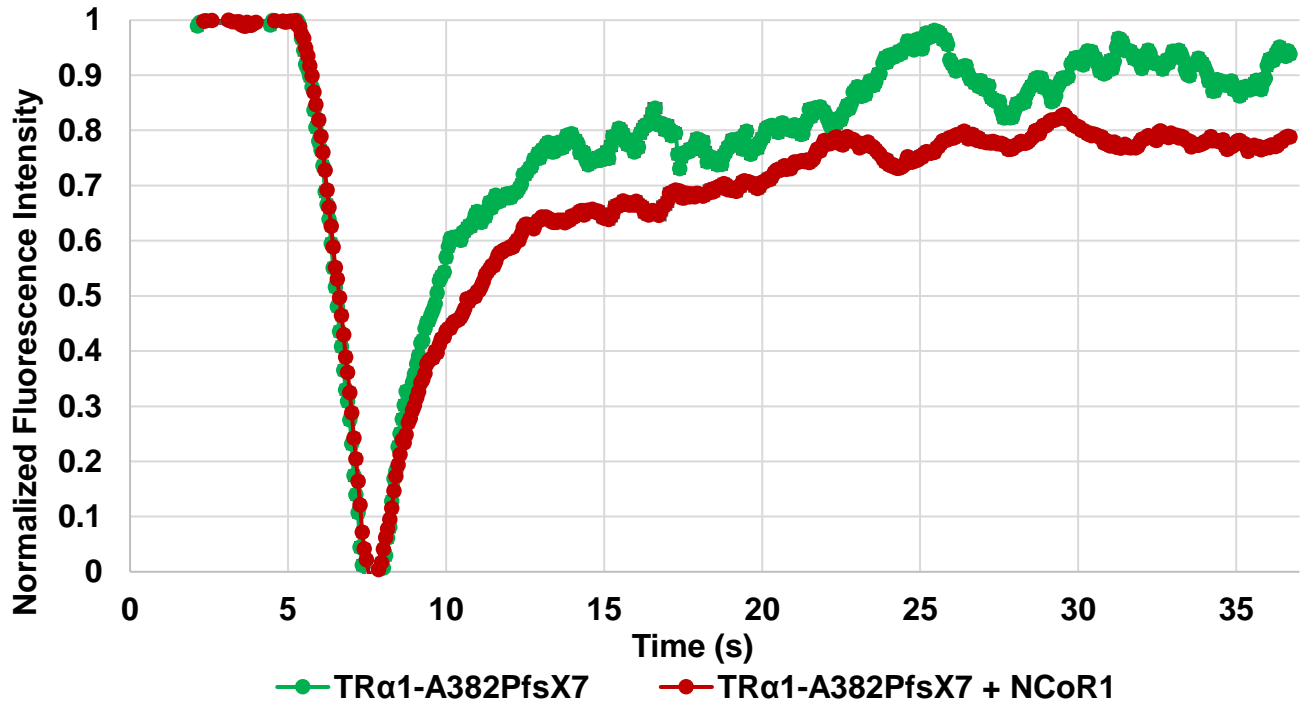
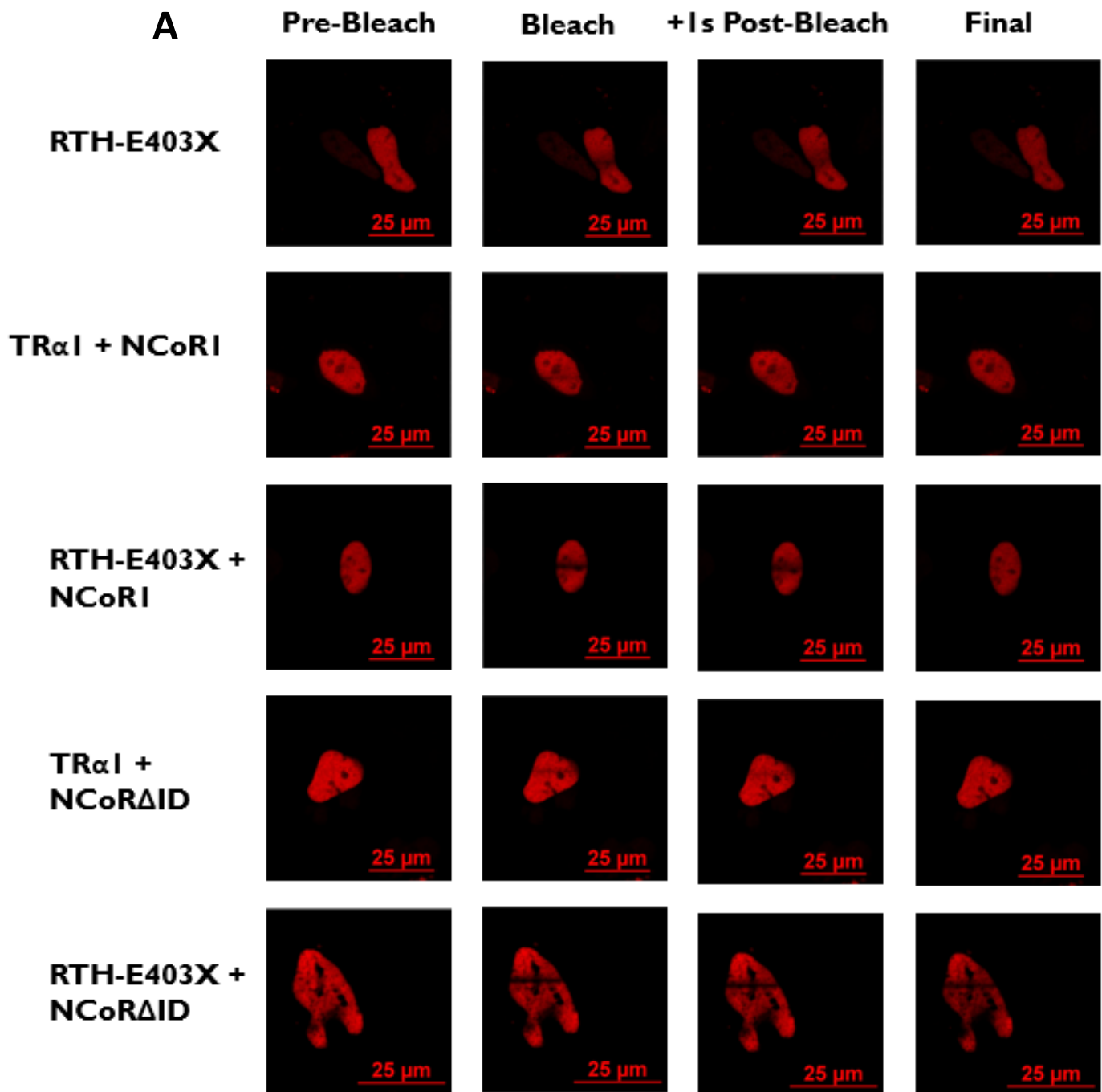
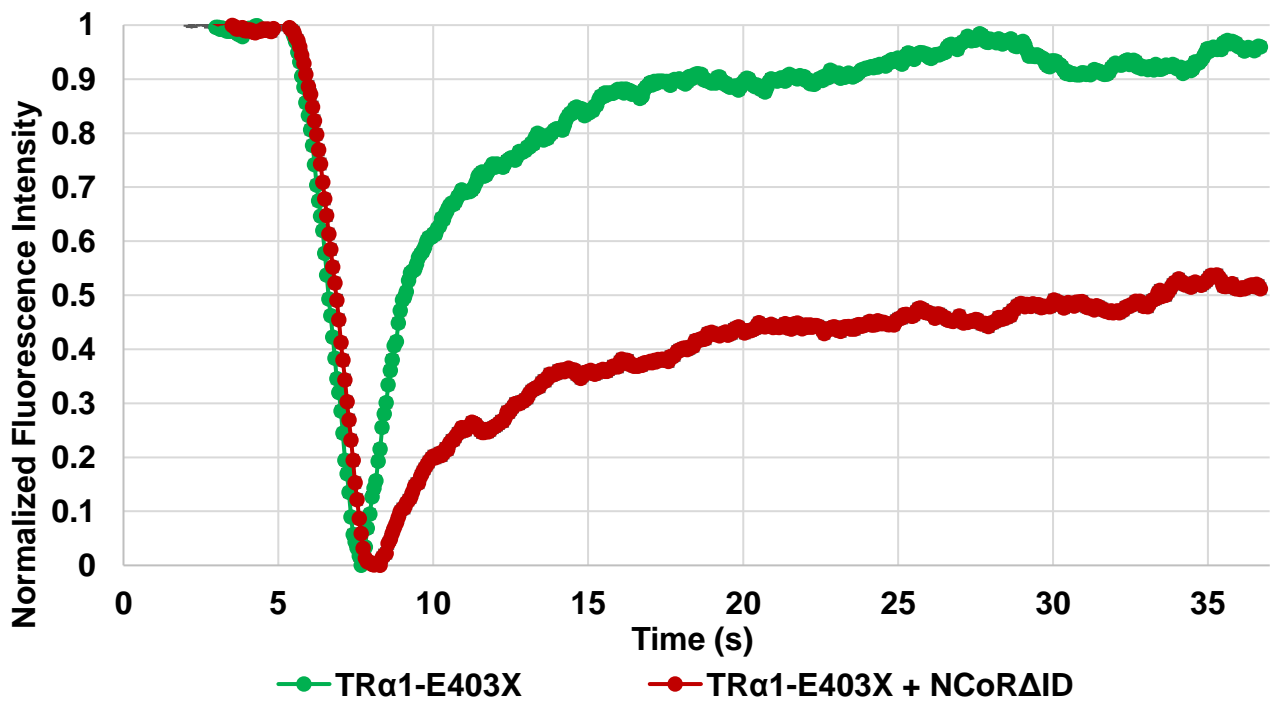
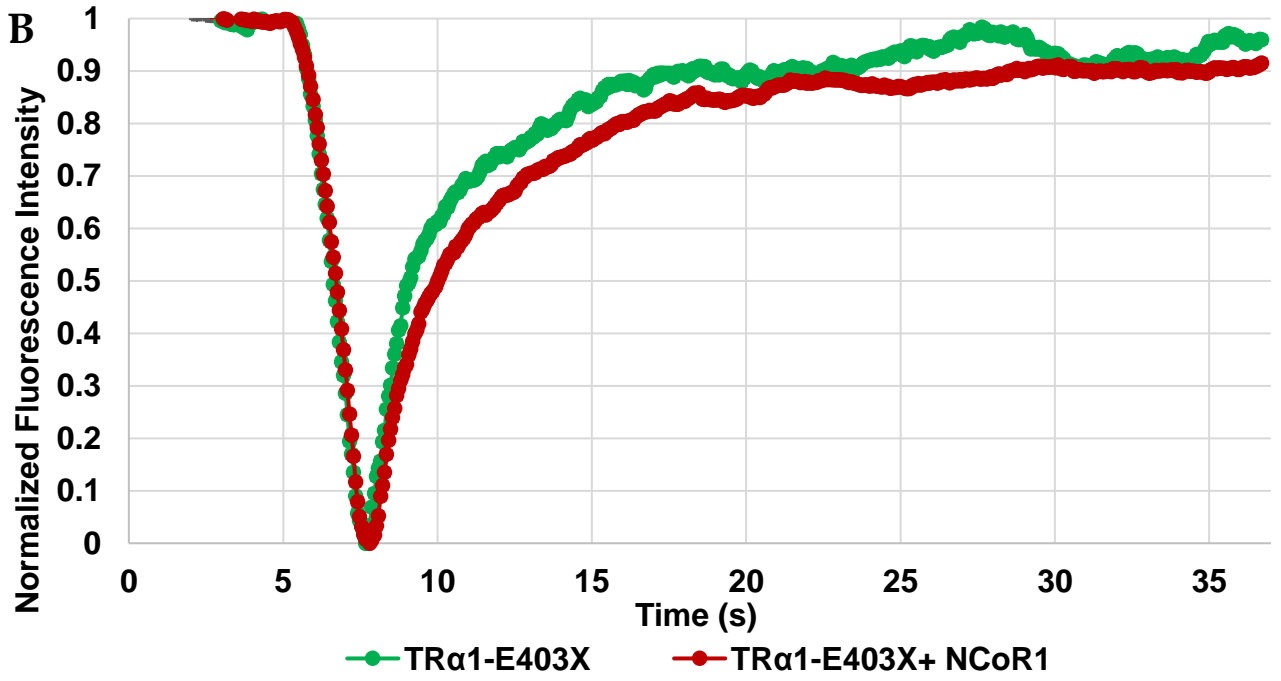


Figure 10: Neither NCoR1 nor NCoRΔID impact RTH-A382PfsX7 intranuclear dynamics. FRAP curve and representative images of HeLa nuclei, comparing either mCherry TRα1 or mCherry RTH TRα1-A382PfsX7 alone to mCherry RTH TRα1-A382PfsX7 cotransfected with either GFP-NCoR1 or GFP-NCoRΔID (NCoR1/ΔID). **(A)** HeLa cells were transfected with expression plasmids for either mCherry RTH TRα1-A382PfsX7 alone, or cotransfected with mCherry RTH TRα1-A382PfsX7 and GFP-

NCoR1/ Δ ID as well at a ratio of 2:1, TR to NCoR1/ Δ ID. **(B)** Strip-FRAP was conducted on 5 nuclei for each of two biological replicates. Data were normalized to a scale of 0 to 1.





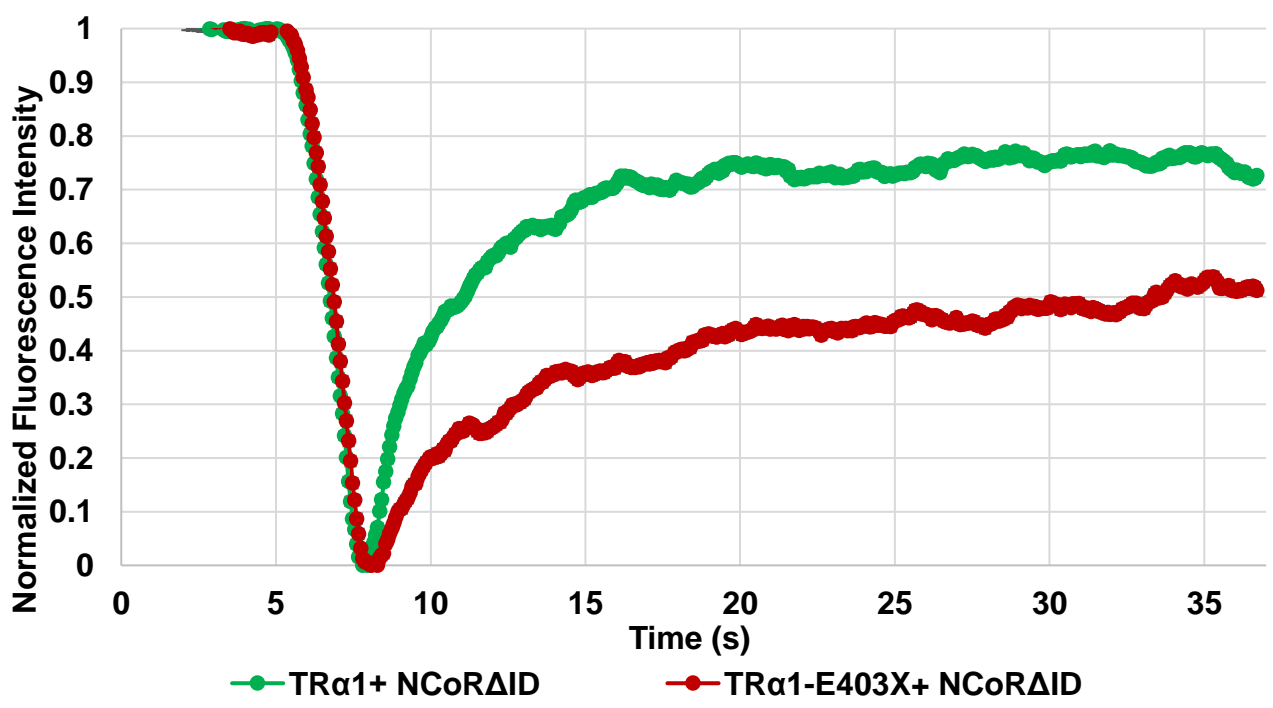
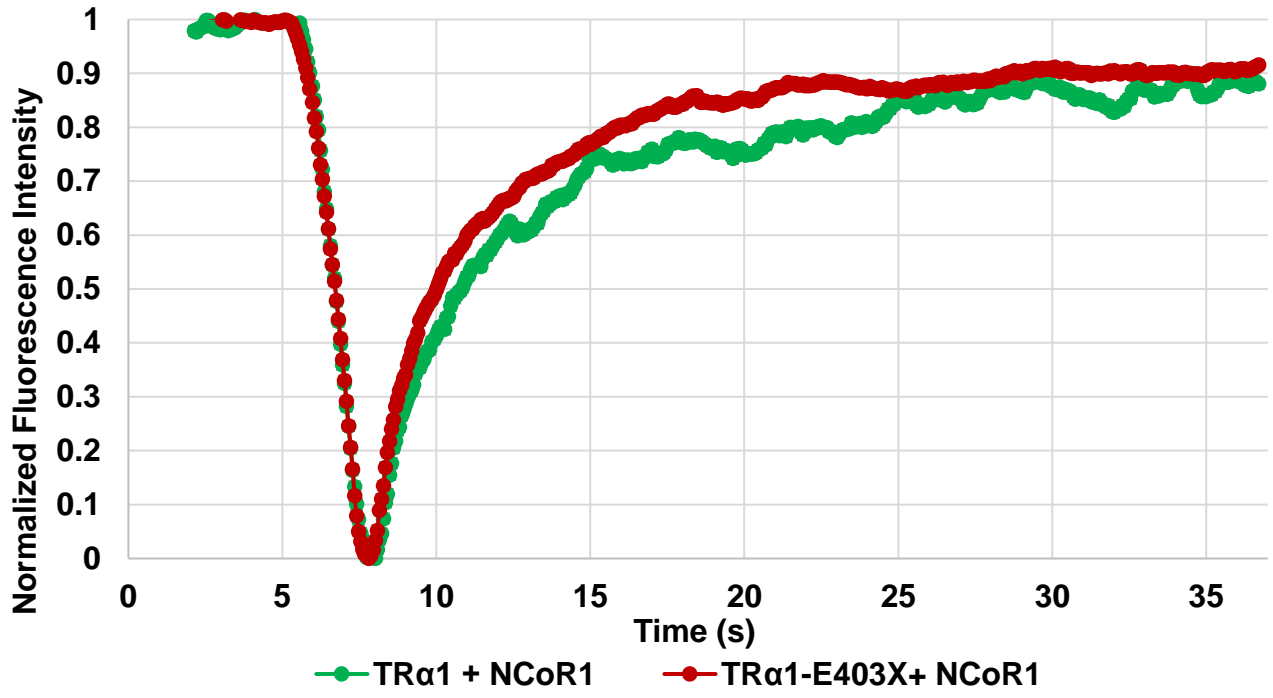


Figure 11: NCoR1 does not impact RTH-E403X intranuclear dynamics, yet NCoRAID reduces its mobility. FRAP curve and representative images of HeLa nuclei, comparing either mCherry TRα1 or mCherry RTH TRα1-E403X alone to mCherry RTH TRα1-E403X cotransfected with GFP-NCoR1 or GFP-NCoRAID (GFP-

NCoR1/ Δ ID). **(A)** HeLa cells were transfected with expression plasmids for either mCherry RTH TR α 1-E403X alone, or cotransfected with mCherry RTH TR α 1-E403X and GFP-NCoR1/ Δ ID as well at a ratio of 2:1, TR to NCoR1/ Δ ID. **(B)** Strip-FRAP was conducted on 5 nuclei for each of two biological replicates. Data were normalized to a scale of 0 to 1.

	Mobile Fraction	Immobile Fraction	t-half (s)	t-half Slope
TR α 1-F397fs406x	0.976258587	0.023741413	1.328158766	0.222161401
TR α 1-F397fs406x + NCoR1	0.971369223	0.027024289	1.485045426	0.22775898
P-Value	0.823208215	0.823208215	0.464993856	0.76926651
TR α 1	0.922262162	0.077737838	1.325700606	0.213999054
TR α 1 + NCoR1	0.97200887	0.02799113	1.737424879	0.159083963
P-Value	0.285869414	0.285869414	0.333263509	0.238515375
TR α 1-F397fs406x + NCoR1	0.971369223	0.027024289	1.485045426	0.22775898
TR α 1 + NCoR1	0.97200887	0.02799113	1.737424879	0.159083963
P-Value	0.978155946	0.978155946	0.545518394	0.092564954
TR α 1-A382PfsX7	1.003798407	-	1.661932266	0.170954241
TR α 1- A382PfsX7 + NCoR1	0.80909281	0.003798407	1.86030239	0.140267293
TR α 1	0.915052399	0.084947601	1.148266833	0.25836812
TR α 1 + NCoR1	0.9999	1E-04	1.652664426	0.18160183
TR α 1- A382PfsX7 + NCoR1	0.971369223	0.027024289	1.485045426	0.22775898
TR α 1 + NCoR1	0.9999	1E-04	1.652664426	0.18160183
TR α 1-E403X	0.944961989	0.055038011	1.414548756	0.153720046
TR α 1-E403X + NCoR1	0.905391245	0.094608755	1.861287238	0.109239526
TR α 1	0.970790516	0.029209484	1.676764528	0.165121574

TR α 1 + NCoR1	0.914849318	0.085150682	2.256236776	0.111627344
TR α 1-E403X + NCoR1	0.905391245	0.094608755	1.861287238	0.109239526
TR α 1 + NCoR1	0.914849318	0.085150682	2.256236776	0.111627344

Table 2: FRAP parameters comparing NCoR1 coexpressed with wild-type TR α 1 to NCoR1 coexpressed with either RTH-F397fs406X, A382PfsX7, or E403X. FRAP analysis parameters (averages) and statistics for RTH α mutants and TR α 1, both coexpressed with NCoR1. HeLa cells were cotransfected with expression plasmids for either mCherry TR α 1 or mCherry RTH-F397fs406X, A382PfsX7, or E403X, in addition to GFP-NCoR1. Strip-FRAP was conducted on cells 23-27 hours post transfection. For RTH-F397fs406X, N=3, 5 nuclei per replicate, p>0.05. For RTH-A382PfsX7 and E403X, N=2, 5 nuclei per replicate.

As shown in Figures 9-11 and Table 2, NCoR1 did not have a significant effect on the intranuclear dynamics of RTH-F397fs406X and did not appear to have a substantial effect on RTH-A382PfsX7 and E403X. The curves of RTH-F397fs406X alone compared to RTH-F397fs406X coexpressed with NCoR1 closely followed each other (Figure 9), with no significant difference between the slopes at time t-half (Table 2; t-half slope, p = 0.7692). When comparing RTH-F397fs406X alone to the mutant coexpressed with NCoR1, neither the mobile fractions nor t-half values were significantly different (p = 0.8232 and 0.4650 respectively). The mobile fractions had a difference of 0.49%, t-half values at 0.1569s, and t-half slopes at 0.0056. This trend was also observed when comparing RTH-F397fs406X with NCoR1 to TR α 1 with NCoR1. Figure 9 demonstrated that the curves for the two groups closely followed each other, and no significant differences were found in the parameters listed in Table 2. The mobile fractions were comparable at 97.1% and 97.2% (p = 0.9782), and the t-half values and t-half slopes were not significantly different (p=0.5455 and 0.0925, respectively).

RTH- E403X demonstrated a similar trend to RTH-F397fs406X, and while RTH-A382PfsX7 appeared to recover more slowly when coexpressed with NCoR1, the

differences in t-half values, t-half slopes, and mobile fractions between single transfections and cotransfections, and between TR α 1 and RTH-A382PfsX7, were similar to those of the other two mutants (Figure 10). Due to technological issues with the confocal microscope, only two biological replicates were performed for RTH-A382PfsX7 and E403X (N=2, 5 nuclei per replicate in each transfection group, so an additional replicate will be required prior to statistical analyses of the data. However, the trends seen in Figure 11 and Table 2, suggest that the intranuclear mobility of RTH-E403X is likely not affected by NCoR1. RTH-E403X alone compared to the mutant coexpressed with NCoR1 showed minimal differences in the mobile fractions (3.96%), a difference of 0.4468s for t-half values, and 0.0445 for t-half slopes. When comparing NCoR1 coexpression with RTH-E403X and TR α 1, the parameter value differences were even smaller, with a mobile fraction difference of 0.946%, 0.3949s for the t-half difference, and 0.0023 for t-half slopes.

When comparing the parameters in Table 2, RTH-A382PfsX7 showed the same trend as RTH-F397fs406X and E403X, with NCoR1 not demonstrating an effect on RTH-A382PfsX7 intranuclear dynamics. When comparing RTH-A382PfsX7 with and without NCoR1, the t-half time difference was only 0.19 seconds, similar to RTH-F397fs406X's difference of 0.16 seconds (Table 2). The t-half slope and mobile fraction differences for RTH-A382PfsX7 with and without NCoR1 were also similar to those of the former two mutants (0.0307 and 2.8% for slope and mobile fractions, respectively), as were those of the mutant and TR α 1 with NCoR1 (0.0462 and 0.0285, respectively, with a t-half difference of 0.1676s; Table 2). When comparing differences between TR α 1 and RTH-A382PfsX7 when both are coexpressed with NCoR1, we saw mobile fractions with a

difference of 2.76%, t-half values with a 0.1676s difference, and t-half slopes with a difference of 0.0462.

	Mobile Fraction	Immobile Fraction	t-half (s)	t-half Slope
TR α 1-F397fs406x	0.976258587	0.023741413	1.328158766	0.222161401
TR α 1-F397fs406x + NCoR Δ ID	0.966938932	0.033061068	1.321711647	0.119544208
P-Value	0.196717295	0.196717295	0.050314257	0.044548016
TR α 1	0.922262162	0.077737838	1.325700606	0.213999054
TR α 1 + NCoR Δ ID	0.900792225	0.099207775	1.281294566	0.156312661
P-Value	0.71341891	0.71341891	0.74813597	0.106573464
TR α 1-F397fs406x + NCoR Δ ID	0.966938932	0.033061068	1.321711647	0.119544208
TR α 1 + NCoR Δ ID	0.900792225	0.099207775	1.281294566	0.156312661
P-Value	0.202296592	0.202296592	0.703566752	0.332621829
TR α 1-F397fs406x + NCoR Δ ID	0.966938932	0.033061068	1.321711647	0.119544208
TR α 1-F397fs406x + NCoR1	0.971369223	0.027024289	1.485045426	0.22775898
P-Value	0.202296592	0.202296592	0.703566752	0.332621829
TR α 1-A382PfsX7	1.003798407	-	1.661932266	0.170954241
TR α 1- A382PfsX7 + NCoR Δ ID	0.998872882	0.001127118	1.856286607	0.164531946
TR α 1	0.915052399	0.084947601	1.148266833	0.25836812
TR α 1 + NCoR Δ ID	0.894344796	0.105655204	1.875483154	0.164993274
TR α 1- A382PfsX7 + NCoR Δ ID	0.998872882	0.001127118	1.856286607	0.164531946
TR α 1 + NCoR Δ ID	0.894344796	0.105655204	1.875483154	0.164993274

TR α 1- A382PfsX7 + NCoR Δ ID	0.998872882	0.001127118	1.856286607	0.164531946
TR α 1- A382PfsX7 + NCoR1	0.80909281	0.19090719	1.86030239	0.140267293
TR α 1-E403X	0.944961989	0.055038011	1.414548756	0.153720046
TR α 1-E403X + NCoR Δ ID	0.605411323	0.394588677	4.154810418	0.068587839
TR α 1	0.970790516	0.029209484	1.676764528	0.165121574
TR α 1 + NCoR Δ ID	0.752275781	0.247724219	1.635850126	0.132492647
TR α 1-E403X + NCoR Δ ID	0.605411323	0.394588677	4.154810418	0.068587839
TR α 1 + NCoR Δ ID	0.752275781	0.247724219	1.635850126	0.132492647
TR α 1-E403X + NCoR Δ ID	0.605411323	0.394588677	4.154810418	0.068587839
TR α 1-E403X + NCoR1	0.905391245	0.094608755	1.861287238	0.109239526

Table 3: FRAP parameters comparing NCoR Δ ID coexpressed with wild-type TR α 1 to NCoR Δ ID coexpressed with either RTH-F397fs406X, A382PfsX7, or E403X.

FRAP analysis parameters (averages) and statistics for RTH α mutants and TR α 1, both coexpressed with NCoR Δ ID. HeLa cells were cotransfected with expression plasmids for either mCherry TR α 1 or mCherry RTH-F397fs406X, A382PfsX7, or E403X, in addition to GFP-NCoR Δ ID. Strip-FRAP was conducted on cells 23-27 hours post transfection. For RTH-F397fs406X, N=3, 5 nuclei per replicate, $p < 0.05$. For RTH-A382PfsX7 and E403X, N=2, 5 nuclei per replicate.

Interestingly, while NCoR Δ ID did not appear to affect WT TR α 1's intranuclear mobility as expected, it did have a significant effect on the t-half of F397fs406X's mobility compared to the mutant TR alone (0.0064s, $p = 0.050$), as well as on the t-half slope (0.1026 $p = 0.045$). However, the mobile fractions were not significantly different, with a difference of 0.932% and a p-value of 0.1967.

While no statistical analyses could be performed on RTH-A382PfsX7 and RTH-E403X, the two replicates obtained demonstrated interesting trends for the effect of NCoR Δ ID on the mutants. Just as in NCoR1-coexpression, RTH-E403X appeared to follow a

similar trend to RTH-F397fs406X with NCoR Δ ID coexpression, showing a substantially slower intranuclear mobility for RTH-E403X coexpressed with NCoR Δ ID (Figure 11), and with a t-half average difference of just under 2.5 seconds between RTH-E403X and RTH-E403X coexpressed with NCoR Δ ID (Table 3). Unlike RTH-F397fs406X, RTH-E304X also appeared to have a considerable difference between the intranuclear mobilities of RTH-E403X with NCoR Δ ID and TR α 1 with NCoR Δ ID, showing a t-half average difference of just over 2.5 seconds between the two groups (Table 3). RTH-A382PfsX7 did not appear to be affected by NCoR Δ ID; RTH-A382PfsX7 + NCoR Δ ID appeared to follow the curves of RTH-A382PfsX7 alone and TR α 1 + NCoR Δ ID (Figure 8).

These results prompted us to confirm the intracellular localization of NCoR1 and NCoR Δ ID alone versus cotransfected (Figure 12). Astapova et al (2008) demonstrated that both NCoR1 and NCoR Δ ID had a nuclear distribution, which was expected given NCoR1's function as a nuclear corepressor. We therefore examined the localization of NCoR1 and NCoR Δ ID on their own to see if there were any intracellular localization differences that could explain our results, representative images of which are found in Figure 10. Both proteins maintained a nuclear distribution, noting a relatively speckled appearance especially in GFP-NCoR1-transfected cells. Our FRAP analysis also assessed this nuclear distribution, as all cotransfected cells used were confirmed to be coexpressing GFP-NCoR1 or GFP-NCoR Δ ID, and either mCherry-TR α 1 or mCherry-RTH-A382PfsX7, F397fs406X, or E403X, as shown in Figure 13.

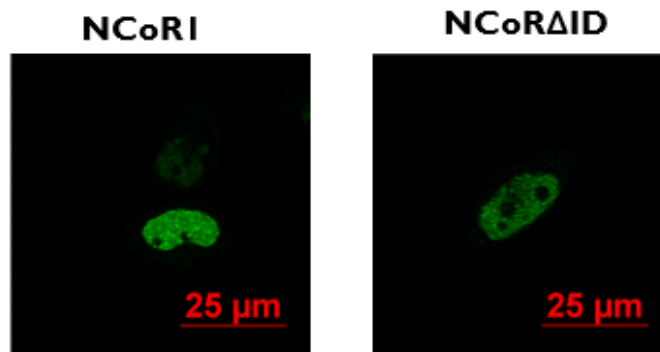


Figure 12: Intracellular localization of NCoR1 and NCoR Δ ID. Representative images of HeLa cells transfected with expression plasmids coding for either GFP-NCoR1 or GFP-NCoR Δ ID. Live cells were analyzed 24 hours post transfection using confocal microscopy.

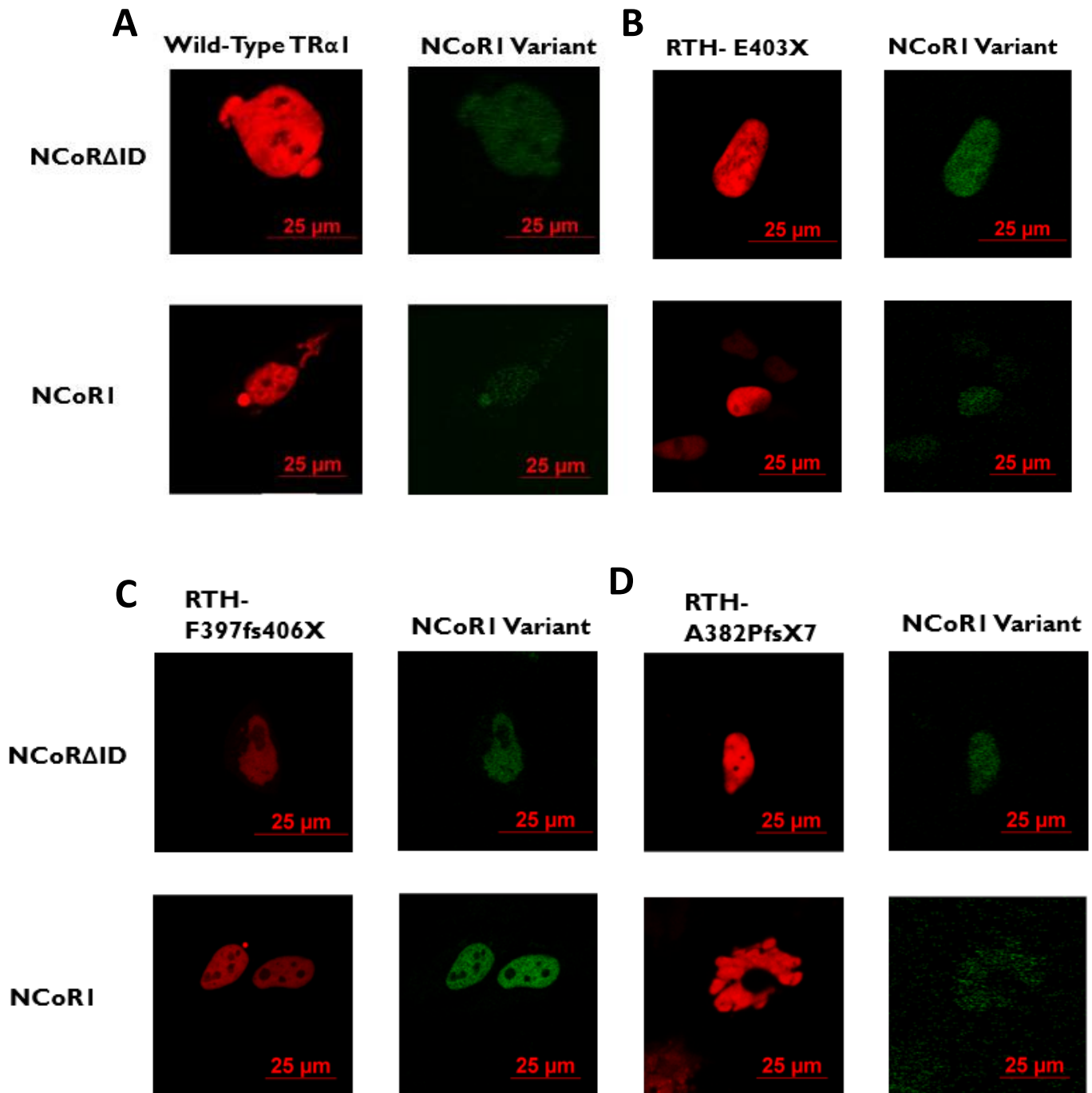


Figure 13: Intracellular localization of NCoR1 and NCoR Δ ID in cotransfected cells. Representative images of HeLa cells transfected with expression plasmids coding for either GFP-NCoR1 or GFP-NCoR Δ ID, as well as cotransfected with mCherry wild type TR α 1 (A) or mCherry RTH-E403X (B), F397fs406X (C), or A382PfsX7(D) expression plasmids. Live cells were analyzed 24 hours post transfection using confocal microscopy.

RTH-A382PfsX7 undergoes nucleocytoplasmic shuttling

The primarily nuclear localization of the three RTH α mutants A382PfsX7, F397fs406X, and E403X raised questions not just in their intranuclear mobility, but also in their ability to shuttle between the nucleus and the cytoplasm. Nucleocytoplasmic shuttling provides a key step in TR α 1's regulation, as it regulates the receptor's exposure to DNA and associated target genes (Roggero, et al. 2016; Subramanian, et al. 2015).

Previous work performed by Rochelle Evans in her Master's Thesis (Evans, 2019) demonstrated that the RTH α mutants of interest were still able to be imported to the nucleus, given their primarily nuclear localization. This finding was confirmed here, noting a primarily nuclear localization of the RTH α mutants during FRAP. However, these mutations result in either the complete loss of NES-H12 in the case of A382PfsX7, or a truncation of the NES in the case of E403X and F397fs406X. Of note, two NESs, spanning helices 3 and 6 (NES H3/H6), remain at full length. As such, we wished to determine if the NES-H12 truncations or deletion had any significant impact on nucleocytoplasmic shuttling.

To do so, we performed heterokaryon assays between mouse (NIH/3T3) cells and human (HeLa) cells, with HeLa cells serving as the transfected donor cells and NIH/3T3 cells as the nontransfected recipients. Using heterokaryons allowed for us to ensure that any fluorescent proteins seen in the recipient mouse nuclei were indeed due to shuttling and were not previously transfected cells. To differentiate between the two species, Hoescht stain was used instead of DAPI, as Hoescht staining of DNA creates bright blue/white speckles in NIH/3T3 nuclei in addition to diffuse blue fluorescence. In contrast, Hoescht staining is diffuse blue in HeLa nuclei, with a similar presentation to

DAPI staining. Therefore, any heterokaryon required at least one nucleus without speckles (HeLa) and one with speckles (NIH/3T3). Like DAPI, Hoescht stain is excited by a wavelength of 405 nm. Evidence of a speckled nucleus containing, in this case, mCherry-fusion proteins would demonstrate nucleocytoplasmic shuttling. Preliminary results were obtained for heterokaryons transfected with either mCherry TR α 1 or mCherry TR α 1-A382PfsX7 (Figure 14).

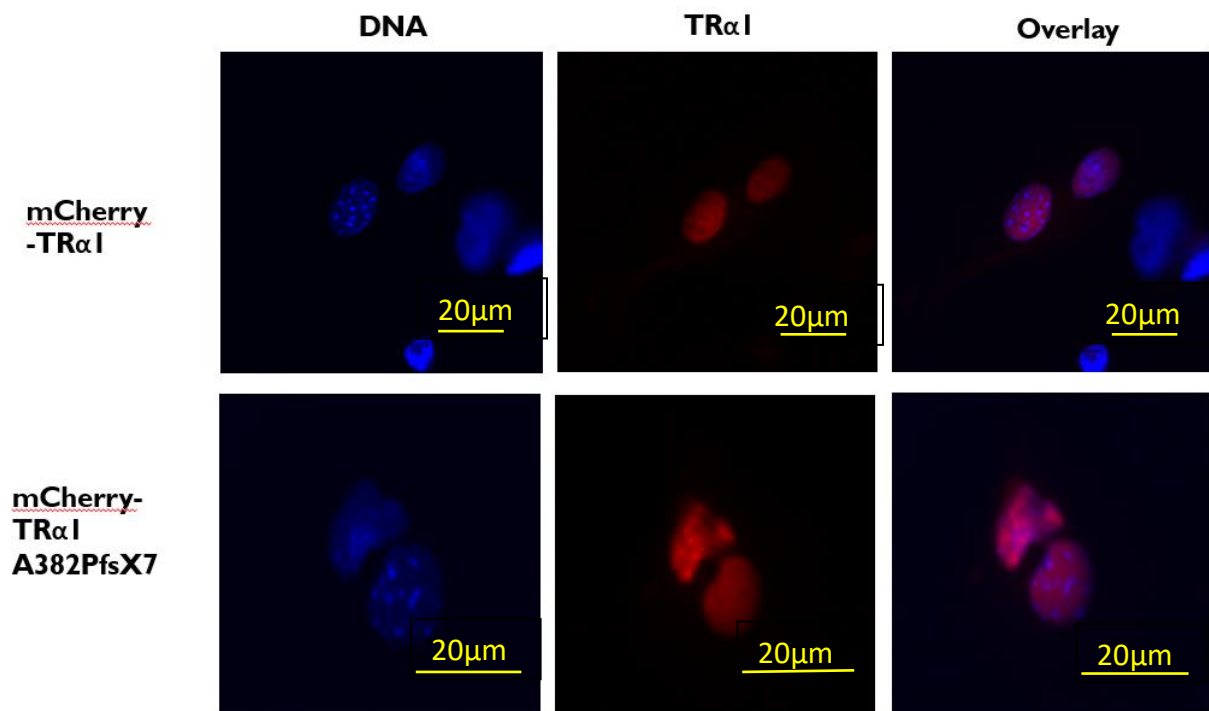


Figure 14: Deletion of Helix 12 does not impact TR α 1-A382PfsX7 nucleocytoplasmic shuttling. Representative images of preliminary heterokaryon assay results, depicting heterokaryons transfected with either wild type mCherry-TR α 1, or mCherry TR α 1-A382PfsX7. Heterokaryons were created by first transfecting HeLa cells, then seeding NIH/3T3 cells on top of the transfected HeLas. Once settled, the cells were fused, left to incubate for two hours to allow for shuttling, then fixed and analyzed using fluorescence microscopy. Blue fluorescence depicts Hoescht-stained nuclei of the heterokaryons. NIH/3T3 nuclei contain bright-blue speckles. TR α 1 depicts TR α 1 localization in the nucleus, and Overlay depicts the two channels together. Two biologically independent replicates were performed.

As seen in Figure 14, preliminary results demonstrated the presence of continued nucleocytoplasmic shuttling of TR α 1-A382PfsX7, despite the loss of NES- H12. Qualitatively, the receptor's shuttling capabilities appear to be similar to wild type TR α 1 shuttling.

Chapter 4: Discussion

RTH α is becoming more easily recognized in the medical world, with increased publications of clinician's guides and reviews detailing symptoms, treatments, and up to date information on what is known about the genetics behind the disease (Erbaş & Demir, 2021; Singh & Yen, 2017; van Gucht et al., 2017; Weiss et al., 2016). Since its first documentation in 2012, the number of mutations attributed to RTH α has grown to 25 known mutations today (*RTH α — Institut de Génomique Fonctionnelle de Lyon*, 2022.) Though it is known that the mutants discussed in this thesis—RTH-A382PfsX7, F397fs406X, and E403X—have impaired binding to T3, the molecular effects and mechanisms this causes remain elusive (Bochukova et al., 2012; Moran et al., 2013; van Mullem et al., 2012; van Mullem et al., 2013; Zavacki & Larsen, 2013).

The first mechanism of interest to our lab was the mutants' intracellular localization, especially since prior research done on RTH α mutants R384H and R384C for an Honors Thesis displayed increased cytoplasmic localization compared to wild type TR α 1 (Trampenau, 2019). Studies performed by Rochelle Evans demonstrated that RTH-A382PfsX7, F397fs406X, and E403X retained a nuclear distribution, and she went on to demonstrate they also maintained similar intranuclear mobility as wild-type, the next mechanism of interest to our lab (Evans, 2019).

Intranuclear mobility provides insight into intranuclear protein activity and function. The nucleoplasm does not contain cytoskeletal scaffolding, so movement is assumed to follow Brownian diffusion, with proteins, RNA, and other molecules of interest localizing to target areas when bound to their target structure(s) (Boulon et al., 2002; Grünwald et al., 2006; Kues et al., 2001). Multiple experimental methods have been used to evaluate

molecular mobility, including FRAP, fluorescence correlation spectroscopy (FCS), and photoactivation (PA) (Kues et al., 2001). However, we opted for FRAP given its frequent use in analyzing protein movement in a localized area within the cell or nucleus (Evans, 2019; Femia et al., 2019; Houtsmueller et al., 1999; Köster et al., 2005; Hughes et al., 2020).

As such, our aim was to elucidate better the molecular mechanisms that RTH-A382PfsX7, F397fs406X, and E403X follow due to their mutations. Because Evans (2019) had demonstrated that the mutations alone did not appear to affect the intranuclear mobility, any affects seen on the mutants' intranuclear mobility and associated function would likely come from an external source. Therefore, for our first aim we focused on NCoR1—TR α 1's primary corepressor that has been hypothesized to bind increasingly readily to these three mutants, since all three mutations cause a partial truncation or complete lack of H12 (Bochukova et al., 2012; Moran et al., 2013; Mottas et al., 2013; van Mullem et al., 2012, van Mullem et al., 2013)

We had predicted that NCoR1 would decrease the RTH α mutants' intranuclear mobility due to its increased binding affinity to the mutants, as well as its overall size (Bochukova et al., 2012; Moran et al., 2013; van Mullem et al., 2012, van Mullem et al., 2013). We therefore introduced a synthetic NCoR1 isoform to control for the binding affinity, NCoR Δ ID, which had two of three RIDs deleted inhibiting its ability to bind to TR α 1 (Astapova et al., 2008, Han, Park & Cheng, 2017). Interestingly, the results suggested the opposite: coexpressed NCoR1 did not have a significant effect on the intranuclear mobility of RTH-F397fs406X, compared to WT TR. RTH-A382PfsX7 and E403X followed a similar trend. While the trends for RTH-A382PfsX7 did not follow

those set by RTH-F397fs406X as closely, they still suggested that the mutant remained relatively unaffected by coexpressed NCoR1. Contrary to our prediction, NCoR1's increased binding affinity did not seem to interfere with the intranuclear dynamics of the mutants. While the results did not rule out the possibility of other potential effects of the increased binding affinity, they did rule out any effects on the receptors' intranuclear mobility. As to why NCoR1 did not affect the receptors' intranuclear mobility, it is possible that the RTH mutant TRs may be able to dissociate from NCoR1 more readily than anticipated, and that TR's intranuclear mobility is not as dependent on that of NCoR1 as we had predicted. It is also possible that helix 12 in the LBD is not as crucial for NCoR1 dissociation as previously hypothesized. This would need to be confirmed via coimmunoprecipitation assays in future studies. As such, the results raise questions as to whether TR's intranuclear mobility is impacted by other associated coregulators, including coactivators like MED1. MED1 has been shown to impact the intranuclear dynamics of wild-type TR and other RTH mutants (Femia et al., 2019; Wang, 2022). Curiously, we found instead that NCoR Δ ID significantly decreased the intranuclear mobility of RTH-F397fs406X when compared to the mutant's baseline intranuclear mobility via t-half and t-half slope values ($p = 0.050$ and $p = 0.045$, respectively). RTH-E403X also appeared to be substantially affected by NCoR Δ ID, but interestingly the intranuclear mobility of RTH-A382PfsX7 was not affected. NCoR Δ ID is a synthetic mutant and is only found in vivo in synthetic mouse models. These mouse models, like those seen in Astapova et al. (2008) and Han, Park & Cheng (2017) were created to model RTH β and RTH α , respectively. Astapova et al. (2008) had demonstrated that NCoR Δ ID maintained the nuclear distribution seen in wild-type NCoR1, which our

studies confirmed (Figure 12). Interestingly, while both isoforms maintained a speckled appearance, NCoR1 did appear to be a bit more speckled (Figure 12 and 13). The speckles suggested target gene localization, noting that HeLa cells do maintain some endogenous nuclear receptor expression, specifically androgen receptor (AR), retinoic acid receptor beta (RAR β), and growth hormone receptor (GHR) (Rouillard et al., 2016). However, overexpression of either NCoR1 or NCoR Δ ID when coexpressed with TR α 1 or any of the three RTH α mutants of interest would override this interaction, and any aggregation would have been due to TR α 1 target gene binding. The decrease in aggregation seen in NCoR Δ ID alone and when cotransfected with wild type TR α 1 may have been due the loss of ID2 and ID3, since NCoR Δ ID would not have been able to bind to any endogenous nuclear receptors nor be recruited to associated target genes. Interestingly, we did see some speckles maintained more in cells cotransfected with NCoR Δ ID and either RTH-F397fs406X and E403X, and less so in A382PfsX7, suggesting potential interactions between the two former receptors and corepressor (Figures 12 and 13).

Although we had intended NCoR Δ ID to serve as a control for NCoR1's increased binding affinity to RTH α -A382PfsX7, F397fs406X, and E403X, its effect on RTH-F397fs406X and E403X and lack of effect on WT TR α 1 and RTH α A382PfsX7 suggested that while it could serve as a control for WT TR α 1, the lack of the two more C-terminal RIDs does not completely inhibit NCoR Δ ID binding to RTH α F397fs406X and E403X. As a reminder, RTH α F397fs406X and E403X's mutations resulted in a truncated helix 12 (H12) in TR α 1's LBD, whereas RTH α A382PfsX7's mutation resulted in the complete deletion of helix 12 and the truncation of helix 11 (H11). This difference

may explain the lack of an effect on RTH α A382PfsX7 while its counterparts, F397fs406X and E403X, were significantly impacted. NCoR1 was hypothesized to have a higher binding affinity to the three RTH α mutants of interest in this thesis because it was hypothesized that H12 was crucial in the mechanics behind NCoR1 dissociation from the RTH-TR α mutants.

Prior studies by Han, Park & Cheng (2017) demonstrated through chromatin immunoprecipitation (ChIP) assays that WT TR α 1 and NCoR Δ ID do not associate with each other, however no such assays have been performed on RTH α A382PfsX7, F397fs406X, and E403X, and would benefit from such assays in the future. While RTH α A382PfsX7 was not significantly impacted by NCoR Δ ID in this study, it would still be worth performing a CoIP assay to establish whether or not RTH α A382PfsX7 and NCoR Δ ID were associated. This would allow for some insight into the mechanics behind our findings, chiefly because A382PfsX7 has a complete deletion of H12, while F397fs406X and E403X retain truncated helix 12s. Further replicates of RTH-A382PfsX7 and E403X must be done to confirm their trends. Future studies would also benefit from obtaining and analyzing NCoR Δ ID's predicted structures, as this may provide insight into its interaction mechanics with RTH-A382PfsX7, F392fs406X, and E403X.

Interestingly enough, the study performed by Han, Park & Cheng (2017) showed that in mouse models, TR α 1-PV mice (mutant mice expressing a mouse variant of the F397fs406X mutation) with NCoR Δ ID coexpression phenotypically recovered to near wild-type parameters. Specifically, anemic TR α 1-PV mice with NCoR Δ ID coexpression saw partial recovery of total bone marrow cells, number of mature erythrocytes, and de-

repressed erythropoietic genes that TR α 1-PV alone had repressed (Han, Park & Cheng, 2017). However, beyond changes in gene expression, they did not discern the molecular mechanisms behind the phenotype recovery. Looking back at our results, it is possible that NCoR Δ ID coexpression in TR α 1-PV mice allows for phenotypic recovery because NCoR Δ ID is decreasing TR α 1-PV's intranuclear mobility. This could ameliorate TR α 1-PV's dominant negative effect on WT TR α 1, allowing WT TR α 1 to perform closer to its standard level and result in a phenotypic recovery similar to those seen in mice. Our second aim was to characterize any impact, if present, that RTH-mutants have on nucleocytoplasmic shuttling. TR α 1 normally undergoes shuttling from the cytoplasm to the nucleus and as needed, back to the cytoplasm, adding a layer of regulation in gene transcription (Anyetei-Anum et al., 2018). TR α 1 relies on several motifs to be able to shuttle, two NLSs, located in the N-terminal transactivation and hinge domains, and multiple nuclear export motifs, including two well-characterized NESs overlapping H3 and H6 (NES-H3 and NES-H6) in the receptor's ligand binding domain (LBD), one located in the LBD's twelfth helix (NES-H12), and an uncharacterized CRM1-dependent NES (Mavinakere et al., 2012; Zhang et al., 2018; Salomon et al., 2020). RTH-A382PfsX7, F397fs406X, and E403X all have a compromised NES-H12; for the former, it is completely missing, and for the latter two mutants, it is truncated (Moran & Chatterjee, 2016; Evans, 2019). This posed the question as to whether the loss of NES-H12 would impact the mutants' nucleocytoplasmic shuttling, and thereby the transcription of TR α 1's target genes. Heterokaryon assays were performed to investigate this question, as they provide easy qualitative data as the presence, absence, or spectrum of shuttling via fluorescence intensity in the heterokaryon's

mouse nucleus. Our lab has used heterokaryon assays in the past to evaluate TR α 1's nucleocytoplasmic shuttling with success (Bunn et al., 2001; Rosenberg et al., 2020). Due to time constraints, only RTH-A382PfsX7 was able to be studied. Our preliminary results showed that the loss of NES-H12 had no qualitative impact on RTH-A382PfsX7's shuttling ability. Both WT TR α 1 and RTH-A382PfsX7 appeared to have relatively similar fluorescence intensities in both mouse and HeLa nuclei in the heterokaryons, suggestive of unimpaired shuttling. As such, it appears that the loss of NES-H12 is not as drastic as we had predicted. This raises questions as to how significant NES-H3/H6 are to the shuttling process, how much they are compensating for the loss of NES-H12, and what are the mechanisms behind this loss. The first step to answering these questions, however, would be to perform this assay on RTH-F397fs406X and E403X as well. These two mutants have the first few N-terminal amino acids of NES-H12, which could potentially cause these mutants to act differently compared to RTH-A382PfsX7, which has a completely missing NES-H12. Not only could this provide insight into these RTH α mutants' dynamics, but this knowledge could provide insight into the importance of each NES to the nuclear export mechanism.

Chapter 5: Conclusions

As clearly shown in the case reports that first documented RTH-E403X (Bochukova et al., 2012), F397fs406X (van Mullem et al., 2012), and A382PfsX7 (Moran et al., 2013), single nucleotide changes to TR α 1's ligand binding domain (LBD) can have drastic impacts on a person's development, physiology, metabolism, and intellect. This is due primarily to the mutants' poor binding affinity to thyroid hormone and their dominant-negative effect on TR α 1 (Bochukova et al., 2012, van Mullem et al. 2012, Moran et al., 2013). While most mutations in the ligand binding domain of TR α 1 would result in poor hormone binding and associated activity changes, these mutations created the possibility for changes in TR's protein-protein interactions and nucleocytoplasmic shuttling due to the total loss or truncation of the LBD's twelfth helix; this helix contained not just a nuclear export motif (NES-H12), but also is hypothesized to allow for NCoR1 dissociation—any compromise of H12 could result in NCoR1 increased binding affinity to the mutants and affect their functionality. We therefore evaluated the mutants' functionality based on their intranuclear mobility with FRAP, and began pilot studies into nucleocytoplasmic shuttling, beginning with RTH-A382PfsX7. Our FRAP assays revealed some unforeseen results with equally interesting implications. Despite the exposed H12 (RTH-F397fs406X and E403X) or completely missing H12 (RTH-A382PfsX7), NCoR1's increased affinity to these mutants does not impact their intranuclear mobility. Therefore, NCoR1 interaction is likely not a mechanism that results in the decreased functionality of these mutants, beyond poor thyroid hormone binding. However, a synthetic NCoR1 mutant, NCoR Δ ID, that does not bind to wild-type TR α 1 was able to slow down the intranuclear mobility of RTH-F397fs406X and E403X,

yet not that of A382PfsX7. As for the heterokaryons, it was evident that the total loss of H12 does not impact RTH-A382PfsX7's ability to undergo nucleocytoplasmic shuttling. Whether or not a partial truncation of NES-H12 impacts shuttling remains to be seen in future heterokaryon assays involving RTH-F397fs406X and E403X. Our results therefore pose a new model, as shown in Figure 15. Specifically, we suggested that despite the loss of ID2 and ID3, NCoRΔID may still be interacting with RTH-F397fs406X and E403X with its remaining interaction domain, ID1, and affecting the receptors' behavior. It is possible that because the corepressor slowed down the receptors, NCoRΔID may not be able to dissociate from RTH-F397fs406X and E403X. Further investigation may be required into this question, by introducing to this experiment another NCoR1 mutant with all interaction domains. When taken together with *in vivo* heterogenous RTH studies performed by Astapova et al. (2008; 2013) and Han, Cheng, & Park (2017), NCoRΔID may be ameliorating RTHα-F397fs406X phenotypes due to its effect on the mutant's intranuclear mobility, allowing any wild-type TRα1 present to behave in a wild-type fashion. Taken together, our results offer new insight into both RTHα's molecular phenotype and TRα1's baseline functionality.

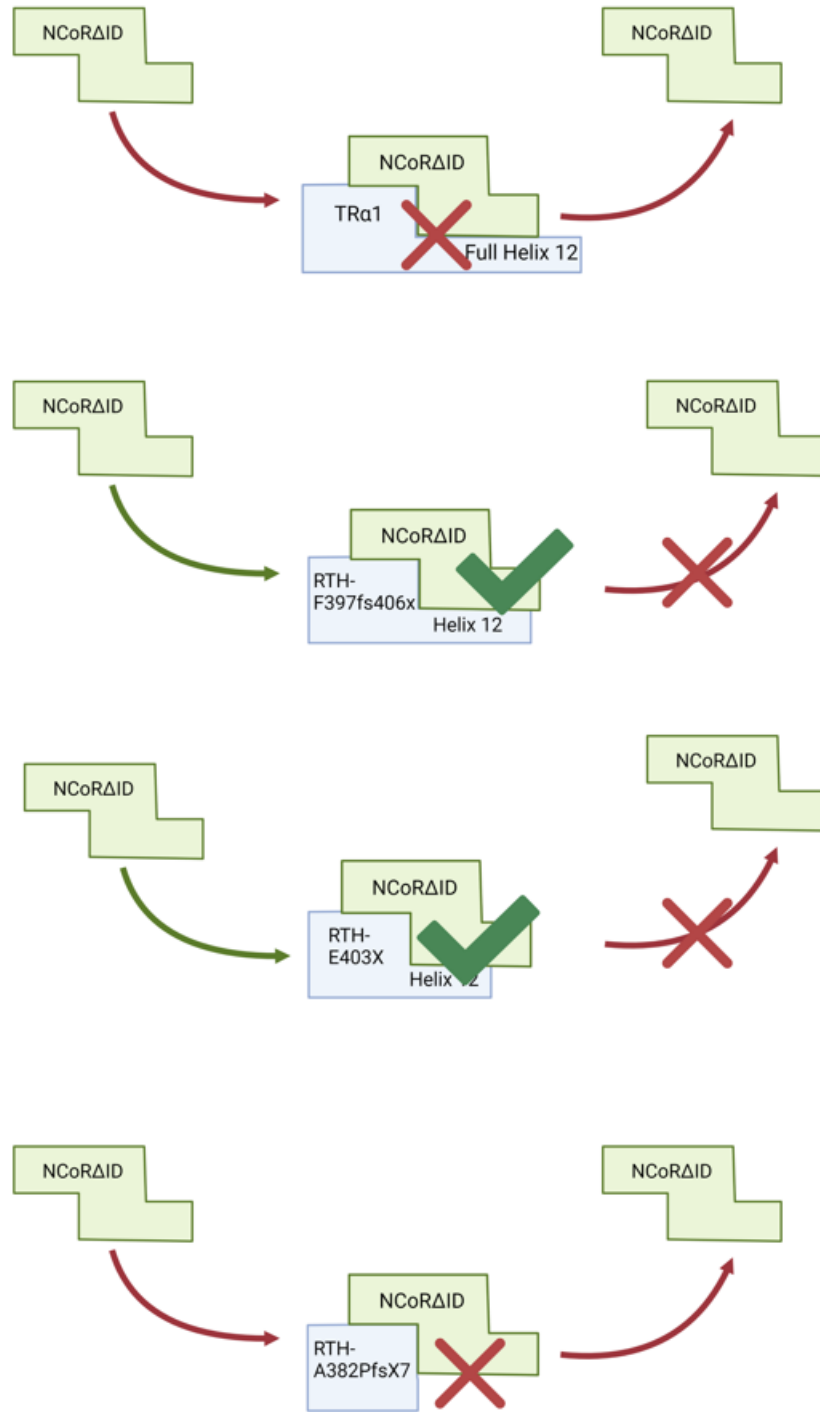


Figure 15: Suggested Model: NCoRΔID may bind to RTH-F397fs406X and E403X. Here we present a new model – NCoRΔID may be able to bind to RTH-F397fs406X and E403X and have trouble dissociating despite the loss of ID2 and ID3. Created with BioRender.

Appendix

The following is the Keyence BZ-X800 user manual created for the Allison Lab.

Keyence BZ-X800

Allison Lab

COMPLETE SOFTWARE OPERATIONS MANUAL



WILLIAM
& MARY

CHARTERED 1693

Foreword

Hi there! I'm glad that you have decided to take the time to learn how to not to break this wonderful piece of equipment. Karma has already begun to work in your favor – congrats! If you want it to keep building up your karma, please continue to peruse through this manual and learn how to use, love, and care for it so it will not hate you, break just to spite you, and ruin all of your data. I have included the tips and tricks I have learned while using it so that if you want, you can go from knowing how not to break it to knowing how to use it and make pretty photos! ALL THE PRETTY PHOTOS (which is, let's be honest, the real reason we are here – the ultimate DIY desktop background). I hope you enjoy using this microscope as much as I have, and that my instructions are easy to follow – if not, find Vinny or Liz – they know some stuff too. Good luck, and may the Force be with you and your data!

Best,
Page T.

P.S. If you discover anything new or interesting that isn't covered in this manual, or if there is a software update after I graduate, write down your discovery! Put it in the binder! There's only so much I know about this microscope, so the more fun things you all discover about it, the better!

OPERATIONS MANUAL

TABLE OF CONTENTS

	<u>Page #</u>
1.0 GENERAL INTRODUCTION.....	71
1.1 System Overview	71
1.2 Authorized Use Permission	72
2.0 SYSTEM OVERVIEW	74
2.1 System Overview	74
2.2 BZ-X800 Viewer Software Overview	74
2.3 BZ-X800 Analyzer Software Overview	75
3.0 STARTING IP	3-79
4.0 SOFTWARE OPERATION.....	4-Error! Bookmark not defined.
4.1 Operating the BZ-X800 Viewer Software.....	4-83
4.2 Operating the BZ-X800 Analyzer Software	4-Error! Bookmark not defined.
5.0 SHUT DOWN PROTOCOL	5-1

1.0 GENERAL INTRODUCTION

GENERAL INTRODUCTION

Thanks for continuing your interest in learning how not to break the microscope! Before you can begin using it, let's cover the most important part of operating any microscope: its component parts.

In this section, we will cover key parts of the Keyence itself, and any other introduction to help you get started.

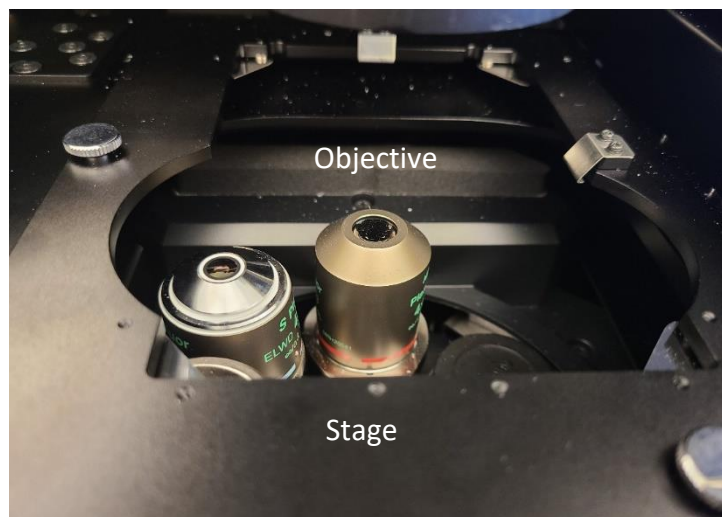
1.1 System Overview

The Keyence BZ-X800 condenses component, hardware parts of a fluorescence microscope into one, compact machine. This includes:

- Objectives (room for 6 in this microscope)
- Light Source (Brightfield and Phase Contrast)
- Lasers
- Excitation Filters
- Emission Filters

among other things (all of which have equally fancy-sounding names). However, there is one piece missing - the eyepiece. This has been replaced with a viewing software that allows you to see your specimen on a desktop computer. The scope also includes:

- Its own darkroom, provided by the lid
- Fully motorized stage with changeable holders





1.2 Authorized Use Permission

Prior to using the scope, please sign up on the calendar for a designated time. Upon signing up, please keep to that time frame. A lot of lab members use this scope, and we want to ensure that they have time to create beautiful images. Thanks in advance!

2.0 System Overview

SYSTEM OVERVIEW

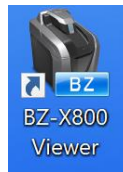
2.1 System Overview

This section provides an overview of the softwares associated with the microscope – the Viewing software and the Analyzing software. More specifically, it will provide an overview of the component parts of each software that you are likely to use. For more details on how to use the softwares, please refer to **Software Operations**.

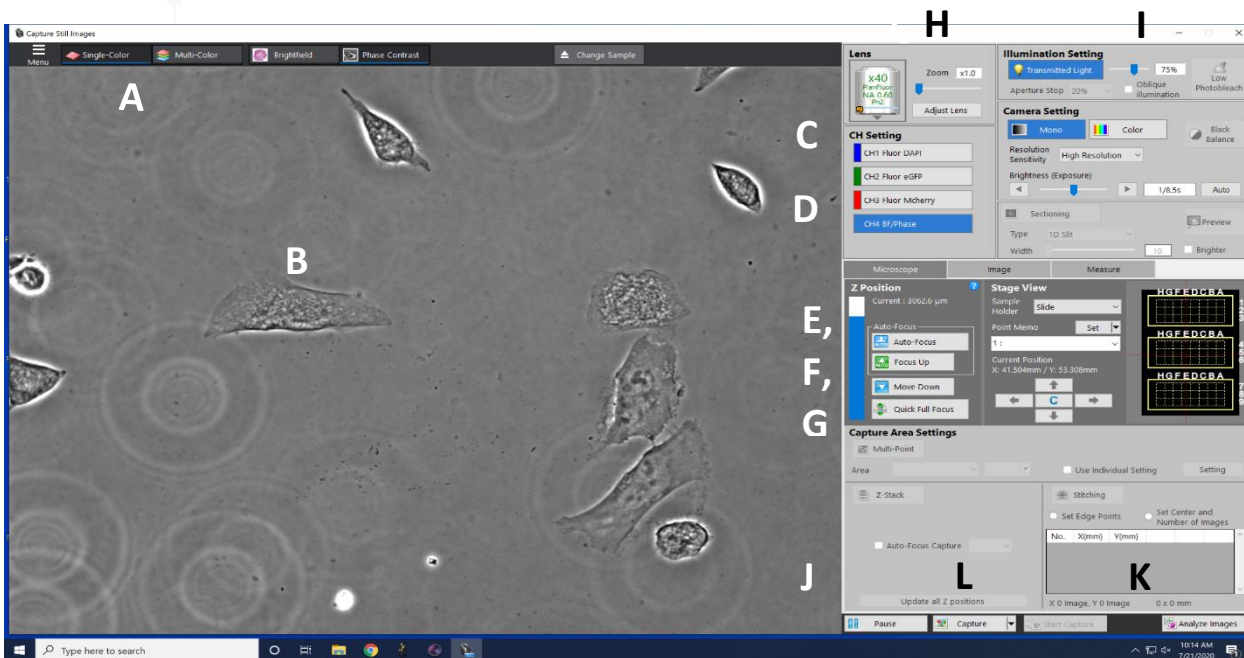
2.2 BZ-X800 Viewer Software Overview

This software serves as the viewer for your specimen given the lack of an eyepiece, as well as serving as the interface that controls the mechanics of the microscope – aspects such as focus, exposure, and light sources. Below is a list of what you see upon opening the Viewer Software, as well as an image of the screen. Each part is lettered to match corresponding labels on the screen.

To access the software, select the following desktop icon:



An overview of what you will see upon opening the software:

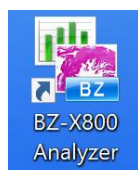


- A. Viewing Pane:** View of your specimen in the software as the microscope sees it. This is also where you can control the stage.
- B. Light Control:** select what light source(s) you wish to use. The options available are bright field, phase contrast, and fluorescence. Select which fluorescence excitation wavelengths to use by selecting their corresponding channels.
- C. Channels:** The channels listed show what laser excitation wavelengths are available to you when examining fluorescence.
- D. Lens:** which objective is in use
- E. Microscope:** control position of the stage in the X, Y, and Z dimensions
- F. Image:** control aspects of the image, such as contrast and saturation
- G. Measure:** add measurement aspects to your image, such as scale bars
- H. Illumination:** How much light you want shined on the specimen
 - a. **Photobleach Mode:** select low photobleach mode to protect your samples from photobleaching.
- I. Camera Setting:** where to control the camera's settings to obtain the ultimate photo (ex. Brightness, resolution)
- J. Capture Area Settings:** perform more advanced options not included in our current software update.
- K. Capture:** Capture a photo of your specimen. It will capture what you see in the Viewing Pane.
- L. Live/Pause :** change between live scanning and paused scanning

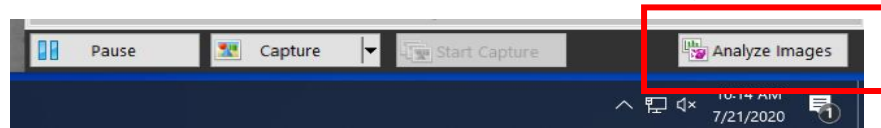
2.3 BZ-X800 Analyzer Software Overview

This software allows you to begin analyzing your images from the Viewer. Important component parts will be listed below, and an image of the screen will be included. Each part will be labeled on the image, corresponding to the list. The software can be accessed three ways:

Select the following desktop icon,



Select **Analyze Images** in the Viewer Software at the bottom right corner,



or access it upon capturing an image – once an image is captured, the Analyzer will open automatically.

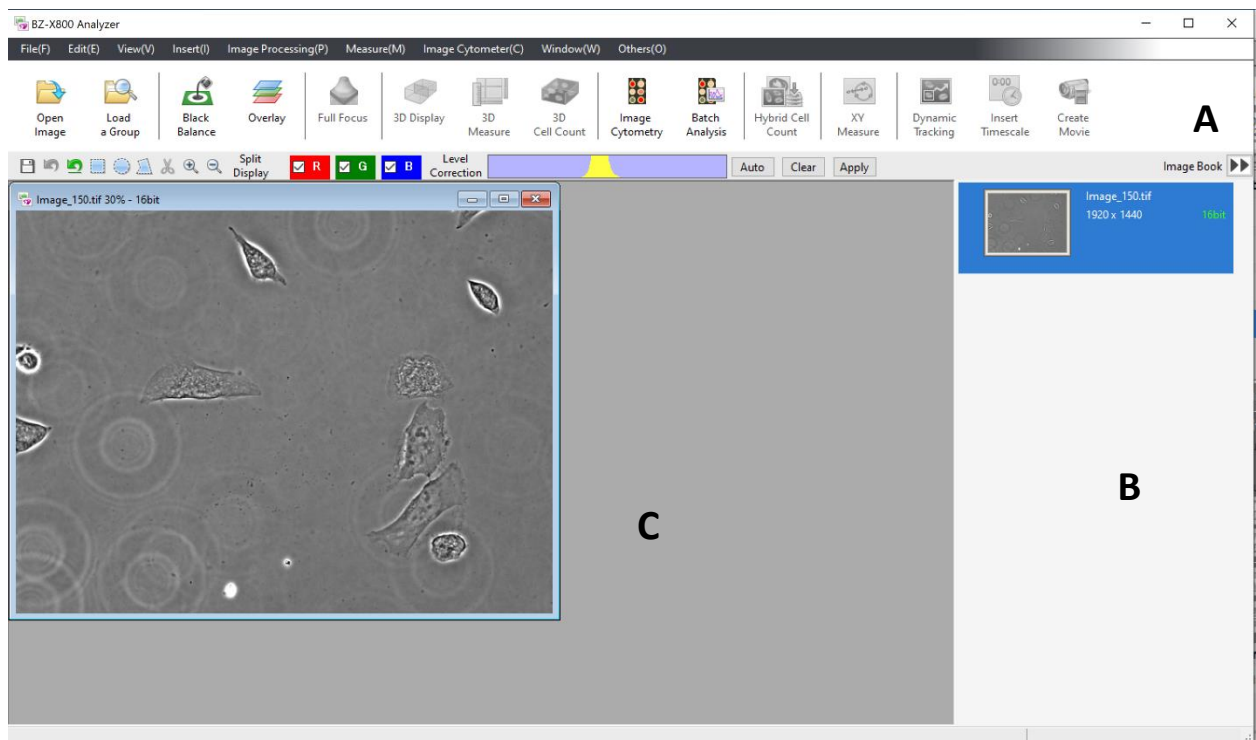
Overview of the software:

A. Shortcut Toolbar: Pre-loaded shortcuts to certain functions

- a. **Note:** As of July, 2020 we do not have the software necessary for all functions listed on this bar – only the software for what we need. If grey, we either do not have that software, or it is not necessary for the type of image analysis you are performing. If it is necessary, the icon will colorize.

B. Image Book: A list of all images pulled into the software

C. Viewer: what image you want to work on



NOTE: For some analysis functions to work, a flashdrive with all of the necessary components has been inputted into the back of the CPU case (big black box next to the desktop). **DO NOT REMOVE ANY COMPONENTS PLUGGED INTO THE BACK.** If you wish to load some information onto a personal flashdrive, plug your drive into one of the three USB ports located in the front of the case.

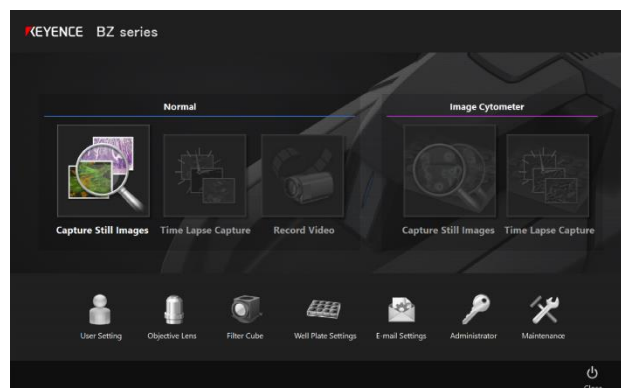
3.0 STARTING UP

3.1 Starting Up

STOP- did you sign up for a time slot? If not, SIGN UP FOR A SLOT.
Thanks!

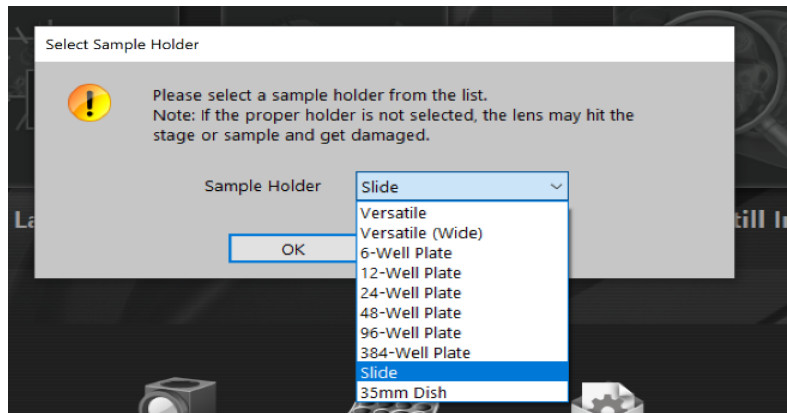
Assuming you signed up for a slot and know when the next person is coming in, feel free to follow these steps to start up the Keyence, the Viewing Software, and the Analyzer Software.

1. Turn on the **Precision 3630** (CPU case) and desktop, and log in
 - a. **Username:** .\Allison Lab
 - b. **Password:** Thyroid
2. Press power button on the bottom right corner of the front of the microscope.
3. Ensure the correct stage is in place according to how you are viewing your specimen (slide, 6 well plate, etc.)
 - a. **To change the holder**, grab the long edges of the current holder and gently lift up. To place a different holder in, gently press the holder into the stage until it clicks in place.
4. Place your specimen in the stage
 - a. **FIXED SLIDE:** Place coverslip – side down
 - b. **WELL-PLATES:** Place face-up – do not invert! The scope will be able to see your specimen as long as your cells (HeLa or otherwise) are seeded on a coverslip
5. Access the imaging software by clicking the **BZ-X800 Viewer** icon. The following window will open:



6. Select **Capture Still Images**

7. Select what you sample holder you are using (slide, 6 well plate, etc) and open



the software.

8. When in the software, check under **Lens** to see which lens is selected. Ensure the lowest objective is selected (ex., 4x)

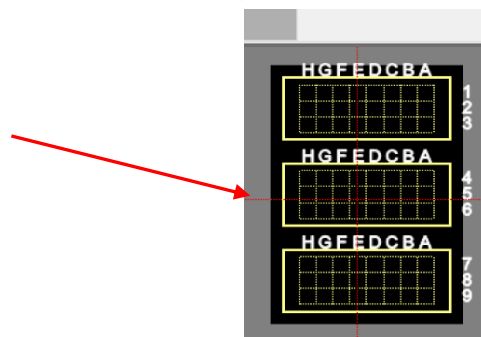
- a. REMINDER: to change the lens, click the icon below and select the lowest objective available



9. Stand up, stretch, then proceed to watch a bunch of Facebook videos- you've done so much already over the course of 2 minutes, you deserve a break!

10. Center the lowest objective on your specimen: there are 3 methods to do so

- i. Click the location of your specimen on the available stage grid (ex. if you were using slides)



1. Where the red lines intersect shows you where you are on the slide/well, etc.
 2. The layout of the grid will change depending on what sample holder you have selected. The above sample is the slide holder grid
- ii. Click and drag along the **Viewing Pane**

Continue scrolling through Facebook, or Instagram, until you are ready to start creating your new background! Have fun!

4.0 SOFTWARE OPERATION

4.0 SOFTWARE OPERATION

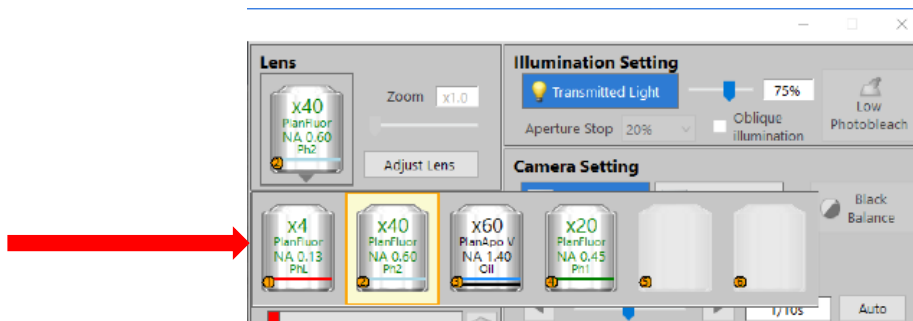
This section provides more detail into operating the Keyence BZ-X800's Viewer and Analyzer softwares, once set up. For a brief reminder of component parts, refer to the previous section. Images will be provided to help direct you with more specific functions and associated buttons.

4.1 Operating the BZ-X800 Viewer Software

The BZ-X800 Viewing Software may seem intimidating at first, but obtaining your new desktop background will be oh, so much easier. If you need a refresher on the components of the software, see **Getting to Know the Keyence BZ-X800**.

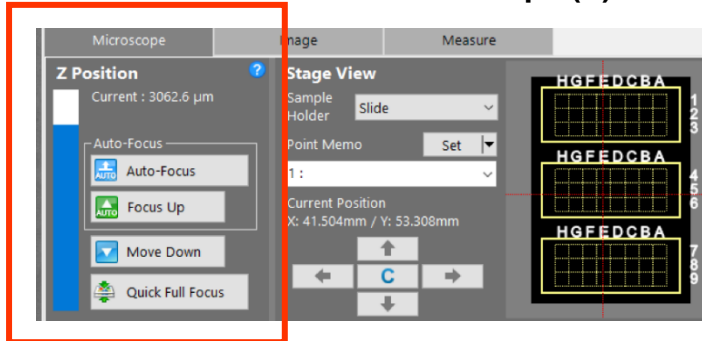
NOTE: the Allison Lab has a **DATA** hard drive, which can be accessed on all associated computers. I recommend you save all images there, under a folder with your name on it.

- **Changing Objectives:** This was briefly introduced in **Starting Up**, but I will reintroduce how to change the objective used. The lens you are using will be shown under the **Lens** tab in the viewing software. To change between lenses:
 - Click on the image of the current lens
 - Select which lens you want to use from the menu below



- **Changing light intensity:** scroll through **Brightness (Exposure)** under **Camera Setting**
- **Focus:** Moving in the Z dimension: must have the **Microscope** tab selected
 - **Manual Focus:**
 - **Coarse Focus:** press **Ctrl** and scroll with the mouse.

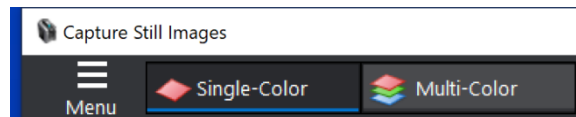
- **Fine Focus:** Scroll with the mouse. No additional keys required.
- **Extra Fine Focus:** press **Shift** and scroll with the mouse.
- **Auto Focus:** Found under the **Microscope (E)** tab as Z-Position



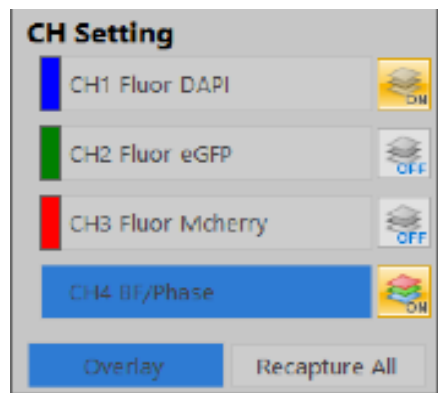
- **Auto-Focus:** select to automatically focus on specimen
- **Focus Up:** automatically focus on the layer of your specimen above your current position (in the Z-Dimension)
- **Move Down:** move the stage down to the lowest height (~2365 μ m)
- **Quick Full Focus:** automatically creates a full-focus image of a thick sample (for example, a live image)
 - *NOTE:* this is not necessary for fixed slides – the cells are too flat
- *NOTE:* I prefer using only **Manual Focus** since it provides more control. Auto Focus is incredibly convenient, but it can at times focus on particles of dust or other random specks that may be inadvertently in your sample. If this is the case, I recommend **Manual Focus**. Quickly fix an incorrect focus with **Coarse Focus** until you see your specimen.
- *NOTE II:* You can only move the stage up until just under 3600 μ m. Do not force the software to go past this as you will hit the objective against the specimen and potentially break the glass on the lens
- **Moving the Stage:** XY Dimension
 - **Manual:** Click and drag on the viewing pane to move the stage around
 - **Automated:** Select an area on the Stage Grid (see Starting Up, step 10) to direct the stage to focus on the area of interest.

- *NOTE:* basic microscope optics still apply: your specimen will be inverted and flipped on your screen as it would if you were using a standard compound microscope.
 - Track where you are using the stage grid in the **Microscope** tab – where the red lines intersect indicates where you are

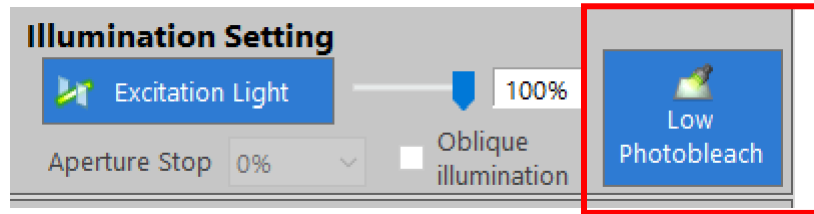
- **Changing Light Source**



- Select how many light sources you want to use, located at the top bar:
 - **Single-Color:** allow only one light source at a time
 - **Multi-Color:** allow for multiple light sources to be shown
 - aka **OVERLAYING** your light sources. For example, if you want to show DAPI and eGFP fluorescence at the same time
- **Channels:** click on the desired fluorescence excitation channel / light source you need to change the channel



- **NOTE** – if using fluorescence, **MAKE SURE Low Photobleach** is clicked! Otherwise your sample will photobleach and the fluorophores won't fluoresce



- **To overlay:** select the **Multi-Color** button at the top of the screen to overlay, then select all of the light sources you want to see
 - In the example above, the DAPI and BF/Phase contrast are overlaid

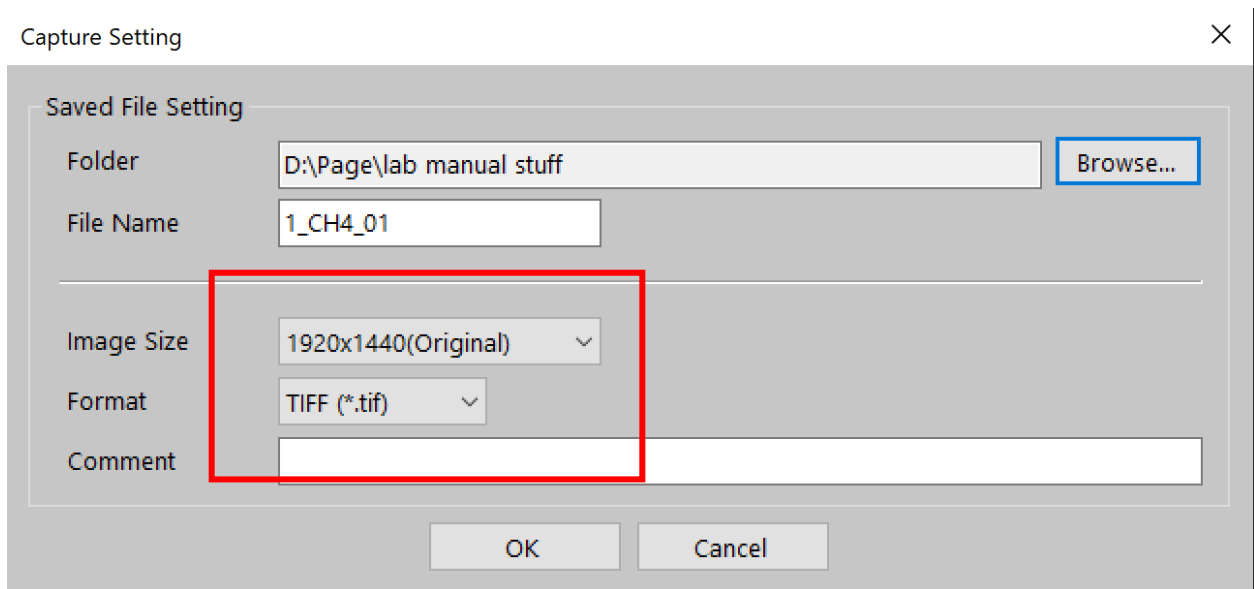
- **To change Phase Contrast/ Brightfield:** Click on which you would prefer while you have the BF/Phase channel selected and open

- You can select as many fluorescence excitation channels as desired, but can only choose one traditional light source option at a time – bright field or phase contrast
- **Capturing an Image:** in both instances below, make sure imaging is live and press Capture in the bottom right corner to take the photo (should look like this):

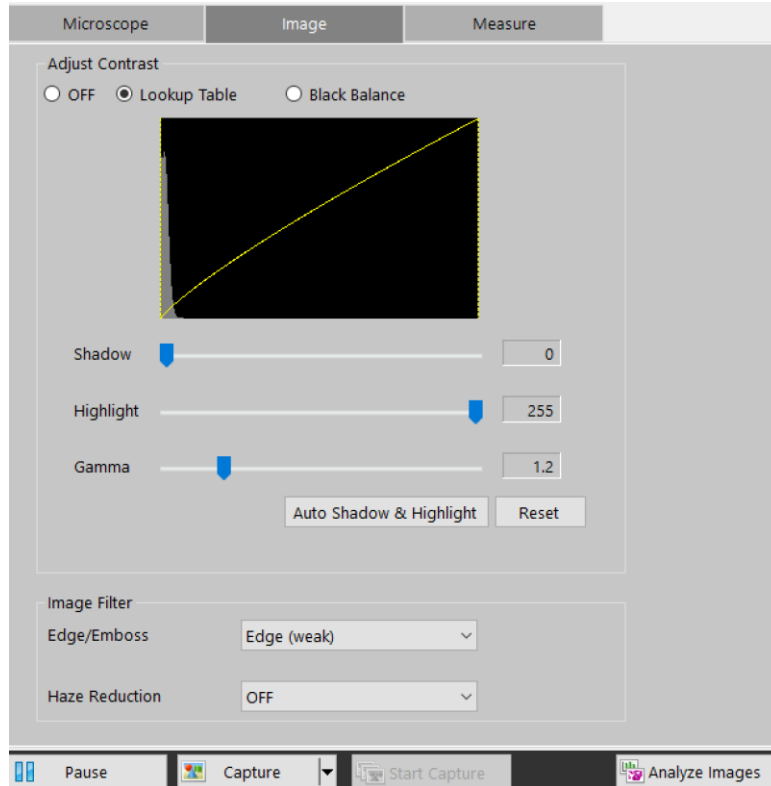


- **Single Color:** use if you want an image using only one light source. Have the color option selected to **Single Color**, then **Capture**.
- **Overlay:** use if you want to capture an overlay image. View your image in Multi-Color mode and Capture.
 - When prompted, select how many layers you want, and where to save the images, and press **OK**
 - How many layers you have depends on how many light sources you have. For example – a bright field with DAPI and eGFP is three-layered, so the software will take and save 4 images – one of each layer, and one final overlaid image

- **NOTE: IMAGE SIZE – please keep at the following image size to ensure consistent analysis**

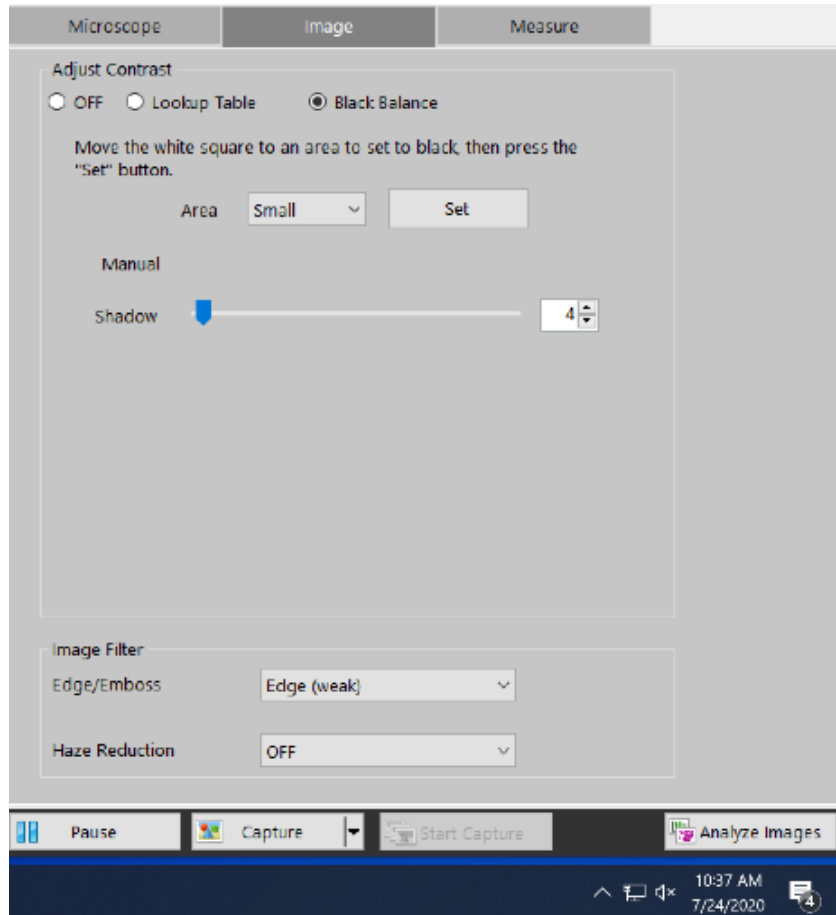


- **Extra Imaging Techniques:** You can change certain aspects of the images in real time, such as enhancing contrast and balancing a black background. For this, we will be working in the **Image** tab in the Viewing Software

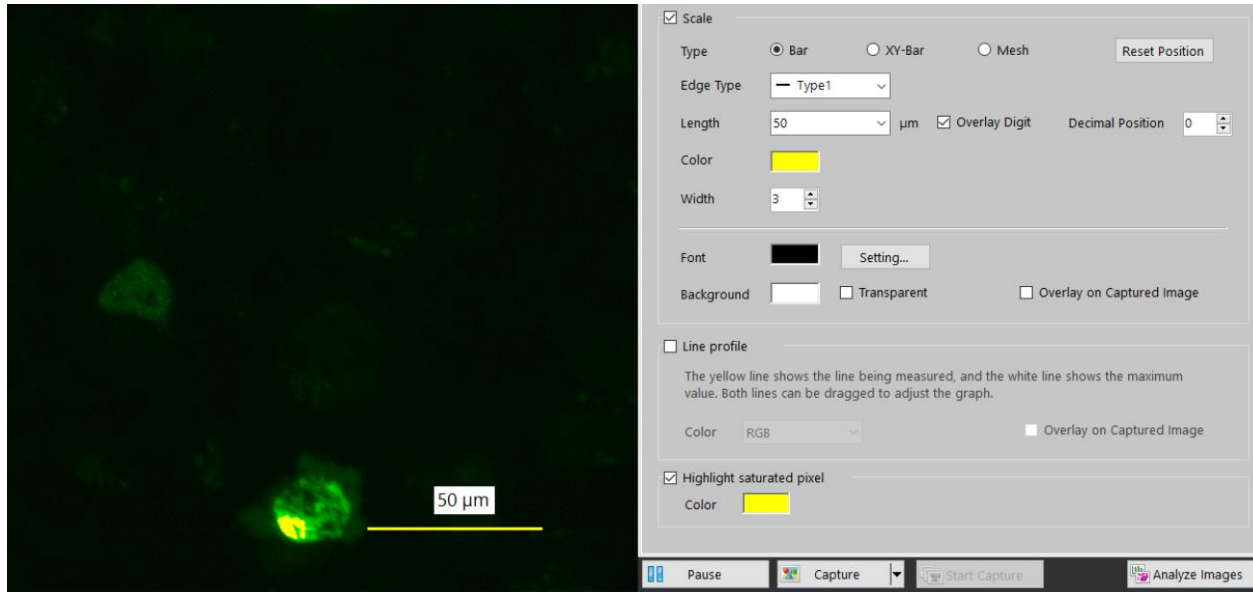


- **Contrast:** Select **Lookup Table** and adjust the shadow, highlight, and gamma correction
 - **Gamma correction** is a photography concept that helps bring out shadows, and makes the curve in the graph above less linear
- **Edge/Emboss:** Select how much edge or embossing you want to see around and in your cells.
 - The higher the edge level, the harsher the image looks.
 - The higher the embossing, the easier it is to see the outline of the cell, but with loss of intracellular detail
 - *NOTE:* For this reason, I find using phase contrast alone helps with ensuring the edges are neat while maintaining detail

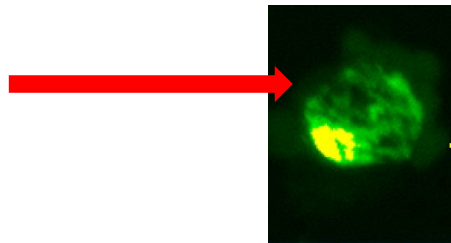
- **Haze Reduction:** Use for Brightfield / Phase Contrast settings. Increasing the haze reduction will sharpen your images to a certain degree, but can overcompensate if your images are not hazy to begin with. Use sparingly
 - **Black Balance:** Use primarily for fluorescence without Phase Contrast or Brightfield. Reduce noise.



- Select Black Balance under **Image**,
 - Select a black area in your image, scaling the square in the Viewer Software's **Viewing Pane** to your desired size
 - Use the **Shadow** bar to shift how much shadow you want to see in the image, based on the background scanned in the square
- **Adding Measurements: Found under Measure (G):** This is where you can add things like scale bars, as well as keep track of fluorescence oversaturation – see next page



- **Scale:** select what type of scaling tool you want to use – bar, XY-bar, or mesh- what it looks like, how long is it, color, and width.
 - *NOTE:* the Keyence automatically knows how long a given area is under each objective, and will scale the length of the bar according to what you want (50μm, 100μm, etc.)
- **Line Profile:** measure the fluorescence intensity along the X axis of your image at any Y position
- **Highlight Saturated Pixel:** Use to track if your are oversaturating the fluorophores with too much laser intensity. It will highlight the saturated/oversaturated area a color of your choosing (see arrow for example)



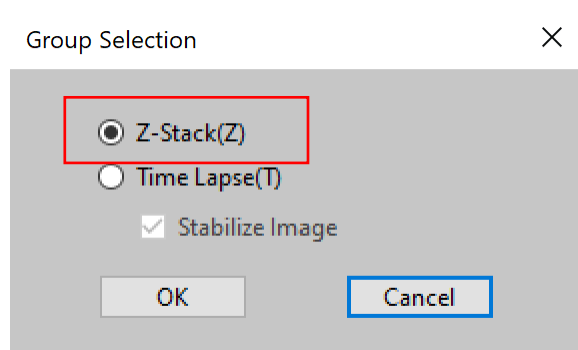
3.2 Operating the BZ-X800 Analyzer Software

Now that we have some gorgeous images, we need to analyze them. The analysis software allows us to do some initial analyses, however if looking at features such as fluorescence intensity for an N/C ratio, other softwares can be useful as well.

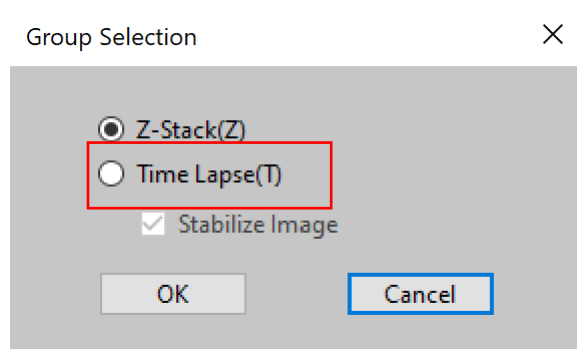
This software also has the capability of combining multiple images into varying animated images, as well as merging multiple images together as needed. Please see below to learn how to do Z-stacks, Time Lapses, and Merged Images.

NOTE: for each of these options, save your multiple images in an easy-to-access folder.

- **Z-Stack:** use to create a three-dimensional image of your specimen (assuming it's live and not fixed flat on a slide - I'm afraid there's not much depth to look at in that scenario).
 - Scroll in the Z-dimension through your specimen, beginning at the bottom and working incrementally to the top. At each increment (say, 2 μ m), capture the image and save it to your easy-to-access folder.
 - *NOTE:* if you want to perform a Z-Stack on an **Overlay**, move your final, overlay images out of the automatically generated folder with all captured images to a separate, Overlay- only folder that you can easily access
 - Drag your folder with your saved images to the **Analysis Viewer**
 - *NOTE:* you must drag the FOLDER and not individual images. It will not work on individual images
 - When prompted, select **Z-Stack**, then OK. The software will compile all images in your folder to one Z-Stack image that you can scroll through

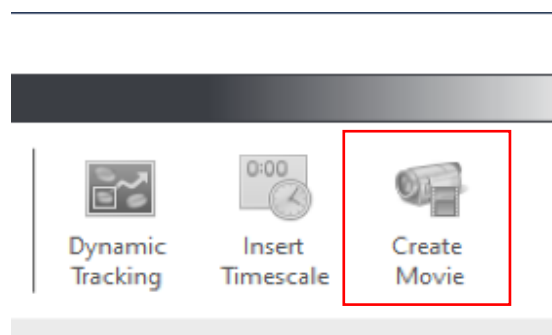


- Save the Z-Stack in your **DATA** hard drive folder for easier access
- **Time Lapse:** use to create a time lapse of live cells (again, won't do much good if fixed flat on a slide – your specimen just may find it hard to move).
 - **Capture** images of your specimen at desired time increments (say, every 10 minutes), and save them to an easy-to-access folder.
 - *NOTE:* if you want to perform a Time Lapse on an **Overlay**, move your final, overlay images out of the automatically generated folder with all captured images to a separate, Overlay- only folder that you can easily access
 - Drag the folder with your saved images to the **Analysis Viewer**
 - *NOTE:* you must drag the FOLDER and not individual images. It will not work on individual images
 - When prompted, select **Time Lapse**, then OK. The software will compile all images in your folder into a time lapse slideshow that you can click

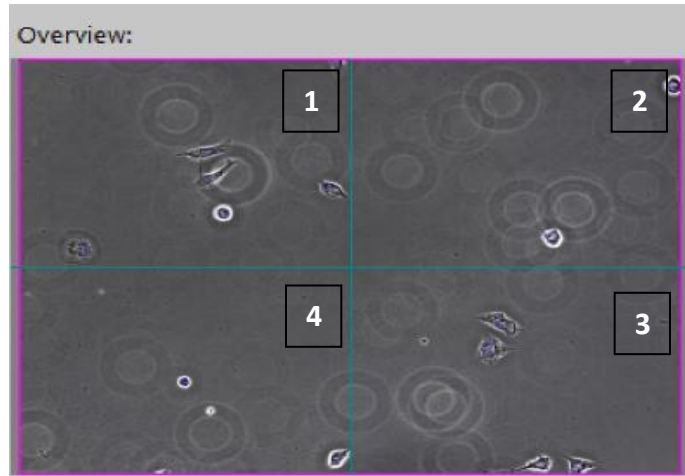


through.

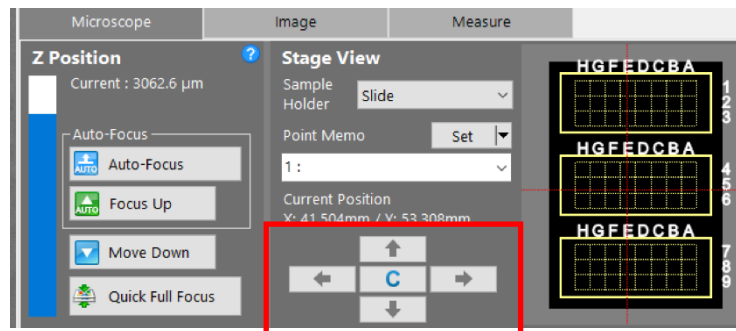
- To make a **Time Lapse Movie** out of your slideshow, keep your slideshow open and in the Analyzer, click **Create Movie** in the **Shortcut Toolbar**



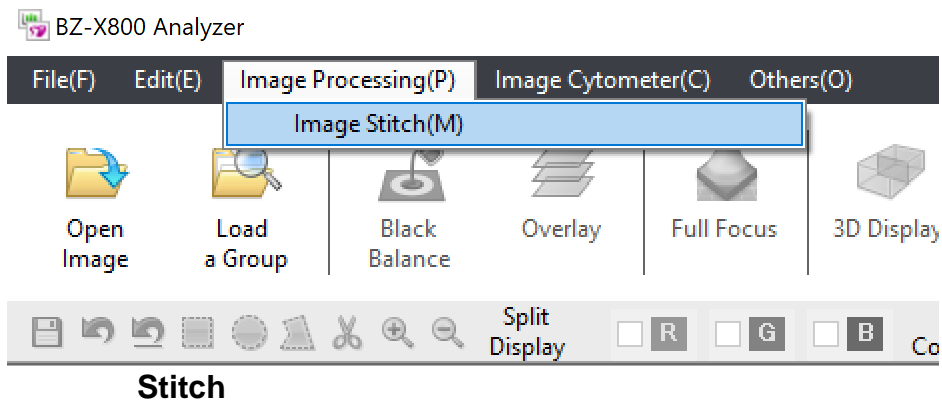
- Save your time lapse in your **DATA** hard drive folder for easier access
- **Stitched Images:** use to join, or “stitch,” multiple images into one larger image
 - **Capture** images of your specimen at given intervals, following a “grid of squares/rectangles,” with each square representing each image you take
 - Ex: below is a final stitched image with a 2 x 2 grid. The numbers mark the order in which the images were taken



- *Image 1:* Capture your first image and think about where it is in your grid.
 - In the example above, the first image taken was the top left image
- *Image 2:* Using the arrows surrounding the **Current Position** button (aka the **C**) under **Microscope** in the viewing software, move to the next square in your grid, then **Capture**

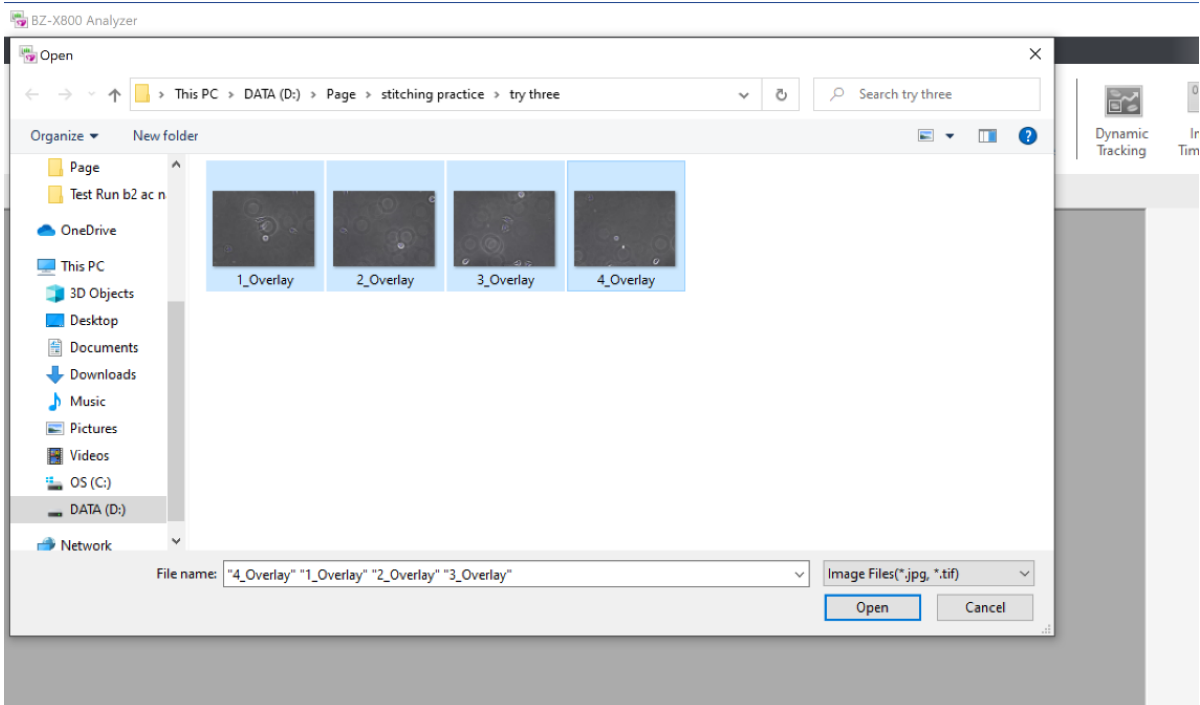


- *NOTE:* The arrows are preset in distance moved (1 μ m) – do not change! Instead, change how many times you click to increase the distance
- In the example above, the right arrow was clicked twice for a 2 μ m shift to the right to create the second image
 - REPEAT for all further images, going row by row. After you complete your first row, go down one square in your grid to begin the next row. Continue back through the row to complete the second. Repeat as needed
- Save your images to an easy to access folder
- Stitch your images using the following steps
 - In the Analysis software, select **Image Processing**, then **Image**

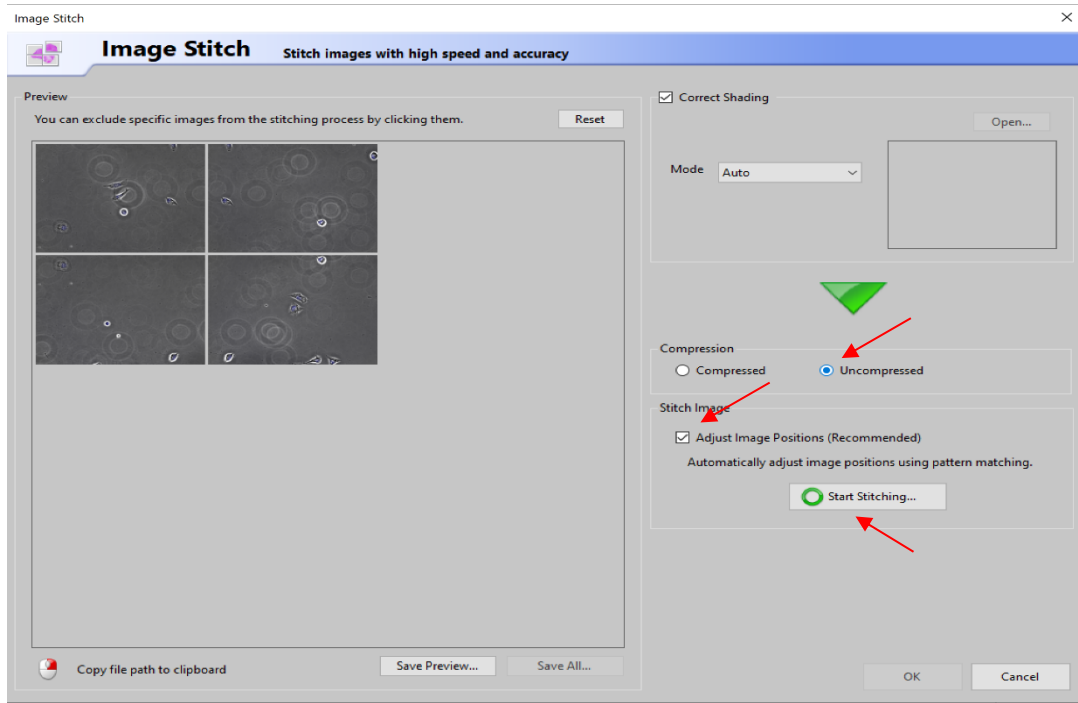


- Select the images you want stitched in your folder, and click **Open**

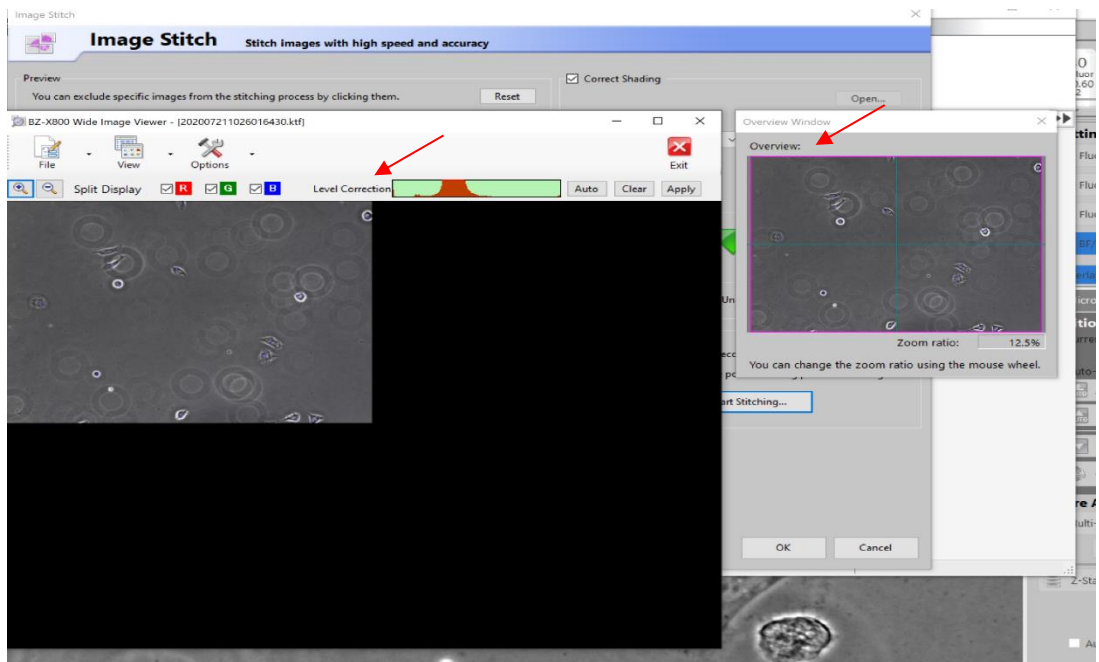
- **NOTE:** The Keyence will memorize where on your slide the image was taken and store that info in the images, so when you upload the images it may seem out of order, but the Analyzer software will know how to organize the images along your grid



- In the new pop up window, select **Uncompressed**, keep **Adjust Image Positions** clicked, then press **Start Stitching** to create the final image



- The final image will pop up in a window like the one below. You may scroll through it, change the contrast with **Level Correction**, and change the area of interest on your stitched image based on the location of the purple square in the **Overview**



- Save your image to your folder in the **DATA** hard drive

5.0 SHUT DOWN PROTOCOL

5.0 Shut down protocol

This part's pretty straightforward compared to the earlier procedures. But just in case you want to make sure you don't break it during this part of the day (I don't blame you – you made it this far without breaking it!), then I've created a little checklist below to complete to ensure you shut down everything correctly.

- Ensure all images, z-stacks, and time lapses you have created are saved to an easy access folder in the aforementioned **DATA** hard drive, lest we want to lose all of our hard work and beautiful images!
- Set the microscope to the lowest objective (generally, the **4x**)
- Close out of the Viewer and Analyzer softwares
- Turn off the desktop and CPU case, but leave the microscope on for now
- If you haven't already, remove your specimen from the stage and store it properly
- Clean off any objectives used with lens paper
- Turn off the microscope and close the lid
- **Place the cover over the microscope**

And that's it! Thank you for taking the time to learn how to use / not break this microscope. Continue down this path, and beautiful images will await you! Don't be afraid to ask senior lab members for help if you are unsure about anything. And again, if you discover something new about the microscope that wasn't covered here, write it down and pass on the information. The more we learn about the scope, the better it will serve us.

Good luck and have fun!

References

- Anyetei-Anum, C. S., Roggero, V. R., & Allison, L. A. (2018). Thyroid hormone receptor localization in target tissues. *The Journal of Endocrinology*, *237*(1), R19–R34.
<https://doi.org/10.1530/JOE-17-0708>
- Aranda, A., Alonso-Merino, E., & Zambrano, A. (2013). Receptors of Thyroid Hormones. *Pediatric Endocrinology Reviews*, *11*(1), 13.
- Arnold, L. A., Kosinski, A., Estébanez-Perpiñá, E., & Guy, R. K. (2007). Inhibitors of the Interaction of a Thyroid Hormone Receptor and Coactivators: Preliminary Structure–Activity Relationships. *Journal of Medicinal Chemistry*, *50*(22), 5269–5280.
<https://doi.org/10.1021/jm070556y>
- Astapova, I. I. (2016). Role of co-regulators in metabolic and transcriptional actions of thyroid hormone. *Journal of Molecular Endocrinology*, *56*(3), 73–97.
<https://doi.org/10.1530/jme-15-0246>
- Astapova, I., Lee, L. J., Morales, C., Tauber, S., Bilban, M., & Hollenberg, A. N. (2008). The nuclear corepressor, NCoR, regulates thyroid hormone action in vivo. *Proceedings of the National Academy of Sciences*, *105*(49), 19544–19549.
<https://doi.org/10.1073/pnas.0804604105>
- Astapova, I., Vella, K. R., Ramadoss, P., Holtz, K. A., Rodwin, B. A., Liao, X.-H., Weiss, R. E., Rosenberg, M. A., Rosenzweig, A., & Hollenberg, A. N. (2011). The Nuclear Receptor Corepressor (NCoR) Controls Thyroid Hormone Sensitivity and the Set Point of the Hypothalamic-Pituitary-Thyroid Axis. *Molecular Endocrinology*, *25*(2), 212–224.
<https://doi.org/10.1210/me.2010-0462>

Black, B. E., & Paschal, B. M. (2004). Intranuclear organization and function of the androgen receptor. *Trends in Endocrinology & Metabolism*, 15(9), 411–417.

<https://doi.org/10.1016/j.tem.2004.09.006>

Bochukova, E., Schoenmakers, N., Agostini, M., Schoenmakers, E., Rajanayagam, O., Keogh, J. M., ... Chatterjee, K. (2012). A Mutation in the Thyroid Hormone Receptor Alpha Gene. *New England Journal of Medicine*, 366(3), 243–249.

<https://doi.org/10.1056/NEJMoa1110296>

Bonamy, G. M. C., & Allison, L. A. (2006). Oncogenic conversion of the thyroid hormone receptor by altered nuclear transport. *Nuclear Receptor Signaling*, 4, e008.

<https://doi.org/10.1621/nrs.04008>

Bonamy, G. M. C., Guiochon-Mantel, A., & Allison, L. A. (2005). Cancer promoted by the oncoprotein v-ErbA may be due to subcellular mislocalization of nuclear receptors. *Molecular Endocrinology (Baltimore, Md.)*, 19(5), 1213–1230.

<https://doi.org/10.1210/me.2004-0204>

Bondzi, C., Brunner, A. M., Munyikwa, M. R., Connor, C. D., Simmons, A. N., Stephens, S. L., Belt, P. A., Roggero, V. R., Mavinakere, M. S., Hinton, S. D., & Allison, L. A. (2011). Recruitment of the Oncoprotein v-ErbA to Aggresomes. *Molecular and Cellular Endocrinology*, 332(0), 196–212.

<https://doi.org/10.1016/j.mce.2010.10.012>

Boulon, S., Basyuk, E., Blanchard, J.-M., Bertrand, E., & Verheggen, C. (2002). Intra-nuclear RNA trafficking: Insights from live cell imaging. *Biochimie*, 84(8), 805–813.

[https://doi.org/10.1016/S0300-9084\(02\)01438-4](https://doi.org/10.1016/S0300-9084(02)01438-4)

- Bunn, C. F., Neidig, J. A., Freidinger, K. E., Stankiewicz, T. A., Weaver, B. S., McGrew, J., & Allison, L. A. (2001). Nucleocytoplasmic Shuttling of the Thyroid Hormone Receptor. *Molecular Endocrinology*, 15(4), 512–533. <https://doi.org/10.1210/mend.15.4.0619>
- Conway-Campbell, B. L., Wooh, J. W., Brooks, A. J., Gordon, D., Brown, R. J., Lichanska, A. M., Chin, H. S., Barton, C. L., Boyle, G. M., Parsons, P. G., Jans, D. A., & Waters, M. J. (2007). Nuclear targeting of the growth hormone receptor results in dysregulation of cell proliferation and tumorigenesis. *Proceedings of the National Academy of Sciences*, 104(33), 13331–13336. <https://doi.org/10.1073/pnas.0600181104>
- Davis, P. J., Goglia, F., & Leonard, J. L. (2015). Nongenomic actions of thyroid hormone. *Nature Reviews Endocrinology*, 12, 111.
- DeLong, L. J., Bonamy, G. M. C., Fink, E. N., & Allison, L. A. (2004). Nuclear export of the oncoprotein v-ErbA is mediated by acquisition of a viral nuclear export sequence. *The Journal of Biological Chemistry*, 279(15), 15356–15367. <https://doi.org/10.1074/jbc.M308214200>
- Duma, D., Jewell, C. M., & Cidlowski, J. A. (2006). Multiple glucocorticoid receptor isoforms and mechanisms of post-translational modification. *The Journal of Steroid Biochemistry and Molecular Biology*, 102(1), 11–21. <https://doi.org/10.1016/j.jsbmb.2006.09.009>
- Erbaş, İ. M., & Demir, K. (2021). The Clinical Spectrum of Resistance to Thyroid Hormone Alpha in Children and Adults. *Journal of Clinical Research in Pediatric Endocrinology*, 13(1), 1–14. <https://doi.org/10.4274/jcrpe.galenos.2020.2019.0190>
- Evans, R.M. (2019). *Intranuclear Dynamics of RTHα Mutant Thyroid Hormone Receptors* (Unpublished Master's Thesis). College of William and Mary, Williamsburg, United States.

- Femia, M.R. (2017). *Subcellular Localization Dynamics of Thyroid Hormone Receptor and Mediator Complex Subunit 1* (Unpublished Undergraduate Honors Thesis). College of William and Mary, Williamsburg, United States.
- Femia, M. R., Evans, R. M., Zhang, J., Sun, X., Lebegue, C. J., Roggero, V. R., & Allison, L. A. (2019). Mediator subunit MED1 modulates intranuclear dynamics of the thyroid hormone receptor. *Journal of Cellular Biochemistry*, *n/a*(*n/a*).
<https://doi.org/10.1002/jcb.29532>
- Fernandez, E. J., Gahlot, V., Rodriguez, C., & Amburn, J. (2017). DNA-induced unfolding of the thyroid hormone receptor α A/B domain through allostery. *FEBS Open Bio*, *7*(6), 854–864. <https://doi.org/10.1002/2211-5463.12229>
- Fondell, J. D., Guermah, M., Malik, S., & Roeder, R. G. (1999). Thyroid hormone receptor-associated proteins and general positive cofactors mediate thyroid hormone receptor function in the absence of the TATA box-binding protein-associated factors of TFIID. *Proceedings of the National Academy of Sciences of the United States of America*, *96*(5), 1959–1964.
- Fozzatti, L., Kim, D. W., Park, J. W., Willingham, M. C., Hollenberg, A. N., & Cheng, S.-Y. (2013). Nuclear receptor corepressor (NCOR1) regulates in vivo actions of a mutated thyroid hormone receptor α . *Proceedings of the National Academy of Sciences of the United States of America*, *110*(19), 7850–7855.
<https://doi.org/10.1073/pnas.1222334110>
- Gereben, B., Zavacki, A. M., Ribich, S., Kim, B. W., Huang, S. A., Simonides, W. S., ... Bianco, A. C. (2008). Cellular and Molecular Basis of Deiodinase-Regulated Thyroid

Hormone Signaling¹. *Endocrine Reviews*, 29(7), 898–938.

<https://doi.org/10.1210/er.2008-0019>

Grespin, M. E., Bonamy, G. M. C., Roggero, V. R., Cameron, N. G., Adam, L. E., Atchison, A. P., Fratto, V. M., & Allison, L. A. (2008). Thyroid Hormone Receptor α 1 Follows a Cooperative CRM1/Calreticulin-mediated Nuclear Export Pathway. *The Journal of Biological Chemistry*, 283(37), 25576–25588. <https://doi.org/10.1074/jbc.M710482200>

Hager, G. L., Lim, C. S., Elbi, C., & Baumann, C. T. (2000). Trafficking of nuclear receptors in living cells. *The Journal of Steroid Biochemistry and Molecular Biology*, 74(5), 249–254. [https://doi.org/10.1016/S0960-0760\(00\)00100-X](https://doi.org/10.1016/S0960-0760(00)00100-X)

Houtsmuller, A. B., Rademakers, S., Nigg, A. L., Hoogstraten, D., J, J. H., Hoeijmakers, & Vermeulen, W. (1999). Action of DNA Repair Endonuclease ERCC1/XPF in Living Cells. *Science*, 284(5416), 958–961. <https://doi.org/10.1126/science.284.5416.958>

Hughes, J., Chisholm, D., Ambler, C., Whiting, A., & Girkin, J. (2020). Using FRAP as a Technique to Quantitate Local Reactive Oxygen Species (ROS) Production. *Microscopy and Microanalysis*, 26(S2), 1336–1337. <https://doi.org/10.1017/S1431927620017742>

Köster, M., Frahm, T., & Hauser, H. (2005). Nucleocytoplasmic shuttling revealed by FRAP and FLIP technologies. *Current Opinion in Biotechnology*, 16(1), 28–34.

<https://doi.org/10.1016/j.copbio.2004.11.002>

Laudet, V., & Gronemeyer, H. (2002). *The Nuclear Receptor Facts Book*. Academic Press.

Makowski, A., Brzostek, S., Cohen, R. N., & Hollenberg, A. N. (2003). Determination of Nuclear Receptor Corepressor Interactions with the Thyroid Hormone Receptor.

Molecular Endocrinology, 17(2), 273–286. <https://doi.org/10.1210/me.2002-0310>

- Marimuthu, A., Feng, W., Tagami, T., Nguyen, H., Jameson, J., Fletterick, R., ... West, B. (2002). TR Surfaces and Conformations Required to Bind Nuclear Receptor Corepressor. *Molecular Endocrinology*, 16, 271–286.
<https://doi.org/10.1210/mend.16.2.0777>
- Maruvada, P., Baumann, C. T., Hager, G. L., & Yen, P. M. (2003). Dynamic Shuttling and Intranuclear Mobility of Nuclear Hormone Receptors. *Journal of Biological Chemistry*, 278(14), 12425–12432. <https://doi.org/10.1074/jbc.M202752200>
- Martínez-Iglesias, O., Alonso-Merino, E., & Aranda, A. (2016). Tumor suppressive actions of the nuclear receptor corepressor 1. *Pharmacological Research*, 108, 75–79.
<https://doi.org/10.1016/j.phrs.2016.04.027>
- Mavinakere, M. S., Powers, J. M., Subramanian, K. S., Roggero, V. R., & Allison, L. A. (2012). Multiple Novel Signals Mediate Thyroid Hormone Receptor Nuclear Import and Export. *Journal of Biological Chemistry*, 287(37), 31280–31297.
<https://doi.org/10.1074/jbc.M112.397745>
- Mottis, A., Mouchiroud, L., & Auwerx, J. (2013). Emerging roles of the corepressors NCoR1 and SMRT in homeostasis. *Genes & Development*, 27(8), 819–835.
<https://doi.org/10.1101/gad.214023.113>
- Nascimento, A. S., Dias, S. M. G., Nunes, F. M., Aparício, R., Ambrosio, A. L. B., Bleicher, L., Figueira, A. C. M., Santos, M. A. M., de Oliveira Neto, M., Fischer, H., Togashi, M., Craievich, A. F., Garratt, R. C., Baxter, J. D., Webb, P., & Polikarpov, I. (2006). Structural rearrangements in the thyroid hormone receptor hinge domain and their putative role in the receptor function. *Journal of Molecular Biology*, 360(3), 586–598.
<https://doi.org/10.1016/j.jmb.2006.05.008>

- Normanno, D., Dahan, M., & Darzacq, X. (2012). Intra-nuclear mobility and target search mechanisms of transcription factors: A single-molecule perspective on gene expression. *Biochimica et Biophysica Acta (BBA) - Gene Regulatory Mechanisms*, 1819(6), 482–493. <https://doi.org/10.1016/j.bbagr.2012.02.001>
- Ortiga-Carvalho, T. M., Chiamolera, M. I., Pazos-Moura, C. C., & Wondisford, F. E. (2016). Hypothalamus-Pituitary-Thyroid Axis. *Comprehensive Physiology*, 6(3), 1387–1428. <https://doi.org/10.1002/cphy.c150027>
- Passero, Kristin, "Characterizing the Intracellular Distribution of Mutant Thyroid Hormone Receptor α -1 A382PfsX7" (2018). *Undergraduate Honors Theses*. William & Mary. Paper 1187. <https://scholarworks.wm.edu/honorstheses/1187>
- Rachez, C., & Freedman, L. P. (2001). Mediator complexes and transcription. *Current Opinion in Cell Biology*, 13(3), 274–280. [https://doi.org/10.1016/S0955-0674\(00\)00209-X](https://doi.org/10.1016/S0955-0674(00)00209-X)
- Rachez, C., Suldan, Z., Ward, J., Chang, C.-P. B., Burakov, D., Erdjument-Bromage, H., Tempst, P., & Freedman, L. P. (1998). A novel protein complex that interacts with the vitamin D3 receptor in a ligand-dependent manner and enhances VDR transactivation in a cell-free system. *Genes & Development*, 12(12), 1787–1800.
- Refetoff, S., Weiss, R. E., & Usala, S. J. (1993). The Syndromes of Resistance to Thyroid Hormone. *Endocrine Reviews*, 14(3), 348–399. <https://doi.org/10.1210/edrv-14-3-348>
- Rivas, A. M., & Lado-Abeal, J. (2016). Thyroid hormone resistance and its management. *Proceedings (Baylor University. Medical Center)*, 29(2), 209–211.

Rosenberg, D. P., Kolla, L., Heo, D. S., Cassio, E. E., Veenstra, M. J., Vakaki, M., Zhang, J., Anyetei-Anum, C., Allison, L. A., & Buchser, W. J. (2020). *Modulating Intra-Nuclear LC3 with Small Molecules Rescues Cells from a Docetaxel-Induced Phenotype* [Preprint]. *Molecular Biology*. <https://doi.org/10.1101/2020.10.28.355826>

Rouillard AD, Gundersen GW, Fernandez NF, Wang Z, Monteiro CD, McDermott MG, Ma'ayan A. *The harmonizome: a collection of processed datasets gathered to serve and mine knowledge about genes and proteins*. *Database (Oxford)*. 2016 Jul 3;2016. pii: baw100.

RTH α —Institut de Génomique Fonctionnelle de Lyon. (2022). Retrieved June 3, 2022 from <http://igfl.ens-lyon.fr/equipes/f.-flamant-functional-genomics-of-thyroid-signaling/projets-en-cours/rthalpha>

Salomon, M. S., Malapati, S. H., O' Dwyer, J., Silva, C. L., Williams, C. C., Barbeau, M. C., Yip, D., Punzalan, P., Nagle, V. L., Hinton, S. D., Roggero, V. R., & Allison, L. A. (2020). Mislocalization of Cancer-associated Thyroid Hormone Receptor Mutants. *Nuclear Receptor Research*, 2020, <https://web.archive.org/web/20210227193123/https://www.kenzpub.com/journals/nurr/inpress/2020/101453/>.

Singh, B. K., Sinha, R. A., Ohba, K., & Yen, P. M. (2017). Role of thyroid hormone in hepatic gene regulation, chromatin remodeling, and autophagy. *Molecular and Cellular Endocrinology*, 458, 160–168. <https://doi.org/10.1016/j.mce.2017.02.018>

Singh, B. K., & Yen, P. M. (2017). A clinician's guide to understanding resistance to thyroid hormone due to receptor mutations in the TR α and TR β isoforms. *Clinical Diabetes and Endocrinology*, 3(1), 8. <https://doi.org/10.1186/s40842-017-0046-z>

- Sinha, R., & Yen, P. M. (2018). Cellular Action of Thyroid Hormone. In K. R. Feingold, B. Anawalt, A. Boyce, G. Chrousos, K. Dungan, A. Grossman, J. M. Hershman, G. Kaltsas, C. Koch, P. Kopp, M. Korbonits, R. McLachlan, J. E. Morley, M. New, L. Perreault, J. Purnell, R. Rebar, F. Singer, D. L. Trence, ... D. P. Wilson (Eds.), *Endotext*. MDText.com, Inc. <http://www.ncbi.nlm.nih.gov/books/NBK285568/>
- Subramanian, K. S., Dziedzic, R. C., Nelson, H. N., Stern, M. E., Roggero, V. R., Bondzi, C., & Allison, L. A. (2015). Multiple exportins influence thyroid hormone receptor localization. *Molecular and Cellular Endocrinology*, 411, 86–96.
<https://doi.org/10.1016/j.mce.2015.04.014>
- Sun, X. (2019). *Thyroid Hormone Receptor and Coregulators* (Unpublished Undergraduate Honor's Thesis). College of William and Mary, Williamsburg, United States.
- THRA | gnomAD v2.1.1 | gnomAD. (2021). Retrieved October 13, 2021, from https://gnomad.broadinstitute.org/gene/ENSG00000126351?dataset=gnomad_r2_1
- THRA thyroid hormone receptor alpha [Homo sapiens (human)] – Gene – NCBI. (2019, October 12). Retrieved November 12, 2019, from <https://www.ncbi.nlm.nih.gov/gene/7067>.
- Trampenau, Elizabeth, "Mutations in Thyroid Hormone Receptor Alpha 1 and Their Implications for Resistance to Thyroid Hormone Alpha" (2019). *Undergraduate Honors Theses*. William & Mary. Paper 1327.<https://scholarworks.wm.edu/honorstheses/1327>
- Tylki-Szymańska, A., Acuna-Hidalgo, R., Krajewska-Walasek, M., Lecka-Ambroziak, A., Steehouwer, M., Gilissen, C., ... Chrzanowska, K. H. (2015). Thyroid hormone resistance syndrome due to mutations in the thyroid hormone receptor α gene (THRA).

Journal of Medical Genetics, 52(5), 312–316. <https://doi.org/10.1136/jmedgenet-2014-102936>

Usala, S. J., Bale, A. E., Gesundheit, N., Weinberger, C., Lash, R. W., Wondisford, F. E., ... Weintraub, B. D. (1988). Tight Linkage between the Syndrome of Generalized Thyroid Hormone Resistance and the Human c-erbA β Gene. *Molecular Endocrinology*, 2(12), 1217–1220. <https://doi.org/10.1210/mend-2-12-1217>

van Mullem, A., van Heerebeek, R., Chrysis, D., Visser, E., Medici, M., Andrikoula, M., ... Visser, T. J. (2012). Clinical Phenotype and Mutant TR α 1. *New England Journal of Medicine*, 366(15), 1451–1453. <https://doi.org/10.1056/NEJMc1113940>

van Mullem AA, Chrysis D, Eythimiadou A, et al. Clinical phenotype of a new type of thyroid hormone resistance caused by a mutation of the TR α 1 receptor; consequences of LT4 treatment. *J Clin Endocrinol Metab*. 2013;98:3029–3038

Vlaeminck-Guillem, V., Espiard, S., Flamant, F., & Wémeau, J.-L. (2015). TR α receptor mutations extend the spectrum of syndromes of reduced sensitivity to thyroid hormone. *La Presse Médicale*, 44(11), 1103–1112. <https://doi.org/10.1016/j.lpm.2015.07.022>

Wang, X., & Li, S. (2014). Protein mislocalization: Mechanisms, functions and clinical applications in cancer. *Biochimica et Biophysica Acta*, 1846(1), 13–25. <https://doi.org/10.1016/j.bbcan.2014.03.006>

Webb, P., Anderson, C. M., Valentine, C., Nguyen, P., Marimuthu, A., West, B. L., ... Kushner, P. J. (2000). The Nuclear Receptor Corepressor (N-CoR) Contains Three Isoleucine Motifs (I/LXXII) That Serve as Receptor Interaction Domains (IDs). *Molecular Endocrinology*, 14(12), 1976–1985. <https://doi.org/10.1210/mend.14.12.0566>

- Weiss, R. E., & Refetoff, S. (2000). Resistance to Thyroid Hormone. *Reviews in Endocrine and Metabolic Disorders*, 1(1–2), 97–108.
- Weiss, R. E., Dumitrescu, A. M., & Refetoff, S. (2016). Chapter 9—Syndromes of Impaired Sensitivity to Thyroid Hormone. In R. E. Weiss & S. Refetoff (Eds.), *Genetic Diagnosis of Endocrine Disorders (Second Edition)* (pp. 137–151). Academic Press.
<https://doi.org/10.1016/B978-0-12-800892-8.00009-9>
- Weinberger, C., Thompson, C. C., Ong, E. S., Lebo, R., Gruol, D. J., & Evans, R. M. (1986). The c-erb-A gene encodes a thyroid hormone receptor. *Nature*, 324(6098), 641–646.
<https://doi.org/10.1038/324641a0>
- Yen, P. M. (2001). Physiological and Molecular Basis of Thyroid Hormone Action. *Physiological Reviews*, 81(3), 1097–1142.
<https://doi.org/10.1152/physrev.2001.81.3.1097>
- Yen, P. M. (2003). Molecular basis of resistance to thyroid hormone. *Trends in Endocrinology and Metabolism: TEM*, 14(7), 327–333. [https://doi.org/10.1016/s1043-2760\(03\)00114-0](https://doi.org/10.1016/s1043-2760(03)00114-0)
- Zavacki, A. M., & Larsen, P. R. (2013). RTH α , a newly recognized phenotype of the resistance to thyroid hormone (RTH) syndrome in patients with THRA gene mutations. *The Journal of clinical endocrinology and metabolism*, 98(7), 2684–2686.
<https://doi.org/10.1210/jc.2013-2475>
- Zhang, J., & Lazar, M. A. (2000). The Mechanism of Action of Thyroid Hormones. *Annual Review of Physiology*, 62(1), 439–466. <https://doi.org/10.1146/annurev.physiol.62.1.439>

Zhang, J., Roggero, V. R., & Allison, L. A. (2018). Chapter Three—Nuclear Import and Export of the Thyroid Hormone Receptor. In G. Litwack (Ed.), *Vitamins and Hormones* (pp. 45–66). <https://doi.org/10.1016/bs.vh.2017.04.002>

COMPLIANCE PAGE

Research approved by

Institutional Biosafety Committee

Protocol number(s):

IBC-2020-01-10-14058-laalli

Date(s) of approval: 2022-1-31

2021-1-31

2020-1-31